

A 15 Metre Submillimetre Telescope on La Silla

During its last meeting, on 7 June 1984, the ESO Council approved the agreement between the Swedish Natural Science Research Council and ESO on the joint installation and operation on La Silla of a 15 m submillimetre telescope and the agreement between IRAM and ESO under which IRAM will provide the telescope.

The observing time will be shared equally between Sweden and ESO. Much of the technical responsibility for the project would lie with the Onsala Space Observatory which operates a 20 m millimetre telescope at Onsala. The Swedish/ESO Sub-

millimetre Telescope (SEST) is scheduled to become operational in 1987.

Director General Reappointed

Prof. L. Woltjer has been reappointed by the ESO Council to be Director General for the period 1 January 1985 to 31 December 1989.

The Remote Control Run from La Serena, June 10–17, 1984

G. Raffi and M. Tarenghi, ESO

With the expenditure of missions from Europe to Chile showing a steady increase, not only because of flight prices but also because of the rise in infrastructure upkeep of remote sites, along with a clear tendency to lower the cost of satellite transmission, it seems to us that remote control will become an economical system to operate telescopes.

It is important to underline here that the economic factor is not the only one, and probably not even the major one. The real reason for the modern tendency towards remote control is the hope to make better use of our present and future telescopes. Possible advantages directly or indirectly coming from remote control are:

(1) The telescope can be located on the best possible site, which may in itself not be comfortable for astronomers.

(2) Larger groups of astronomers can participate in observing programmes.

(3) Better use of telescope time. Scheduling of telescopes becomes more flexible and it will be possible to make maximum use of the best seeing nights.

(4) Better collaboration between technical maintenance in Chile and Europe will result. Instrument tests will have the advantage of being carried out under the control of a larger technical team, and in particular by the group who assembled the equipment in Europe.

We are investigating possible systems of communication between the observatory and Europe. The transmission of data between the telescope control system and some type of data processing and visualization equipment in Garching should include the transmission in real time of the telescope's field image and the instrument's data and, in the reverse direction, the transmission of the control commands.

If the operation of the telescope cannot be fully automated, a means of communication between the observer in Garching and a night assistant in La Silla must be provided.

Change of ESO telephone number in Santiago

Please take note that the telephone number of La Silla via the ESO Santiago office has been changed from 88757 to 6988757.

In the case of the NTT, it is intended to implement remote control as a connection of two computers via a long-distance link. Clearly this approach gives some advantages, such as:

- Communication reliability can be increased by retransmissions to such a level that all transmission errors are eliminated.

- The raw data can be sent from one computer to the other. An obvious implication of this is that the full power of an image processing system on the user-end computer can then be applied at will to the data. Furthermore, the user has the data available to him already at the end of his observing night.

To clarify these advantages better, one should think of the alternative of simply having a terminal connected via a long-distance link to a distant computer. In this case all graphics, etc. must be computed on the host distant computer and the result (e.g. a plot) must be sent down the line each time to the user's terminal.

On a slow speed line this requires time, and the terminal does not have the "intelligence" to correct transmission errors, which will probably destroy the graph and the raw data will not be available to the user.

A remote control run from La Serena, last June, was a first relevant step in this direction.

The Technology Used for the La Serena Run

The 2.2 m telescope of ESO was chosen to run this experiment because its control/acquisition software was implemented in a manner suitable for remote control, even if not initially written explicitly for this, and because an auto-guider was available on it. The instruments used were a Boller & Chivens spectrograph with CCD detector and a CCD for direct imaging.

The two computers connected were two HP 1000 systems, one in the 2.2 m telescope and the other in the ESO office in La Serena.

The line in-between was leased by the Chilean PTT Entel and was based on a microwave link from La Silla to the Entel office in La Serena plus a short VHF link in La Serena. The frequency band used was a normal telephone band and Entel provided also modems at 4800 baud.



Fig. 1: La Serena, 16 June 1984. The control room at the ESO La Serena office, during a measurement of the seeing of the La Silla sky.

In practice we used different modems (synchronous) at 9600 baud, which supported also telephone voice communication as an alternative to data transmission.

The Remote Control Software

The communication software was based on DS/1000, at the top of which a package was built to allow programme to programme communication via mailboxes over a link. The control/acquisition software in the 2.2 m had already been built around modules exchanging commands via mailboxes. What was needed for remote control was to separate some of these modules (the "user end") from the others (the "controller" or instrument/telescope end). The "user end" programmes dealing with softkey input and input-output tables were modified to interact with the remote control package.

The "controller" modules remained unchanged, which means that they could run either locally or remotely.

The "user end" programmes were also unchanged as far as appearance to the user is concerned.

Special attention had to be paid to the usage of the image processing IHAP programme. The data acquisition was done on the La Silla computer, reading data into a disk in the IHAP data-base and putting them on tape there.

The IHAP programme at La Silla, called remote IHAP, was made available also to the user in La Serena, allowing a number of examinations on the acquired data. The transmission of data from the La Silla computer to the user-end computer was carried out typically with a file to file copy programme.

A data compression programme was also tested, which allows the sending of data in compressed form without loss of information. An additional advantage of this is the capability to transfer data from remote IHAP to local IHAP and to do a display on a Ramtek display at the same time. By "local IHAP", the IHAP on the user-end computer is of course meant.

Capabilities Offered

The capabilities offered in La Serena are described below.

- The same user interface to instruments (Boller & Chivens and Adapter with CCD) as in La Silla at the 2.2 m telescope and the same devices (instrumentation and graphic terminal, Ramtek image display) were available.
- An extra feature, with respect to normal observation, was the access to both local IHAP (on the La Serena computer) and remote IHAP (on the La Silla computer).
- It was possible to preset, offset, and focus the 2.2 m telescope via the instrument programme. This is an option available also at La Silla, when the user defines an exposure. The instrument programme takes care of sending the appropriate commands to the telescope control system.
- In principle it is also possible to use directly the telescope control system console from La Serena under remote control, having access to all the functions of the telescope. However, operationally it proved to be unnecessary and the telescope control console was left to the night assistant in La Silla, who used it mainly to start autoguiding.
- Data transmission was carried out and was available in two ways.
 - file to file transfer (data were copied from the IHAP data-base to a file and sent down the link as any file).

– IHAP to IHAP communication directly with data compression. (The data compression programme extracted the data directly from the IHAP data-base and also optionally cut them before transmission.)

The transmission of full raw CCD images (320×512 pixels) took about 7 minutes. However, images were normally either cut with threshold levels or truncated to a subset of the full image. This allows the reduction of the size of images to some 10–20%, even without (or before) using data compression.

It is interesting to note anyhow that operationally, the data transmission times went “unnoticed” as, typically, data were sent across the link while the next CCD exposure was taking place.

Data transmission does not clash either with sending commands to the instrument or telescope, as this involves a short exchange of messages on the line.

- An interactive message system was also used to send/receive messages from a dedicated console. This was constantly active and working together with all other operations on the link.
- A voice channel was available as an alternative to the data channel. This is useful in situations like start-up, rebooting, etc. and was routinely used, e.g. during exposures to obtain information in a more direct and informal way than via a message system.

Conclusions

The operation from La Serena proved to be feasible both for the spectrographic mode and imagery. However, particularly for spectroscopy, the addition of a device to digitize the field image of the telescope, and transmit it to the remote site, which was not yet available at this stage, is planned and will be necessary.

Tentative Time-table of Council Sessions and Committee Meetings in 1984

October 8–9	Scientific Technical Committee, Chile
November 13–14	Finance Committee
November 27–28	Observing Programmes Committee
November 28	Committee of Council
November 29–30	Council

All meetings will take place at ESO in Garching unless stated otherwise.

Next Step

The next logical step is to observe from Garching. Various technical alternatives to do this will be possible. They basically are:

- Direct link via satellite transmission and an antenna in La Silla.
- Direct link via a satellite link from Santiago shared by ESO, plus a dedicated telephone line to Santiago.
- A dedicated telephone line to Santiago plus access from Santiago to a public international computer network. In this case, in practice, data would be routed via a computer in Santiago to a USA computer via a communications satellite link and from there to Europe.

We expect that this last possibility will become available in a few months as a service. A test with this might be relatively cheap to run and would take us one step further in the direction of having remote control for the NTT.

We would like to thank M. Ziebell for his contribution to the project, P. Biereichel for his data compression programme, D. Hofstadt and the TRS staff for handling the lease contracts with Entel and for the support in Chile.

Oxygen Abundances in Metal Poor Stars

R. G. Gratton and S. Ortolani, Osservatorio Astrofisico di Asiago, Italy

Introduction

The study of the chemical composition of old stars may give us interesting information about the early phases of evolution of our Galaxy. The Big Bang may have formed only a trace of elements heavier than Be. It is quite consequent that the early generation of stars in our Galaxy (and in any galaxy) must have formed with a low metal abundance; the metals were then formed in the interior of these early stars and returned to the interstellar medium through stellar winds or supernova explosions. Successive generations of stars formed with an increasing metal abundance. This picture is substantiated by the relation existing between metallicity and galactic orbit eccentricities shown by Eggen et al. (1962); this is interpreted as the interaction between a fast collapse of the gas component of the galactic halo and the increase of the mean metallicity of the same gas.

Many points are still obscure in this picture; the absence of observations of very metal poor stars seems to indicate that the Initial Mass Function (IMF) may have been different in the past, being strongly biased to massive or even super-massive stars ($M > 100 M_{\odot}$). The evolution of these candidates to the first generation of stars is far from being clear (see e.g.

Woosley et al., 1982); there is the strong suspicion that they may form large quantities of Oxygen but very small amounts of Iron. On the other side, type I supernovae are probably efficient Fe makers, while there is no available indication of the presence of Oxygen in their ejecta. As type I supernovae do not follow the arms of spiral galaxies and are present also in ellipticals, we think that the lifetimes of their progenitors are long. Thus the timescale of production of Oxygen (and some other light element) may be substantially different from the timescale of Iron (and other heavy elements) production.

It seems thus interesting to study the behaviour of the O/Fe ratio with time. Unfortunately it is quite difficult to derive sufficiently accurate ages for population II objects. We may however assume that age is correlated with metal abundance. This hypothesis is probably good in the solar neighbourhood, though it may be dangerous to extend it naively to other galactic regions.

Observations and Analysis

Early attempts to derive Oxygen abundances for metal poor stars have been made by Sneden et al. (1979) and Clegg et al.

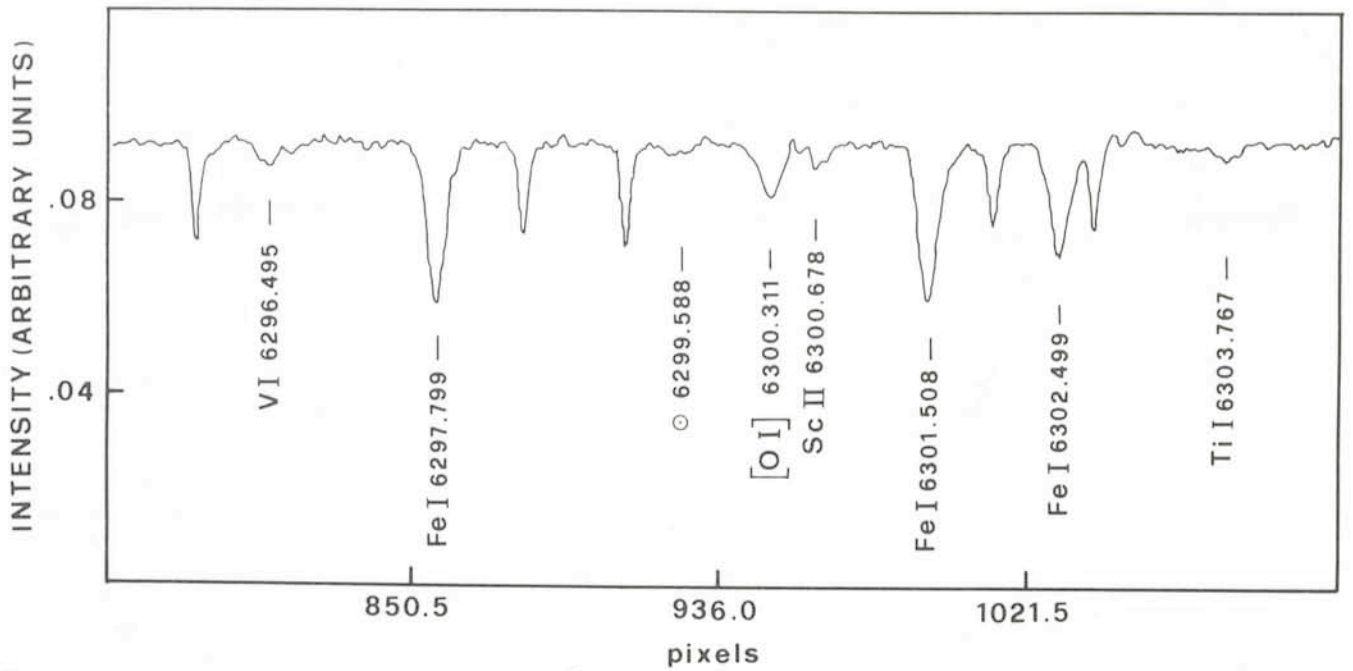


Fig. 1: Tracing of a CAT+CES Reticon spectrum of the 6300 Å region in the metal poor giant HD 26297 ($V = 7.48$). The exposure time was 2 hours; the resolution 100,000. The narrow lines are telluric O lines.

(1981). They make use of the strong infrared Oxygen triplet; this is a high excitation feature which is affected by non-LTE effects. Some doubts about the strong Oxygen overabundances found by these authors seem legitimate.

The best abundance indicators for Oxygen are the forbidden 6300 and 6363 Å lines (Lambert, 1978). However, the observation of these lines is quite difficult, the lines being weak and sometimes contaminated by telluric absorptions and emissions. Further, the lines are strongly gravity dependent. These problems may however be overcome by using the most recent high dispersion instrumentation, like the ESO CES spectrograph at the CAT telescope. The exceptionally high S/N ratio and resolution given by this instrument allow to get accurate equivalent widths for the Oxygen lines (see Fig. 1). It is possible to compare the Oxygen lines directly with other nearby lines having similar atmospheric parameter dependence, like the 6300.68 Sc II line. The abundance ratios that may be obtained in this way are largely model independent, and very small error bars may be obtained.

Observations of the 6300.31 [O I] line region and of other spectral regions were performed at the CAT telescope at La Silla during October 1982 and May 1983. The observational material (Reticon spectra with S/N in excess of 100 and resolution 100,000) was of exceptional quality: it is easy to distinguish atmospheric features from stellar ones by their widths.

Results

A preliminary analysis of the spectra has been performed using model atmosphere analysis programmes available at the Asiago Astrophysical Observatory. We have derived [O/Sc] and [O/Fe] ratios for about twenty stars of different evolutionary phases and chemical compositions. No large differences between dwarfs and giants have been seen. This means that non-LTE or evolutionary effects are unimportant, as expected. The only atmospheric parameter which significantly affects the data is the effective temperature. This was derived from photometric indices. An error of ± 100 K in the

temperatures gives an error of ± 0.04 dex in the [O/Sc] and 0.08 dex in the [O/Fe] ratios respectively. Correction for CO formation was included, assuming that C is depleted by

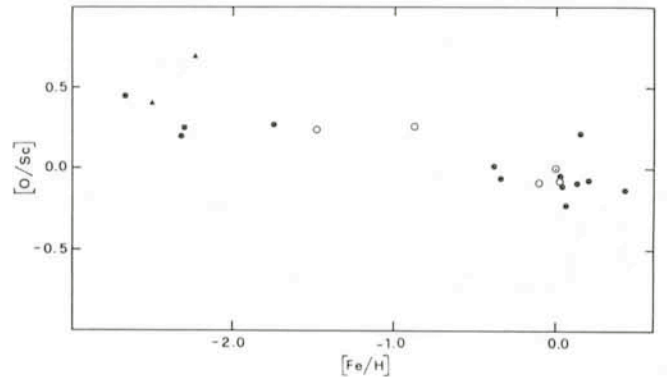


Fig. 2: The [O/Sc] abundance ratio against the metal abundance ($[Fe/H]$). Dots are giants; circles are dwarfs; triangles are data from Lambert et al. (1974).

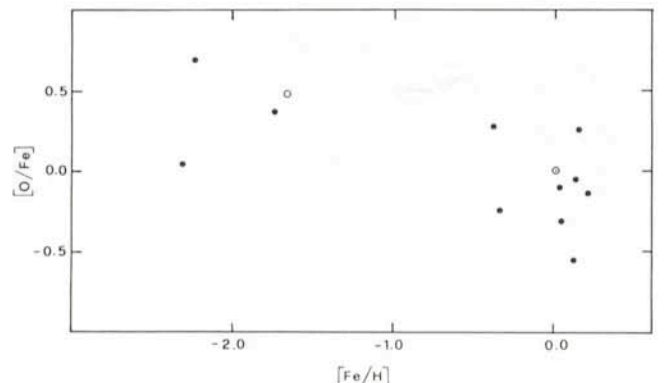


Fig. 3: The [O/Fe] abundance ratio against the metal abundance ($[Fe/H]$). The symbols are the same as in Fig. 2.

0.2 dex in giants (Lambert and Ries, 1977, 1981; Kjaergaard et al., 1982). The effect of this correction is important only for a couple of the cooler population I stars.

Fig. 2 and 3 give the [O/Sc] and [O/Fe] ratios against the iron abundance; an additional star (HD 122563: Lambert et al., 1974) having literature data is plotted in Fig. 2 as a triangle.

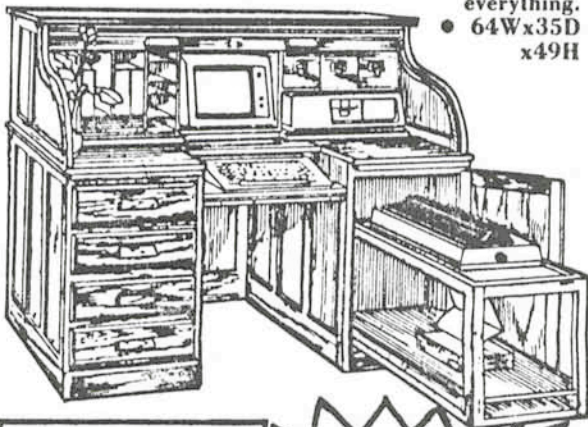
Inspection of Fig. 2 und 3 reveals that metal poor stars are Oxygen overabundant. However, this overabundance is less than indicated by the previous works. Our result refers to a small sample of stars. However, it may be considered as an evidence of a slight (0.3 dex) Oxygen overabundance in metal poor stars.

References

- Clegg, R.E.S., Lambert, D.L., and Tomkin, J., 1981: *Astrophysical Journal* **250**, 262.
 Eggen, O.J., Lynden-Bell, D., and Sandage, A.R., 1962: *Ap. J.* **136**, 748.
 Kjaergaard, P., Gustafsson, B., Walker, G.A.H., and Hultqvist, L., 1981: *Astronomy and Astrophysics*, **115**, 145.
 Lambert, D.L., 1978: *Monthly Notices of the Royal Astronomical Society*, **182**, 249.
 Lambert, D.L., and Ries, L.M., 1977: *Ap. J.* **217**, 508.
 Lambert, D.L., and Ries, L.M., 1981: *Ap. J.* **248**, 228.
 Lambert, D.L., Sneden, C., and Ries, L.M., 1974: *Ap. J.* **188**, 97.
 Sneden, C., Lambert, D.L., and Whitaker, R.W., 1979: *Ap. J.* **234**, 964.
 Woosley, S.E., Axelrod, T.S., and Weaver, T.A., 1982: in *Stellar Nucleosynthesis* (C. Chiosi and A. Renzini, eds.), Reidel, Dordrecht, p. 263.

THE "ULTIMATE" ROLL-TOP COMPUTER DESK

• Superior Quality • Dovetail joint
 drawers on extension glides • Completely
 set up for your IBM • This
 desk has
 everything.
 • 64Wx35D
 x49H




ONLY
\$1799

Image processing at ESO is heavily used and much effort is made to provide the most sophisticated hardware available. A very fashionable and comfortable computer desk terminal has just been chosen from an advertisement published in the Los Angeles Times (15.5.1984).

Visiting Astronomers

(October 1, 1984 to April 1, 1985)

Observing time has now been allocated for period 34 (October 1, 1984 to April 1, 1985). As usual, the demand for telescope time was much greater than the time actually available.

The following list gives the names of the visiting astronomers, by telescope and in chronological order. The complete list, with dates, equipment and programme titles, is available from ESO-Garching.

3.6 m Telescope

October 1984: Hunger/Heber/Drilling/Kudritzki, Alloin/D'Odorico/Pelat, Dravins/Linde/Nordlund/Fredga/Gahm/Ayres/Linsky/Simon, Eriksson/Saxner, Gratton/Ortolani, Maurice/Lequeux/M.L. Prévot/L. Prévot, Cristiani, Moorwood/Cetty-Véron, Richter/Chiosi/Ortolani/Gratton, Beuermann/Pakull/Motch/Krautter, Lindblad/Jörsäter, Kunth/Sargent, Zuiderwijk/v. Paradijs/de Loore.

November 1984: Zuiderwijk/v. Paradijs/de Loore, Alloin/D'Odorico/Pelat, Rosino/Ortolani, Pizzichini/Pedersen, Bergeron/Puget, Marano/Zamorani/Zitelli, Westerlund/Azzopardi/Breysacher, Marano/Zamorani/Zitelli, Westerlund/Azzopardi/Breysacher, Neckel/Staude.

December 1984: Neckel/Staude, Kudritzki/Conti/Gehren/Groth/Husfeld/Simon, Danks, Ferlet/Dennefeld, Rodono/Foing/Cutispoto/Scaltriti/Bonnet/Linsky/Butler/Haisch, Dennefeld, Cristiani, Richtler/Seggewiss, Pakull/Beuermann/Ilovaisky/Chevalier/Motch/van der Klis, Danziger/Cristiani/Shaver.

January 1985: Epchtein/Braz, Israel/Koornneef/de Graauw/Schwering, Westerlund/Jörgensen U.G./Gustafsson, Olofsson/Bergvall/Johansson, van der Kruit, Westerlund/Jörgensen, U.G./Gustafsson, Lequeux/Azzopardi/Breysacher/Westerlund, Schild/Maeder/Kunth, Hensler/Schoembs/Kudritzki/La Dous/Barwig, Chmielewski/Jousson.

February 1985: Chmielewski/Jousson, Kudritzki/Nissen/Gehren/Simon, Reipurth, Cetty-Véron, Bergeron/Boissé, Pottasch/Bouchet/Dennefeld/Karaji, de Grijp/Lub/Miley/de Jong, Pottasch/Bouchet/Dennefeld/Karaji, Preite-Martinez/Persi/Ferrari-Toniolo/Pottasch.

March 1985: Preite-Martinez/Persi/Ferrari-Toniolo/Pottasch, Moorwood/Glass, de Muizon/d'Hendecourt/Perrier, Perrier/Chelli/Léna, Stalio/Ferluga, Gehren/Hartmann/Kudritzki, Krautter.

1.4 m CAT

October 1984: Crivellari/Beckman/Foing/Franco, Ferlet/Vidal-Madjar/Gry/Laurent, Spite, M. and F./François, Danks/Lambert.

November 1984: Danks/Lambert, Pallavicini, Holweger/Gigas/Steenbock, Mauron, Reimers/Hempe/Toussaint.

December 1984: Reimers/Hempe/Toussaint, Foing/Bonnet/Crivellari/Beckman/Galleguillos/Lemaire/Gouttebroze, Gustafsson/Vilhu/Schoembs, Rodono/Foing/Cutispoto/Scaltriti/Bonnet/Linsky/Butler/Haisch, Foing/Bonnet/Crivellari/Beckman/Galleguillos/Lemaire/Gouttebroze, Gustafsson/Vilhu/Schoembs, Barbuy, Baade.

January 1985: Baade, Hanuschik/Dachs, Baade/Ferlet, Furenlid/Kurucz.

February 1985: Baade, Gratton/Ortolani/Sneden, Hanuschik/Dachs.

- March 1985: Hanuschik/Dachs, Thé/Tjin A Djie/Praderie/Catala, Ferlet/Vidal-Madjar, Gry/Laurent, Ruiz/Melnick, Giovanelli/Vittone/Bisnovaty/Sheffer/Lamzin, van Dishoeck/Habing/Black, Groth/Kudritzki/Simon, Cayrel de Strobel.
- December 1984: Thé/Westerlund/Pérez, Bouchet/Chalabaev, Rodono/Foing/Cutispoto/Scaltriti/Bonnet/Linsky/Butler/Haisch, Bouvier/Bertout/Bouchet, Wolf/Appenzeller/Klare/Leitherer/Stahl/Zickgraf/Bastian, Hahn/Lagerkvist/Rickman, Busso/Scaltriti/Cellino.

2.2 m Telescope

- October 1984: Véron, Grewing/Bässgen/Kappellmann/Bianchi/Krämer/Gutekunst, Moorwood/Cetty-Véron, Richter/Ortolani/Gratton/Chiosi, Pizzichini/Pedersen, Danziger/Shaver/Pedersen.
- November 1984: Henry/Arp/Gosset/Swings/Surdej.
- December 1984: Henry/Arp/Gosset/Swings/Surdej, Clausen/Jensen/Giménez/van der Klis, van der Klis/van Paradijs/van den Heuvel/Bonnet-Bidaud/Jansen/Cordova, Crane/Chincarini, Pakull/Beuermann/Ilovaisky/Chevalier/Motch/van der Klis, Lyngå/Westerlund/Linde, Blecha/Rufener.
- January 1985: Jörgensen/Norgaard-Nielsen/Hansen, Weigelt/Koller/Kollatschny/Seggewiss, Schild, Cesarsky/Danziger.
- February 1985: Cesarsky/Danziger, Sadler/Carter, Bertola/Danziger/Sadler, Pottasch/Bouchet/Dennefeld/Karoji, Véron.
- March 1985: Ilovaisky/Motch/Hurley/Pedersen/Chevalier/Angebault.
- January 1985: Busso/Scaltriti/Cellino, Gammelgaard/Kristensen, Bergvall/Olofsson K./Ekman, Lauberts, Hensler/Schoembs/Kudritzki/La Dous/Barwig, Reipurth.
- February 1985: Reipurth, Strupat/Rahe/Drechsel, Bouchet/Chalabaev, Antonello/Mantegazza/Pastori, Maitzen/Schneider/Catalano.
- March: 1985: de Muizon/d'Hendecourt/Perrier, Perrier/Chelli/Léna, Lagerkvist/Rickman/Hahn/Magnusson, Persi/Ferrari-Toniolo/Roth/Tapia, Giovanelli/Vittone/Bisnovaty/Sheffer/Lamzin, Lagerkvist/Rickman/Hahn/Magnusson, Fouqué, Pauls/Kohoutek, Liller/Alcaino.

50 cm ESO Photometric Telescope

- October 1984: Surdej A. and J./Schober/Michalowski, Group for long-term photometry of variables (Sterken-Brussels).
- November 1984: Group for long-term photometry of variables (Sterken-Brussels), Carrasco/Loyola, Schneider/Maitzen, Thé/Westerlund/Pérez.
- December 1984: Thé/Westerlund/Pérez, Schneider/Maitzen, Bouvier/Bertout/Bouchet, Busso/Scaltriti/Cellino, Wolf/Appenzeller/Klare/Leitherer/Stahl/Zickgraf/Bastian.
- January 1985: Wolf/Appenzeller/Klare/Leitherer/Stahl/Zickgraf/Bastian, Group for long-term photometry of variables (Sterken-Brussels).
- February 1985: Group of long-term photometry of variables (Sterken-Brussels), Manfroid/Sterken, Metz/Häfner, Carrasco/Loyola, Metz/Häfner, Thé/Tjin A Djie/Praderie/Catala, Group for long-term photometry of variables (Sterken-Brussels).

1.5 m Spectrographic Telescope

- October 1984: Alloin/D'Odorico/Pelat, Bues/Rupprecht, Prévot M.L./Lequeux/Maurice/Prévot L., Appenzeller/Östreicher, Alloin/D'Odorico/Pelat.
- November 1984: Alloin/D'Odorico/Pelat, Danziger/Maraschi/Tanzi/Treves, Bica/Alloin, Mazure/Capelato/Sleinev/Gerbal/Mathez/Proust/Salvador-Solé, Kollatschny/Colina, Palumbo/Vettolani/Hickson.
- December 1984: Palumbo/Vettolani/Hickson, Thé/Westerlund/Pérez, Heydari-Malayeri/Testor, Bouvier/Bertout/Bouchet, Hahn/Lagerkvist/Rickman, Lub/de Ruiter.
- January 1985: Wolf/Appenzeller/Klare/Leitherer/Stahl/Zickgraf/Bastian, Gomez/Gerbaldi/Floquet/Grenier, Catalano/Marilli/Trigilio, Lundgren, Olofsson G., Bergvall/Olofsson K./Ekman, Capaccioli/Longo, Koester/Zeidler K.T.
- February 1985: Koester/Zeidler K.T., Strupat/Rahe/Drechsel, Koeppen/Finkenzeller/Carsenty, Pastori/Mantegazza/Antonello, Pelat/Clavel, Fricke/Hellwig, Pelat/Clavel, Metz/Häfner, Maitzen/Schneider/Catalano.
- March 1985: Maitzen/Schneider/Catalano, Andersen, Lagerkvist/Rickman/Hahn/Magnusson, Giovanelli/Vittone/Bisnovaty/Sheffer/Lamzin, Chincarini/de Souza/Manousoyannaki/Kotanyi, Nelles, Pauls/Kohoutek.
- October 1984: Martin.
- November 1984: Valbousquet.
- December 1984: Dommagnet/Léonis.
- January 1985: Dommagnet/Léonis, Duerbeck/Tsvetkov/Seitter.
- February 1985: Debehogne/Zappala/De Sanctis/Lagerkvist/Magnusson.
- March 1985: Madsen, Schober, Madsen.

GPO 40 cm Astrograph

- October 1984: Martin.
- November 1984: Valbousquet.
- December 1984: Dommagnet/Léonis.
- January 1985: Dommagnet/Léonis, Duerbeck/Tsvetkov/Seitter.
- February 1985: Debehogne/Zappala/De Sanctis/Lagerkvist/Magnusson.
- March 1985: Madsen, Schober, Madsen.

1.5 m Danish Telescope

- October 1984: Lindgren/Ardeberg/Maurice/Prévot L., Cacciari/Clementini/Prévot L./Lub/de Bruyn, Lindgren/Ardeberg/Maurice/Prévot L., Pedersen, Lequeux Maurice/Prévot L. and M.L., Lindblad/Jörsäter, Fusi Pecci/Renzini/Buonanno/Corsi, Aurière/Cordoni.
- November 1984: Aurière/Cordoni/J.V. Clausen/A. Giménez/K.S. Jensen, A. Reiz/V. Pirola, L. Hansen.
- December 1984: Clausen/Jensen/Giménez/van der Klis, van der Klis/van den Heuvel/van Paradijs/Clausen/Jensen/Bonnet-Bidaud/Jansen, van Paradijs/van der Klis/Cordova, Rosino/Ortolani, Ortolani/Gratton, Ilovaisky/Chevalier/Motch/Angebault.

1 m Photometric Telescope

- October 1984: Cacciari/Clementini / Prévot L. / Lub / de Bruyn, Trefzger/Labhardt/Spaenhauer/Steinlin, Mouchet/Bonnet-Bidaud/Motch, Beuermann/Pakull/Motch/Krautter, Bues/Rupprecht, Fricke/Loose.
- November 1984: Fricke/Loose, Bouchet/Chalabaev, Schneider/Kroll/Voigt, Bica/Alloin/Dottori/Pastoriza, Gosset/Arp/Henry/Surdej/Swings.

- January 1985: B. Reipurth, J. Andersen/A. Blecha/M.F. Walker, A. Reiz, Ilovaisky/Chevalier/Motch/Angebault, Lindgren/Ardeberg/Maurice/Prévot L.
- February 1985: Lindgren/Ardeberg/Maurice/Prévot L., Andersen/Nordström/Olsen, Prévot L. Ardeberg/Lindgren/Maurice, Mayor/Burki, Mayor/Mermilliod, Crane/Capaccioli, de Grijp/Lub/Miley/de Jong.
- March 1985: S. Frandsen/B. Thomsen, K. Gyldenkerne/M. Hawkins, de Grijp/Lub/Miley/de Jong, Liller/Alcaino, Ilovaisky/Chevalier/Motch/Angebault.

50 cm Danish Telescope

- October 1984: Lindgren/Ardeberg/Maurice/Prévot L., Grenon/Oblak, Lindgren/Ardeberg/Maurice/Prévot L., Grenon/Oblak, Foing/Bonnet/Crivellari/Beckman/Galleguillos/Lemaire/Gouttebroze.
- November 1984: Foing/Bonnet/Crivellari/Beckman/Galleguillos/Lemaire/Gouttebroze.
- December 1984: Schneider/Maitzen/Weiss/Vogt, Foing/Bonnet/Crivellari/Beckman/Galleguillos/Lemaire/Gouttebroze, Gustafsson/Vilhu/Schoembs, Foing/Bonnet/Crivellari/Beckman/Galleguillos/Lemaire/Gouttebroze, Gustafsson/Vilhu/Schoembs.
- January 1984: Baade/Ferlet, L.K. Kristensen.
- February 1985: L.K. Kristensen, Sterken, Lindgren/Ardeberg/Maurice/Prévot L., Lodén K.
- March 1985: Lodén K., E.H. Olsen.

90 cm Dutch Telescope

- October 1984: Trefzger/Pel/Blaauw, van Paradijs/Groot, van Paradijs/Charles/Pakull, van Paradijs/Bath/Charles/Groot, van Paradijs/Bath/Zuiderwijk/Groot.
- November 1984: van Paradijs/Groot, van Paradijs/Charles/Pakull, van Paradijs/Bath/Charles/Groot, van Paradijs/Bath/Zuiderwijk/Groot.

December 1984: Diethelm, Lub/de Ruiter.

- February 1985: Grenon/Lub, de Zeeuw/Lub/Blaauw/Koninx, van Paradijs/Groot/van Paradijs/Charles/Pakull, van Paradijs/Bath/Charles/Groot.
- March 1985: van Paradijs/Groot, van Paradijs/Charles/Pakull, van Paradijs/Bath/Charles/Groot, van Paradijs/Bath/Zuiderwijk/Groot.

61 cm Bochum Telescope

- October 1984: Grewing/Bässgen/Kappelman/Bianchi/Krämer/Gutekunst, Bianchi/Cellino/Grewing/Pakull.
- November 1984: Bianchi/Cellino/Grewing/Pakull, Isserstedt.
- December 1984: Isserstedt.
- January 1985: Isserstedt, Feitzinger.
- February 1985: Feitzinger, Musculus.
- March 1985: Musculus.

Applications for Observing Time at La Silla

Period 35 (April 1–Oct. 1, 1985)

Please do not forget that your proposals should reach the Section Visiting Astronomers **before October 15, 1984.**

Applications to observe Comet Halley during Period 36 (October 1, 1985 – April 1, 1986) should also be submitted before October 15, 1984.

First QSO Spectra with EFOSC

H. Dekker and S. D'Odorico, ESO

EFOSC, the ESO Faint Object Spectroscopic Camera, will be available to users as of April 1, 1985 at the Cassegrain focus of the 3.6 m telescope.

The instrument was mounted for the first time at the telescope in June 1984 for a short test period. The optical components were not yet fully optimized, and only part of the grisms and filters were available. It was, however, possible to test successfully the instrument functions and to carry out a few observations in direct imaging and spectroscopic modes. The results prove the high efficiency and the versatility of the instrument. A full description of EFOSC will be given in a next issue of the *Messenger*.

We just report here on the spectra of two QSOs in order to provide users with a first hint of the instrument performance. Table 1 summarizes the parameters of the observations. A thinned, back illuminated, RCA CCD was used as a detector; the chip belongs to the most recent production of RCA and it appears to have good charge transfer properties. The format of the spectra is identical to that of the Boller and Chivens spectrograph plus CCD. A long slit is used so that the sky to

be subtracted can be sampled on either side of the object spectrum.

The radio source PKS 1256-220 has been identified by Condon et al. (1977) with a 20 magnitude stellar object, on the basis of an accurate radio position (the finding chart is labelled

TABLE 1: OBSERVATIONAL PARAMETERS

<i>Detector characteristic:</i>	512 × 320 pixels, 30 μm in size 40 e ⁻ /pixel read out noise	
<i>Dispersion:</i>	230 Å/mm, 7 Å/pixel	
<i>Object:</i>	12 56-22	13 34-00
<i>m_r:</i>	20	17
<i>Slit width:</i>	in arc sec	1.5
	in pixels	2.3
<i>Exposure time: (sec)</i>	1800	600
<i>Seeing: (FWHM)</i>	1.6	1.5
<i>Counts/sec./Å, at λ 5400 Å:</i>	0.24	1.31

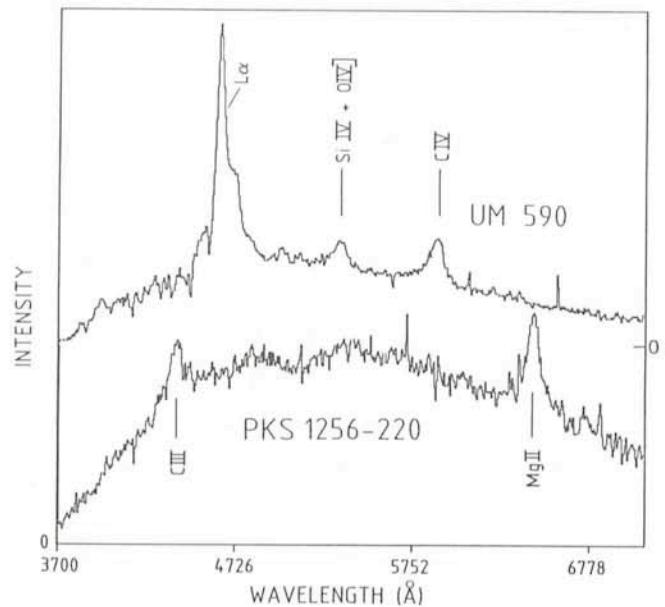
1156-220 instead of 1256-220). The spectrum of this object, exposed for 30 minutes, clearly shows two strong emission lines identified with C III] λ 1909 and Mg II λ 2800 at redshift $z = 1.306$ (Fig. 1).

UM 590 (1334-00) is a 17 magnitude quasar found in an objective prism survey carried out with the 61 cm aperture Curtis Schmidt telescope at the Cerro Tololo InterAmerican Observatory (MacAplaine et al., 1981), with a suggested redshift $z = 2.85$. A 10 minute spectrum (Fig. 1) shows three strong emission lines: Ly α , OIV] λ 1302 and CIV λ 1550 from which a redshift of 2.79 is measured.

References

Condon, J. J., Hicks, P. D., and Jauncey, D. L.: 1977, *Astron. J.* **82**, 692.
 MacAlpine, G. M., and Williams, G. A., 1981, *Astrophys. J. Suppl.* **45**, 113.

Fig. 1: The two sky-subtracted, wavelength-calibrated QSO spectra obtained with EFOSC. No flat fielding or spectral response correction has been applied. The plots show rather effectively the good S/N that was achieved in the two observations. ▶



Study of the Overall Spectrum of the QSO 3C273

T. J.-L. Courvoisier, Space Telescope European Coordinating Facility

Seyfert galaxies, quasars (QSOs) and possibly BL Lac objects have some basic properties in common. We therefore expect them to be different manifestations of the same basic phenomenon and call them Active Galactic Nuclei (AGN). Provided that our estimates of distances based on redshifts are correct, the AGN are the most luminous objects we know. Their luminosities range from 10^{44} ergs/sec for Seyfert nuclei to some 10^{47} ergs/sec for bright quasars (or 10^{11} to $10^{14} L_{\odot}$ where L_{\odot} is the luminosity of the sun). On the other hand, these objects are variable in most of the spectrum on time scales of years and less, which means that they are smaller than a few light years (light weeks for some objects). How to radiate such a large quantity of energy from such a small volume is one of the most puzzling questions of modern astronomy, and as yet unanswered.

The overall spectrum of AGN is very different from that of stars or galaxies. Instead of peaking strongly at one energy (wavelength) characteristic of a temperature, the AGN emit roughly the same quantity of energy in all decades of frequency between the radio and the γ -ray ends of the electromagnetic spectrum (see Fig. 2 for an example). Another common way for AGN to free energy is by means of one or two sided jets.

In order to generate the photon energy distribution of AGN, it is necessary that several regions with very different physical characteristics are involved in emission processes. Two questions must therefore be answered to understand the overall spectra of AGN: 1. Where does the energy come from (in other words, what is the central engine)? And, 2., what are the physical conditions in the different regions and how are they linked together? Or: what is the structure of the emission regions? This paper deals with a theoretical and an observational approach to the second question.

Most of the present conceptions on AGN involve a massive black hole and an accretion disk (see the proceedings of the conference on X-ray and UV Emission from Active Galactic Nuclei, Max-Planck-Institut für Extraterrestrische Physik,

Garching, 1984, for an up-to-date survey). The origin of the radiated energy is thus of gravitational nature and the overall spectrum is explained by the structure of the accretion disk and maybe the presence of a hot corona surrounding it. A different view on this question will be presented in the next section and an observation programme to test it will be described at the end of the paper.

The Wind and Shock Model

In the last two years, M. Camenzind (Institute of Theoretical Physics, University of Zurich) and myself have developed a model to explain the overall structure of the emission spectrum of Active Galactic Nuclei (1). Our effort is aimed at understanding individual objects (say, the QSO 3C 273) rather than global properties of broad classes of AGN. The model can be adapted to different sources by varying its free parameters.

The object at the very centre of an active nucleus (the engine) need not be defined in detail for our purpose. It may be the inner part of an accretion disk, a rotating super-massive star ($\sim 10^8 M_{\odot}$) or a very dense cluster of stars. The radius of this central engine is expected to be of the order of 100 Schwarzschild radii. It is important to note that these objects are radiation pressure dominated and hence marginally stable. In these conditions, a very strong wind accelerated by radiation pressure or magnetohydrodynamic processes is inevitable. The wind velocity will be a few times the escape velocity (approximately 0.1 c) and its kinetic energy comparable to the radiation luminosity of the central object. (The exact ratio is a free parameter in the model). The density in such winds is such that they are optically thick close to their centre and that a photosphere is defined, hiding the central object from direct observation and emitting strongly in the UV.

The outward pressure of the wind decreases with increasing radius, thus, provided the region is surrounded by a magnetic field B (expected to be of the order of a Gauss and a free parameter in the model), there exists a radius R_s where the

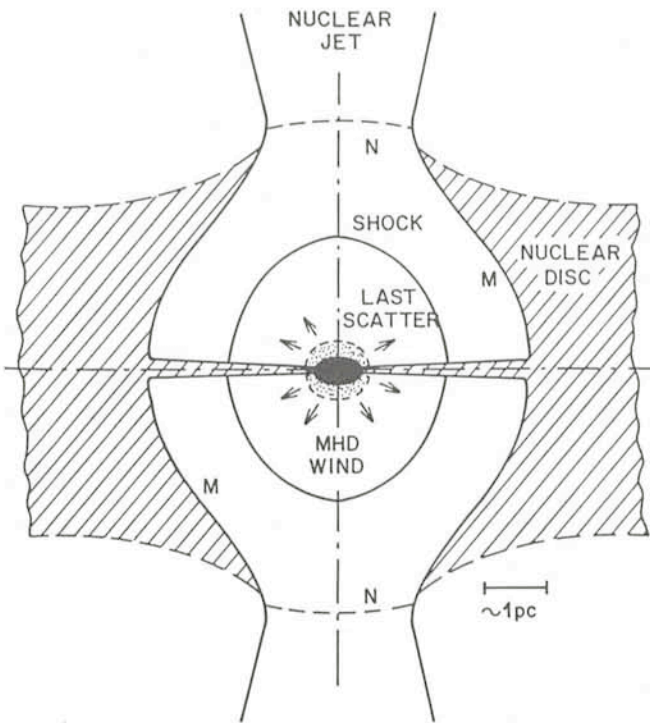


Fig. 1: Schematic (not to scale) representation of the main elements of the wind and shock model for active galactic nuclei. A suprathermal wind is accelerated from the central source to a few times the escape velocity and slowed down in a shock. The shocked region is the source of the non-thermal radiation and the BLR. Matter escapes in two collimated jets. The whole structure lies at the centre of the nuclear disk of the host galaxy.

wind is slowed down and its kinetic energy dissipated. This radius is determined by the equality of the magnetic confining pressure and wind pressure; it is of the order of 10^{18} cm for $B = 1$ G and $\dot{M} \sim 1 M_{\odot}/\text{year}$ (M_{\odot} is the mass of the sun).

The wind is stopped in a strong shock and its kinetic energy transferred to the shocked matter. This matter is heated to a very high temperature which is limited to some 10^9 K by electron-positron pair production. In addition, electron and positron pairs can be accelerated to highly relativistic energies in the shock, producing a power law energy distribution. Two properties of the hot matter are important here. The first is that

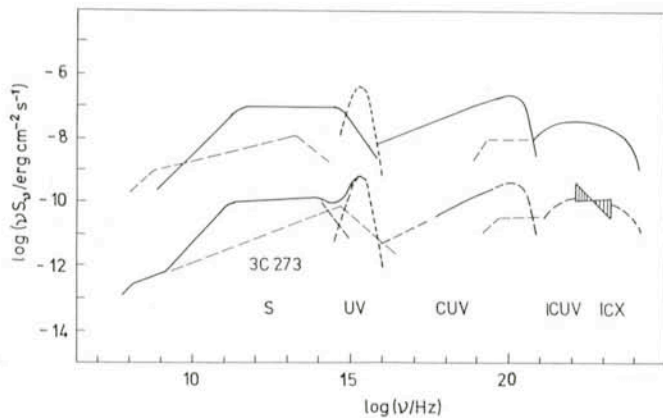


Fig. 2: Emission spectrum of the AGN as calculated in the wind and shock model (arbitrary scaling). Some observations of the QSO 3C 273 are shown for comparison in the lower part of the graph (solid lines). The figure is from Courvoisier and Camenzind, 1983, *Astrophys. and Space Sc.* **93**, 277, where the origin of the observations is quoted.

the electrons can cool by transferring energy to the UV photons (Comptonization), thus producing an X-ray power law spectrum. The second is that a second phase coexists with the hot matter which is cooler and denser ($T \sim 10^4$ K and $n \sim 10^9$ cm $^{-3}$). The matter in this second phase is ionized by the UV and X-ray radiation and cools by line radiation, forming the broad line region (BLR) of AGNs. The velocity characteristic of the BLR is given by the post shock velocity of approximately $\frac{1}{2}$ of the wind velocity or $0.025 c$ (7,500 km/s). The relativistic electrons and positrons moving in the magnetic field produce a power law synchrotron radiation in the IR and optical domains of the spectrum. They can also transfer energy to the softer photons by inverse Compton scattering and boost some photons to γ -ray energies.

The different components of the model are shown in Fig. 1 and a semi-quantitative comparison between the overall spectrum of 3C 273, calculated using the ideas presented here, and some observations is given in Fig. 2. Fig. 2 gives the energy radiated in each decade of frequency versus frequency. Region S (synchrotron) is the IR-optical part of the spectrum where the photons are emitted by relativistic electrons in the magnetic field; the UV part of the spectrum is a thermal black body of 26,000 K emitted at the photosphere of the central body; the CUV photons are emitted by thermal Comptonization of UV photons and the ICUV and ICX photons are emitted by inverse Compton scattering of the UV and X photons on the highly relativistic electrons and positrons.

Coordinated Observations of 3C 273

The observations used in Fig. 2 had not been performed simultaneously. 3C 273 is known to vary by factors of 2–3 in different spectral domains. Even though these variations are small compared to the flux differences in the different spectral domains (see Fig. 3), it is highly desirable to avoid uncertainties due to different observing epochs. This point will become more important as the calculations grow more detailed. In addition, the only way to observe causal relationships between the different physical components of a model (and hence to test the structure proposed by the model) is to study the correlations between temporal variations in the different spectral domains. For these reasons, it seems indispensable

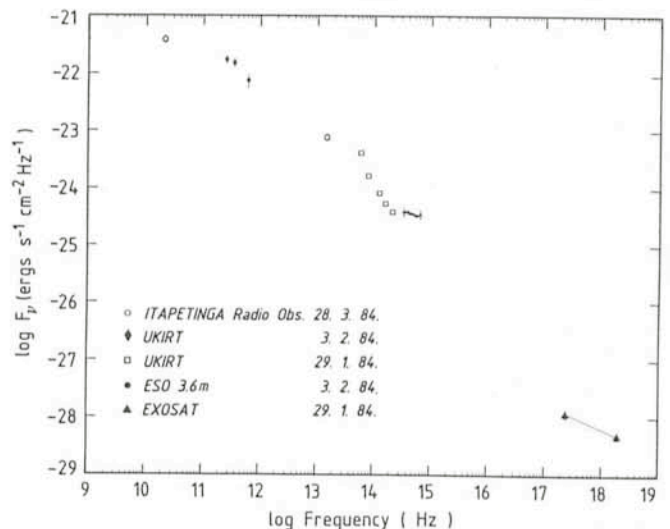


Fig. 3: The spectrum of 3C 273. Infrared to X-ray data were taken within a week at the beginning of February 1984. Radio observation was taken 2 months later. The cut-off in the IR power law at 10^{14} Hz is clearly seen, so is the thermal excess in the optical spectrum. X-ray data are from the Argon chamber of the EXOSAT ME detector.

to observe as large a part of the spectrum as possible quasi simultaneously with different instruments. Ideally, the process should be repeated regularly. The difficulties with this type of studies are the concentration of data from many different groups of workers and the necessity to know the absolute calibration of all the instruments involved.

The availability of the European X-ray satellite EXOSAT (2) since May 1983, and presumably until well into 1987, is an excellent opportunity to attempt several observations between the radio and X-ray ends of the spectrum. 3C 273 is an ideal candidate for this study since it is bright in all relevant wavebands. Several observations of 3C 273 have already been performed with EXOSAT (3) and it seemed useful to extend the observations to several other wavelengths.

We now have 2 quasi-simultaneous spectra of 3C 273 covering 8 decades in energy and separated by 5 months. We intend to continue this monitoring during the lifetime of EXOSAT. Two of the instruments on board EXOSAT can be used for these observations: the LE (low energy imaging telescope) and the ME (medium energy experiment). Spectral information using the LE is obtained by making observations through 3 (overlapping) filters between 0.1 and 2 keV. The Argon chamber of the ME gives the spectrum between 1 keV and 10 keV (the only data used in Fig. 3) and the Xenon chamber can be used to extend the spectrum to approximately 30 keV depending on the background during the observation.

A preliminary reduction of the data obtained in February is shown in Fig. 3. The components of the spectrum described above are clearly recognised: The IR-optical synchrotron emis-

sion described by a power law of index $\alpha = 0.76$ and steepening to $\alpha = 1.6$ at 10^{14} Hz, the thermal component in the optical spectrum (no UV data were available in February), and the comptonized X-ray spectrum of index $\alpha_x = 0.47$.

The data used in the compound spectrum of Fig. 3 are courtesy of D. Molteni, L. C. Botti, E. Scalise (Radio Observation); E. I. Robson, W. K. Gear, P. A. R. Ale (IR photometry); T. Courvoisier and K. Beuermann (Optical Spectrum) and M. Turner, T. Courvoisier, R. Staubert, D. Molteni and J. Trümper (X-ray Spectrum). The spectrum obtained in July includes (in addition to similar observations as in February) an IUE spectrum and a high energy X-ray measurement with which we hope to extend our energy coverage to 150 keV.

The two types of studies mentioned here, theoretical modelling and observations of overall spectrum of an object, give complementary information on the structure of an active galactic nucleus. The observations provide stringent tests and constraints for the proposed model, and the model provides a means of interpreting the measurements in terms of the physics involved in the nucleus. Once our understanding of a few well-studied objects has progressed significantly, it will be possible to use the acquired knowledge together with survey studies to describe the physical structure of active galactic nuclei in general.

References

- (1) M. Camenzind and T. J.-L. Courvoisier: 1983, *Ap. J.* **266**, L83.
- (2) B. G. Taylor, R. D. Andresen, A. Peacock and R. Zobl: 1981, *Space Science Reviews* **30**, 479.
- (3) M. Turner et al., in preparation.

The Sun and α Cen A

I. Furenlid and T. Meylan, Department of Physics and Astronomy, Georgia State University, Atlanta

The closest known star apart from the Sun is a very faint object called Proxima Centauri. The next closest star is Alpha Centauri or *Rigil Kentaurus* which forms a binary system having components designated as α Cen A and α Cen B. The component called α Cen A is of particular interest because it strongly resembles the Sun. As a matter of fact, it resembles the Sun to such an extent that it has been called a solar twin. Several researchers have taken a close look at α Cen A using different means in trying to find out exactly what its properties are. Photometry of an object as bright as α Cen A with a cooler component within 18 arcsec of angular distance may suffer from systematic errors. And analysing spectra of α Cen A is hard to do with sufficient accuracy.

The preliminary result reported here is based on a very strict comparison with the Sun. That means that we cannot give very accurate numbers for example for the temperature or chemical abundance of iron for α Cen A but we can report with considerable accuracy how much hotter α Cen A is than the Sun and how much higher its abundance of iron is.

A fortunate circumstance relating to this work is that a spectrum atlas of the Sun as a star, i.e. using light from the whole solar disk, has recently been prepared by Kurucz, Furenlid, Brault, and Testerman using the Fourier Transform Spectrometer at Kitt Peak National Observatory. The atlas (publication planned for the coming year) covers the wavelength range 3000 to 13000 Å. The resolution in the

visual part of the spectrum is around 500,000 and the signal-to-noise ratio typically 3,000. This unusually good spectrum provides the reference against which we compare the spectra of α Cen A, obtained at ESO with the CAT and Reticon detector. The ESO spectra are also of excellent quality, having a resolution of 100,000 and signal-to-noise ratio of around 500.

The preliminary analysis carried out so far was done in the following way. The solar spectrum was degraded to a resolution of 80,000, the continuum fitted, and a plot made on a uniform wavelength scale. The spectrum of α Cen A was given exactly the same treatment with particular emphasis on locating the continuum in a consistent way for both Sun and α Cen A. Around 25 absorption lines of iron were then selected and their equivalent widths measured. The lines were carefully chosen so that some of them originated at low energy levels and some at high levels while some of the lines are weak and some strong, and some of them arise from neutral iron and some from once ionized iron. By picking lines in this fashion we can assure high sensitivity to temperature effects, microturbulence, and pressure or surface gravity.

The data analysis made use of stellar model atmosphere programme ATLAS 6, kindly brought to us by its author, Dr. R. Kurucz. In an iterative process we varied temperature, surface gravity, and microturbulence for the solar data until all lines gave the same chemical abundance for iron. The requirement

that the deduced abundance be the same whether we use lines from neutral or ionized iron places tight constraints on the stellar model fit. It was rewarding to find the solar abundance of iron in the converged model to be 7.50 ± 0.15 on the logarithmic scale where hydrogen has the abundance 12.00, as the value 7.50 equals the best modern value. At this point we changed the oscillator strengths of all our lines so that the solar iron abundance for all lines became exactly 7.50. These adjusted atomic data were then used for the iterations of α Cen A so that temperature, surface gravity, microturbulence, and iron abundance of α Cen A would be strictly differential to the same parameters in the Sun.

The difference in effective temperature was found to be $+20^{\circ}\text{K} \pm 20^{\circ}$, surprisingly close to the Sun's value. The log of the surface gravity of α Cen A was found to be -0.1 ± 0.1 of the Sun's, pointing towards a somewhat smaller surface gravity than the Sun's. The microturbulence parameter emerges 0.2 km/sec smaller in α Cen A than in the Sun with an error of

± 0.2 . The only significant difference in this analysis between α Cen A and the Sun spectroscopically occurs in the abundance of iron. We find that α Cen A has an iron abundance 65 per cent larger than the Sun's.

We may summarize this preliminary result in the following way: α Cen A has almost exactly the same surface temperature as the Sun but has a diameter around 20 per cent larger. The star is known to have slightly larger mass than the Sun and is probably somewhat more evolved. The iron abundance is sufficiently different from the Sun's that in the full and final analysis we will have to consider the impact of a higher metal abundance on the atmospheric structure of α Cen A. Still the two stars are sufficiently similar in physical properties that we can expect a very accurate differential analysis. In the continuation of this project we are in particular looking forward to the comparison of the enrichment of iron with that of other chemical elements and groups of elements.

Roaming in the Sco OB 1 Association

A. Heske and H.J. Wendker, Hamburger Sternwarte, Hamburg, FRG

OB associations are usually thought to be the youngest stars in a space volume infected by the virus of star formation. The combined effects of strong UV radiation and stellar winds quickly disperse the parent interstellar cloud and thus end the star formation episode. Details of this picture are, however, subject to debate, especially such questions as when, where and how long which types of stars are formed within the parent

cloud. Only a vast amount of observations on as many associations and young open clusters as possible will allow us to draw final conclusions.

During a perusal of the literature on this subject we were struck by several discrepancies which are related to the well-known association Sco OB 1 and several open clusters and an HII region in the same area, e. g. NGC 6231, Tr 24, IC 4628, etc.

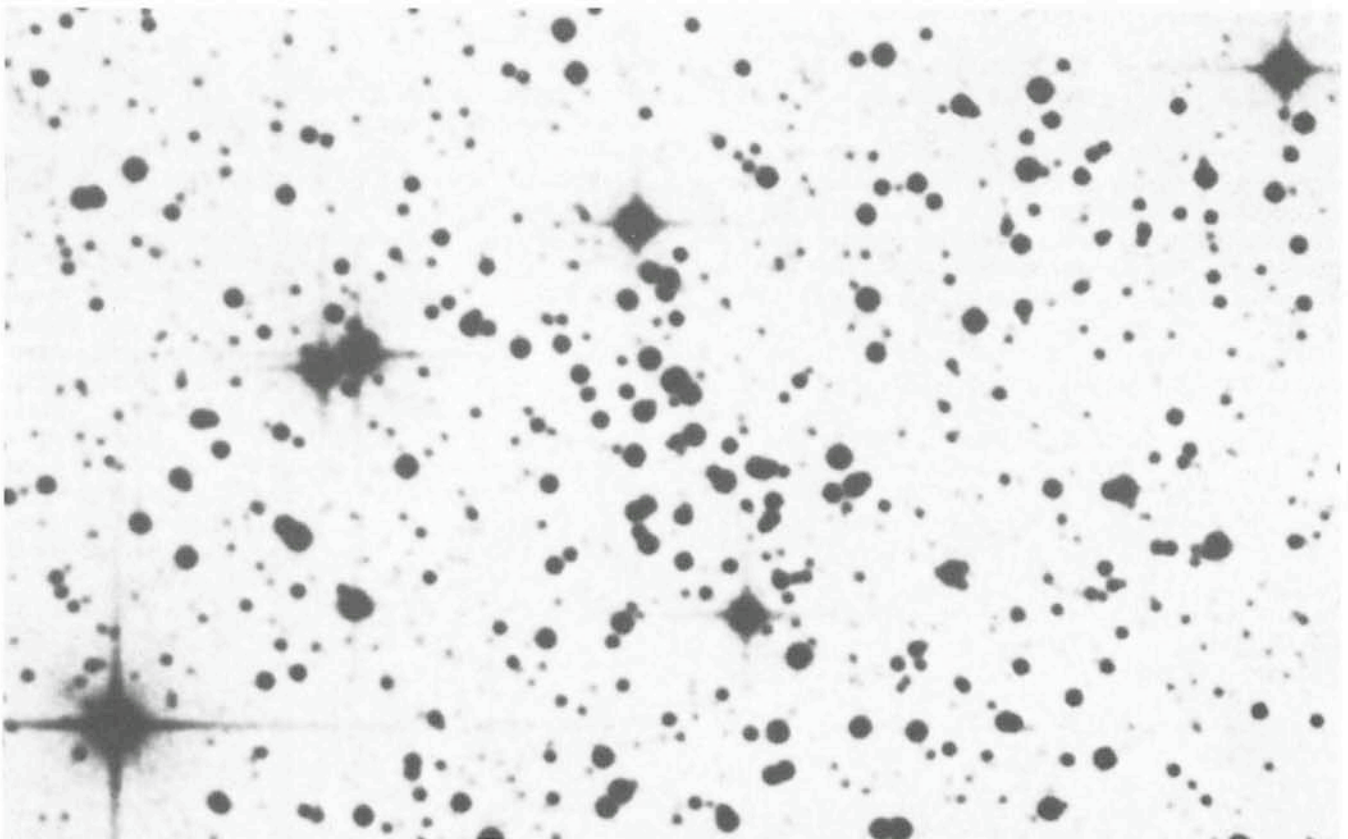


Fig. 1: The "concentration" in Tr 24. Its angular extent is about $12' \times 4'$ and its centre coordinates are roughly $16^{\text{h}}51^{\text{m}}6^{\text{s}}-40^{\circ}8'$. The bright star at lower left is SAO 227443. (Enlargement from the ESO B Sky Survey.)

Among these are a difference in individual distance of Sco OB 1 (2,400 pc) and its alleged core NGC 6231 (1,600 pc), the very peculiar appearance of Tr 24 which seems to contain substructure at different distances in between, and the distribution of the youngest (O-type) stars in a half-ring, with Tr 24 proper in its vertex. Even basic photometric data were missing for most stars fainter than 9^m , except for the well-defined compact open clusters (e.g. NGC 6231) and the brighter OB stars of the association. Thus we obtained observing time in June 1983 for basic, but otherwise unspectacular UBV photoelectric photometry in the area of $1^\circ.3 \times 0^\circ.3$ between NGC 6231 and IC 4628, covering all the apparent substructure of Tr 24. The weather did not permit observations for stars fainter than 14^m with the 1 m telescope. In the range 9^m to 14^m good data were obtained for 288 stars with the Bochum 0.61 m. When we plotted the results in the standard colour-magnitude and colour-colour-diagram we were astonished to find that the stars strewn over such a large area gave one single, well-defined cluster diagram with a reddening of $A_v = 1^m.1$ and a distance of $d = 2,300$ pc. When we then plotted the published data on the stars of the OB association we found a perfect fit in the sense that these stars are a smooth extension to higher absolute magnitudes. We thus concluded that Tr 24 and Sco OB 1 are to be regarded as one giant cluster stretching over roughly 40 pc. The stars which previously defined the association are just those which have left or are leaving the main sequence. A further conclusion seems unavoidable, namely that NGC 6231 is a foreground open cluster albeit of similar youth (age less than 10^7 years). (These results are presently being published in *Astronomy and Astrophysics, Suppl.*)

At later spectral types (A, F) we also found that there are many stars which have apparently not yet reached the main sequence, some of them up to 3^m above it. About one third of our programme stars can be found there distributed all over the cluster area. Here we found another surprise, namely that about 20 of them are clustered in a small area. Such a concentration of pre-main sequence stars is rather unusual, especially as only one true pre-main-sequence star was found in this area. Fig. 1 shows this field (an enlargement from the ESO atlas). The linear extent of the clustering is 8×3 pc. Subject to verification, we dared to regard this configuration as a spatial association of pre-main-sequence stars. In fact, one would expect them to be some sort of RW Aur variables.

Therefore, we again requested observing time for May 1984 with four objectives: first to complete the photometry in the range 9^m to 14^m in a slightly larger area than the year before,

second to test many suspected pre-main-sequence stars for variability, third to obtain photometry for stars fainter than 14^m especially in and around the "concentration", and fourth to observe spectra of all stars in the concentration and a number of the alleged pre-main-sequence stars in its neighbourhood. For objectives 1 and 2 we were again scheduled on the 0.61 m Bochum telescope, for objective 4 on the 1.5 m with IDS and for objective 3 again on the 1 m telescope. As in 1983, the weather again prevented all observations with the 1 m telescope.

We have just finished the data reduction with the help of the standard programmes in Garching. The interpretation is thus very preliminary. First of all, the extension in area contains relatively less cluster stars, which, we think, indicates that the boundary is reached. The linear extent is thus between 40 to 50 pc and we would rather call it a stellar supercluster. Second, most of the suspected pre-main-sequence stars are variable (between 1983 and 1984) a fact which one expects for such stars. The variability ranges up to half a magnitude.

If our assumption is right, namely that all cluster stars which are more than 1^m above the main sequence are genuine pre-main-sequence stars, one should expect them having intermediate spectra between those of normal dwarfs and T Tau stars which are the text book pre-main-sequence stars showing a large number of emission features. Our survey type spectroscopy in a wavelength range 4000 to 5000 Å indeed shows emission line features in almost all spectra but mostly fainter than in genuine T Tau stars. One of these spectra is shown in Fig. 2. Star No. 230 is a star just north of the area of Fig. 1. The iron emission features at 4506 Å and 4722 Å are faint but clearly visible. Together with the asymmetric Balmer lines of hydrogen, they are typical for T Tau, RW Aur and other pre-main-sequence stars.

Although we yet have to analyse all 64 spectra, we are still optimistic that we can prove our hypothesis for the "concentration", namely that it is a rather small volume in space of $8 \times 3 \times 5$ pc containing about 2 dozen stars which have not yet reached the main sequence. We furtheron speculate that these stars are born together in this volume from one and the same filament of the parent molecular cloud. From stellar evolution tracks one would expect that they will be main-sequence stars of late B and early A type (3–5 solar masses). As the contraction time for this mass range is around 10^6 years they are definitely younger than the stars which presently leave the main sequence (about 10^7 years).

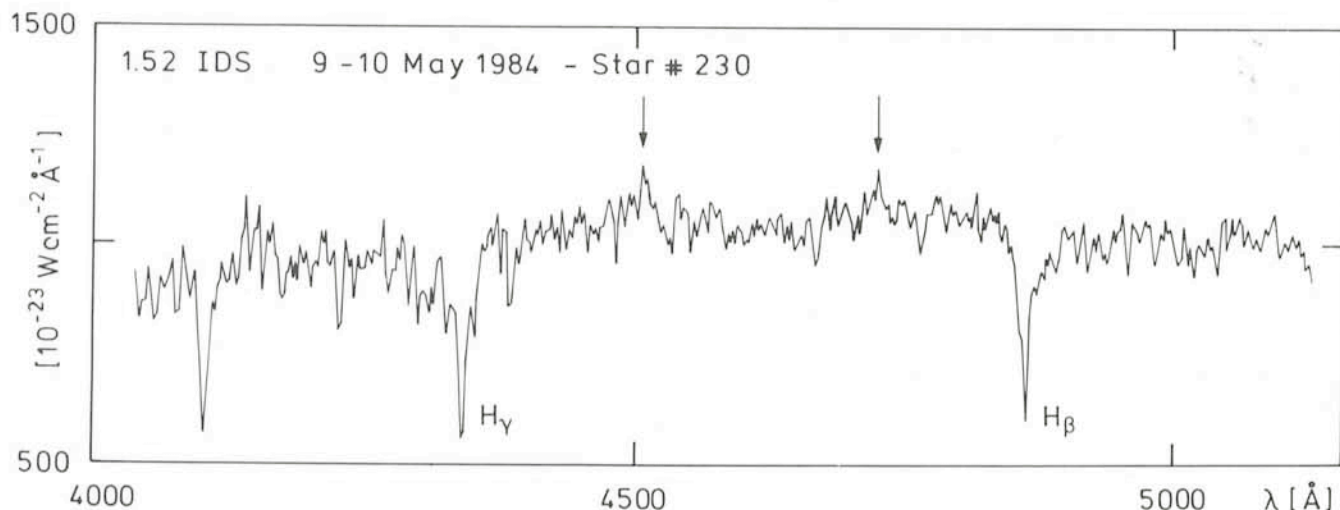


Fig. 2: A sample spectrum of our survey of pre-main-sequence stars. The most prominent emission features are indicated by arrows. The star number is from our working list. (V -magnitude about $11^m.6$). It is situated just north of the field shown in Fig. 1.

Data Saving and Banking at La Silla

S. Vidal, ESO

The main job of the computer operator is organizing and saving the data acquired with all telescopes operating at La Silla in a magnetic tape bank. A short description of his duties and of the standardized procedures is given here intending to make them widely known.

But first a few words regarding ESO rules on this subject:

- Although the observers have the right to keep their data as personal property, they are of course encouraged to hand over their tapes so that they can be banked by the operators.
- All data (saved in the La Silla bank) obtained by any astronomer may only be used by another astronomer if the latter has a written consent of the observer.
- All data saved (bank tapes as well as the copies left as backup at the computer centre) are presently kept indefinitely. New guidelines about the future of the data bank may however restrict this period to e.g. two years. It must be emphasized that the medium now in use for banking (magnetic tapes) under the existing physical conditions (i. e. temperature and humidity) does not guarantee a lifetime exceeding a few years.
- Tape copies taken home by the observers are ESO property and are therefore expected to be back at La Silla or the ESO Headquarters at Garching within 6 months after borrowing them from the Observatory.
- Although the data saving is the operators' duty, the observers share the responsibility for a good saving: they have to use the right day-of-the-week magtape, fill in the labels properly, put tapes in the DATA TAPES mailbox (hotel), request for additional data handling and final tape copies (when needed) well in advance, etc.
- Top priority for the operator's activity as well as for the computer centre resources goes to the daily saving and banking of data. For other common computing services requested, priority is stated by the system manager, or, in his absence, by the operator on duty himself.

General Comments

Although optical disk devices are seriously being considered, magnetic tapes are still used at La Silla as the standard mass data storage. Attention has to be drawn however to a few weaknesses of this medium, in order to improve the integrity of recorded data:

- Magnetic tapes should be kept far from magnetic or any other radiation. We often find tapes on top of, or near to, the terminals or its peripherals. Recorded data might be destroyed within a magnetic field stronger than 50 oersted.
- Sequential access mode of big magnetic tapes is time-consuming and rather tedious, whereas, on the other hand, banking onto small tapes results in waste of physical space and tapes.
- Temperature is a big destroyer of data or even physically of tapes. Long exposure to sunlight in a car caused almost melting of a mag-tape containing a three nights observing run of IDS some years ago. Of course, there was no way to retrieve these data because banking was not running yet and the tape went straight to the trash. Most manufacturers specify environmental ranges between 10°C to 40°C while operating and between -20°C to 65°C in non-operating conditions. Ideal temperatures are in the range 15 to 25 degrees Celsius.

- For long-term banking of data, a dust free operating atmosphere has to be considered since the efficiency of reading and writing magnetic tapes is affected by dust.
- Some other parameters also play a minor role. Among these: relative humidity, atmospheric pressure, physical orientation, etc.

All of these points call for an ideal solution since one cannot take these magnetic bank tapes to the bottom of the cellar, for they will be used from time to time in retrieval of old files. From my side I would say that a well-organized metallic cupboard not too far from the magnetic tape drives, within the special environment of the computer rooms, would make a good "freezer" for those data intended to be kept as long as possible. Tapes coming with hanging plastic rings would do better, if the cupboards were permanently closed to dust, because of space limitations for big libraries.

Two main types of data are found among the various acquisition systems and instruments in use at La Silla: Image data files in IHAP format from CCD, IDS, CES, CASPEC, EFOSC, etc., and photoelectric photometry files; each of these banked separately. Other types, listed according to the amount of data already stored are: Infrared photometry, Fast photometry, Walraven and Exorset photometries, Polarimetry, Coravel (1) measures, etc. . . . Walraven's name stands for a special photometer in use at the Dutch 92 cm telescope, whereas Exorset stands for acquisition and control programmes running on a Motorola 6809 microprocessor installed at the Danish 50 cm telescope which outputs data on floppy disk.

Procedure

At every telescope there are wooden racks containing a "day-of-the-week" set of magnetic tapes with labels to be filled in by the observer, they are intended to keep the original data acquired for at least a week or, usually, an entire observing run. The labels inform the operators about the data of the night (or day). Two "scratch" tapes are also provided for possible breakdowns of the computer and missing EOF marks after the last output of data.

Any suspected abnormal recording must be reported on written labels to operators. Valid data have been unconsciously overwritten and lost for they were not properly labelled.

All tapes (and other data media used) are taken from the DATA TAPES mailbox at the hotel to the computer centre by morning. After banking of the data these tapes are taken back to the telescopes, on the same day if possible, for they might be used for off-line reduction.

Image Data

Since there are no IHAP facilities at the computer centre, three image data banks are handled with the RTE-IVB system operating the ESO 1.52 m telescope in the 3rd floor terminal and banktapes kept there. While the direct CCD image bank from the ESO/MPI 2.2 m telescope is kept at the VAX/750 room in the 3.6 m telescope for off-line reduction facilities, the CCD image bank coming from the Danish 1.54 is being kept in the same building and all other image banks are kept at the computer centre. Banking image data is being organized chronologically since December 1st, 1983, when S. Vidal and R. Arancibia (current computer operators) took over all data

saving and banking at La Silla. Any service concerning data previous to that may lack of promptness due to a kind of chaos in former organization, but well-detailed requests could still be filled out. Two database packages are actually running at the computer centre for the direct CCD imagery from the Danish 1.54 m and the 2.2 m telescopes which allow fast disk access to these banks. Though the trend on handling images is to have them all in database, we lack of disk space, so far, to manage many data banks. On the other hand, the images along with the fast photometry have more than doubled the output from the telescopes in yearly terms, so that we deserve a little more computing power and much more space, I think.

Usually all data from the past night of an observer are entered and added to his copy tape. No "cleaning" of datafiles or purging files like Rasters, Sweeps and calibrations (SP files) are allowed as it was before (i.e. all data are saved as they come from the telescope). Careful track of the number of saved files follows up, paying attention to the date when observers change at each telescope. Each observer receives, on request, a magnetic tape copy of his data as well as any other computer service (print-outs, FITS (2) copies, etc. . .).

Photometric Data

Rather than assuring telescope and instrument control, chief use of the computers nowadays, the first computers arriving on La Silla around 1972 were meant to acquire and handle photometric data. Astronomers used to spend much time patching and winding long streams of broken papertape in bare hands. I developed myself a great skill handling big rolls, even reading with the naked eye (not at the photoreader's speed, for sure) its data coded in holes, at telescopes first and within a damned cold dome later when the first computer centre on the mountain was born by 1974.

A photometer can be appended to almost every telescope on the mountain (exception made of the Schmidt, CAT and GPO), resulting in a big amount of photometric data acquired since the advent of astronomical observations at La Silla. No data banks are possible for photometric observations, due to a wide variety of photometric systems. All measures, except those in the infrared and the so-called fast photometry,

are saved as individual banks under the observer's name and stored in cupboards by telescope. These small banks are, so far, using almost half of the total amount of magnetic tapes. I must stress that such a tape consumption is due to the ASCII format in which these data are recorded, thus making them easier to read.

Future Trends

Some experiments in data transmission via modem and microwaves were successfully carried out last June with direct images between a telescope at La Silla and a computer terminal at La Serena aiming at further remote control of telescopes and instruments from overseas in a near future; they might also be useful for remote data handling. One may expect these results to alleviate a bit the data banking on the mountain (sometimes ten telescopes are sending daily tapes to the computer centre). Yet I foresee a strong increase of output data because new telescopes will still be erected on the site.

Conclusion

We all at La Silla do our best to save the astronomical data and make them readily available for further use.

Software optimization of data banking, i.e. formatting, procedures, database packages, etc., will not reach a real efficiency in managing the forthcoming amount of data if we keep as mass data storage media the slowly accessed magnetic tapes.

Although we intend to make the few procedures described here as standardized as possible, something will always be left out, because the observing programmes, the acquisition systems, the handling environment, the human behaviour and astronomy itself are, as ever, dynamically unstable.

References

- (1) Imbert, M., and Prévot, L., 1981, *The Messenger* **25**, 6.
- (2) Wells, D.C., and Greisen, E.W., 1979, in *Image Processing in Astronomy*, Ed. G. Sedmak, M. Capaccioli, R.S. Allen, Osservatorio Astronomico di Trieste.

Two Bok Globules with Active Star Formation

Bo Reipurth, Copenhagen University Observatory

A number of studies of Bok globules have in the past few years been done at La Silla, mainly with a view to understand how such globules originate and what relation they have to the formation of stars. Bok globules are tiny, very dense, dark clouds composed mainly of molecules and dust, and they are cold rather quiescent structures. Recent work suggests that globules initially are formed as dense condensations, or cores, in large, less dense molecular clouds. The birth of massive OB stars in the neighbourhood of such a large cloud with the subsequent flood of ultraviolet radiation may seriously disrupt the cloud, stripping the cloud cores and leaving them after a compression as isolated Bok globules. In the process, stars may form in or at the edge of the globules. Studies of many southern globules from La Silla have revealed that quite a number of them are associated with various signposts of star formation, such as infrared sources, H α emission stars or

Herbig-Haro objects. Two rather spectacular cases are presented here.

The Horsehead: Birth of a Globule

One of the most famous objects in the sky, widely known from innumerable photos in books and magazines, is the Horsehead. In marked contrast to the celebrity of this object among amateur astronomers and laypersons, professional astronomers have paid it scant attention. However, this lack of interest is not well deserved, because, as it turns out, the Horsehead is in several ways a very remarkable object.

The Horsehead is a Bok globule which is just now in the process of appearing from a large parental dark cloud, known as L 1630. This cloud was once much larger, but the birth of a multiple trapezium-like system of luminous OB stars, σ Orionis

A–E, have had a major influence on the whole region. Today the front of the L 1630 cloud is receding, because the ultraviolet radiation from the young OB stars ionize the outer layers of the cloud, producing an HII region which expands and carries away the evaporated material. The much denser Horsehead was initially embedded as a cloud core in the

L 1630 cloud. It is now being exposed and compressed, but because of its higher density it better withstands the eroding effects of the ultraviolet radiation.

Fig. 1 shows the Horsehead in a reproduction, specially processed by C. Madsen, ESO, of a Gascoigne plate taken by S. Laustsen with the 3.6 m telescope. The sharpness of the



Fig. 1: This photo of the Horsehead nebula was obtained by Dr. S. Laustsen using the 3.6 m telescope with the Gascoigne corrector. The 103a-E plate was exposed 60 min behind a GG 495 filter. The print was obtained by contrast enhancing a masked derivative of the original plate.

right (western) side of the Horsehead is remarkable, and derives from the powerful influence of σ Orionis, which is far outside the right edge of the photo. What gives the Horsehead its name is mainly a luminous feature which forms the "jaw". Deep CCD images obtained with the Danish 1.5 m telescope at La Silla have revealed that the "jaw" is really a large flow-region, where matter is blown away from a newborn star in a highly collimated flow. Radio observations at millimetre wavelengths have in recent years revealed several regions of outflowing material around young stars, often aligned in two oppositely directed jets. A few optically visible jets have also been found, and the one in the Horsehead is a particularly fine example. The young star responsible for this activity can be seen in Fig. 1 at the base of the jet as an optically very faint star. P. Bouchet, ESO, has made near-infrared photometry of this star with the 3.6 m telescope at La Silla, and found it to be much brighter in the infrared than in visible light. The study of such violent phenomena in young stars is very new, and so far no consensus has been reached on the driving processes. However, there is some observational and theoretical evidence that a star recently born in the centre of a slowly rotating disk of molecular material may undergo eruptions when material from the disk accretes onto the star. During these violent flare-ups material may be driven away from the star and guided into oppositely directed jets by the surrounding disk. There could therefore, at least in principle, be a counter-jet in the Horsehead, burrowing into its denser regions, and thus not visible.

Another young star has been born in the Horsehead, in its upper right-hand (north-western) corner. Here a small nebulosity is visible, and CCD images have revealed a faint star half embedded at the bottom of a nebulous cavity. This star has also been observed in the infrared by P. Bouchet, who found it to be a bright infrared source. A few other regions in the Horsehead could also be due to newborn stars; one is a large indented cavity in the northern edge, another is around some structured reflection nebulosity in the southern part.

The Horsehead is thus a newborn Bok globule actively forming stars (probably of low mass), and it appears likely that this activity was triggered by the same processes which are presently excavating it from its parental cloud. Further optical and infrared data supplemented with millimetre observations are now being collected to study how widespread star formation is in this region.

NGC 5367: Demise of a Globule

A globule which has been excavated from a large dark cloud may sometimes be given only a short lease of life. This is so because the OB stars which liberate the globule may also contribute to its destruction. Firstly, the ultraviolet radiation bathing a globule makes a very hostile environment. Secondly, if star formation is triggered in the globule, winds and radiation from the young stars can make significant erosion. And thirdly, if one of the luminous OB stars in the neighbourhood is among the rare, very massive stars, it will after a rather brief evolution become a supernova, and any globules in the region will be run over by a blast wave.

NGC 5367 is a tiny cluster of nebulous stars embedded in the head of the very large cometary globule CG 12. This globule appears to have suffered from all the above-mentioned destructive forces, and may not live for very long. Fig. 2 is an enlargement, also specially processed by C. Madsen, ESO, from a deep ESO Schmidt plate taken by H.-E. Schuster. The globule itself is embedded in the dense bright rims in the front of the cometary object. The tail is about 10 pc long, and shows much structure, partly along the flow direction and partly around obstructions in the flow.

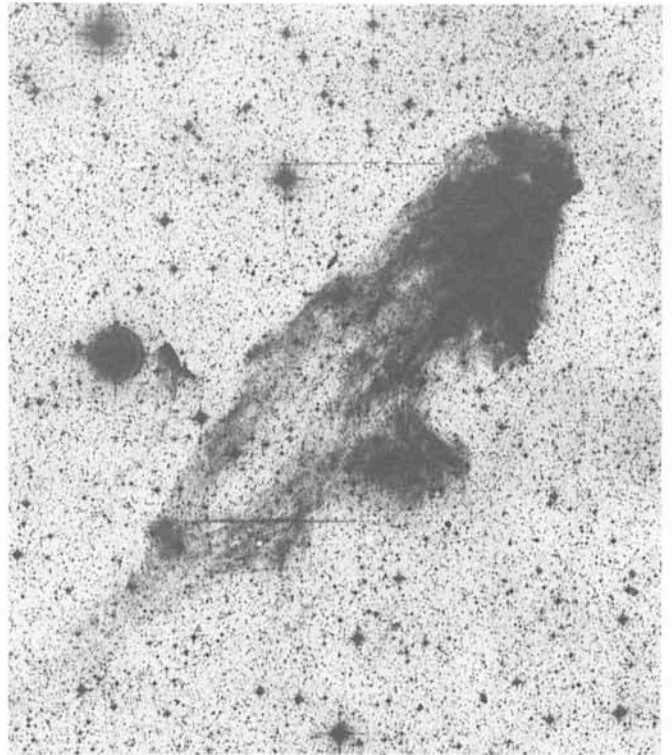


Fig. 2: This photo of NGC 5367 was made by subjecting a standard ESO Schmidt plate (ERS 325) to diffuse light amplification.

The stars in the globule have been studied by several authors, and lately optical and infrared photometry, IDS spectra and CCD images have been obtained at La Silla, and supplemented with IUE spectra. At least 6 stars are associated with the globule. Most prominent is the close visual binary Herschel 4636, consisting of two late B stars, one with and one without $H\alpha$ emission. Three other late B and early A stars are associated with the globule, and an infrared source is embedded in the globule.

It is evident that some outside force has influenced the globule and caused the extraordinary tail structure. There are no obvious OB stars in the direction opposite the tail, but previous investigators found that there is an H I loop, towards the centre of which the globule is pointing. It appears that a very massive star has exploded as a supernova, and a shock wave has passed over the globule. The combined effects of first a luminous OB star, then a supernova explosion, and now a handful of embedded stars will most probably in the end lead to the destruction of the original globule.

The full details of the results mentioned here will appear in articles in *Astronomy and Astrophysics*.

List of Preprints Published at ESO Scientific Group

June – August 1984

327. M.-H. Demoulin-Ulrich, H.R. Butcher and A. Boksenberg: Extended Gaseous Emission in Normal Elliptical Galaxies. *Astronomical Journal*. June 1984.
328. G. Gavazzi, M. Tarengi, W. Jaffe, H. Butcher and A. Boksenberg: Radio and Optical Investigation of UGC 6697 in Abell 1367. *Astronomy and Astrophysics*. June 1984.

329. P.A. Shaver: Clustering at High Redshifts. To appear in "Inner Space/Outer Space", proceedings of a conference held at Fermilab, 2-5 May 1984 (University of Chicago Press. June 1984).
330. M.-P. Véron-Cetty: Study of a Complete Sample of Galaxies. I. UBV Aperture Photometry. *Astronomy and Astrophysics Suppl.* June 1984.
331. B. Reipurth and P. Bouchet: Star Formation in Bok Globules and Low-Mass Clouds. II. A Collimated Flow in the Horsehead. *Astronomy and Astrophysics, Letters.* July 1984.
332. B. Barbanis: The Stochastic Behaviour of a Galactic Model Dynamical System. *Celestial Mechanics.* July 1984.
333. L. Maraschi et al.: Coordinated UV and Optical Observations of the AM-Her Object E 1405-451 in High and Low State. *Astrophysical Journal.* July 1984.
334. E.A. Valentijn and A.F.M. Moorwood: The Stellar Content of the A 496 cD Galaxy. *Astronomy and Astrophysics.* July 1984.
335. A.C. Danks and J. Materne: The Galaxy Group Klemola 25. *Astronomy and Astrophysics.* July 1984.
336. S.R. Federman, A.C. Danks and D.L. Lambert: The CN Radical in Diffuse Interstellar Clouds. *Astrophysical Journal.* July 1984.
337. S. D'Odorico, R.G. Gratton and D. Ponz: A High Dispersion Analysis of a Giant Star in 47 Tucanae. *Astronomy and Astrophysics.* August 1984.
338. F. Matteucci and A. Tornambé: Carbon Deflagrating Supernovae and the Chemical History of the Solar Neighbourhood. *Astronomy and Astrophysics.* August 1984.
339. C. Barbieri, S. Cristiani, S. Omizzolo and G. Romano: The Variable Extragalactic Object 3C 446. *Astronomy and Astrophysics.* August 1984.

Rotation Axes of Gas and Stars in Elliptical Galaxies

D. Bettoni, Padova Astronomical Observatory, Italy

Recent studies (1, 2) of the distribution and kinematics of gas in elliptical galaxies have revealed that in most cases there is no correlation between the position angle of the major axis of the gas and that of the stellar isophotes. In addition, a decoupling is present in the kinematical axes of these components, in that the kinematical major axes of gas and stars do not coincide.

But until now a comparative study of gaseous and stellar dynamics has been made for only very few of these systems; in the past only the stellar or only the gaseous dynamics have been studied in detail. In order to extend this study to a wider sample of objects, it is necessary to have simultaneously the kinematical properties of both gas and stars.

For this purpose we started observations in March and in May 1983 and in March 1984 with the image tube + B & C spectrograph attached to the 1.52 m and 3.6 m ESO telescopes with dispersion of 29 and 39 Å/mm, in order to obtain a complete velocity field for 6 elliptical galaxies, listed in Table 1.

the line strength γ for each position angle (P.A.) observed. The emission lines were measured with the ESO Grant machine and the data were reduced at the Padova Observatory computer centre. An additional measurement of redshift and FWHM of emission lines has been performed by using a non interactive batch IHAP programme, the result being in good agreement with the Grant measurements.

In Table 1 we list the galaxies observed, their morphological characteristics (3) and the distances, obtained from the redshift, assuming $H_0 = 50 \text{ km sec}^{-1} \text{ Mpc}^{-1}$. We report also the dynamical behaviour, i.e. the position angle of maximum rotation, for stars and gas, estimated by means of cosinusoidal interpolation of the central velocity gradients versus P.A., and the value of V_m/σ_0 observed for the central regions. The error in the P.A. of the line of nodes obtained by this procedure is about 10° . All the galaxies follow with little scatter the $L \propto \sigma^4$ (4) and the $\log(V_m/\sigma_0)$ vs M_B (5) relations for elliptical galaxies.

Despite these common morphological and kinematical properties, the galaxies considered show many differences concerning the internal dynamics of gas and stars. All but one case show that gas and stars have different rotation axes, which in most cases are nearly perpendicular.

NGC 2974 is the only galaxy in which gas and stars share the same velocity trend along all the position angles observed. In Fig. 1 a, b are shown the rotation curves along the major and minor axis respectively. The gas seems to be in a disk with the line of nodes coincident with the major axis of the stellar component, in agreement with previous observations (2). The same behaviour is exhibited by the stars. The representative point of NGC 2974 in the V_m/σ_0 - ϵ diagram falls exactly on the line of oblate isotropic rotation, a fact which, together with the previously cited gas and stars spin axes alignment, implies that this galaxy is very similar to a fast spinning disk of stars.

NGC 5077, on the other hand, is a system where the stars do not show appreciable rotation, while the gas, more extended along the apparent minor axis of the galaxy, shows along this axis a well defined rotation curve (Fig. 2 a, b). This behaviour resembles the visible configuration observed in NGC 5128, where the dust lane represents a disk rapidly rotating with the spin axis aligned with the major axis of the stellar body (6).

This interpretation is confirmed by the low value of V_m/σ_0 for the stars which places this bright galaxy ($M = -21.1$) among the low rotators and well down the predicted line of prolate figures. These two properties suggest that this galaxy repre-

TABLE 1

NGC	Type	M_B	P.A. kin. maj. axis		σ_0	V_m/σ_0
			Stars	Gas	(Km sec ⁻¹)	
2325	E4	-21.01	6° (maj. ax.)	-	181 ± 12	0.31
2974	E4	-21.01	45° (maj. ax.)	45° (maj. ax.)	221 ± 30	0.83
3962	E1	-20.91	0° (maj. ax.)	90° (min. ax.)	240 ± 50	0.27
5077	E3 +	-21.05	7°? (maj. ax.)	97° (min. ax.)	307 ± 50	0.095
5846	EO +	-21.22	4°?	90°	244 ± 26	0.25
5898	EO	-20.54	150°	150°	174 ± 40	0.3

The spectra were digitized with the ESO PDS microdensitometer with an aperture of $12.5 \mu \times 50 \mu$. All the spectra were calibrated in intensity and wavelength using the IHAP system of Garching. All the calibrated spectra were finally analysed with the Fourier Quotient Method of the Padova Observatory computer centre in the spectral range $\lambda \lambda 3900-4500 \text{ \AA}$. This method allowed us to obtain simultaneously the radial velocity V_r , the velocity dispersion σ and

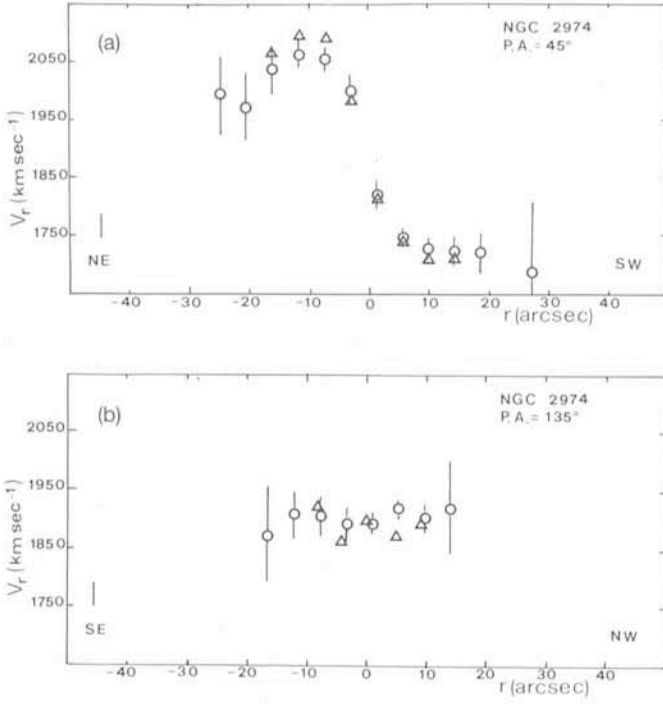


Fig. 1: Rotation curves of NGC 2974 along the major (a) and minor (b) axes for gas (Δ) and stars (\circ). The error bars for the rotation curve of the stars are from the Fourier Quotient Method. The mean error for the Grant measurements of emission lines (30 km sec^{-1}), is indicated by a bar at the lower left of the diagrams. (The data are from two $60''$ exposure spectra from the ESO 1.5 m telescope.)

sents a case in which the gas disk, even though not obscuring the stellar body, lies in the equatorial plane of a prolate or almost prolate galaxy.

NGC 3962 is rounder than NGC 5077 but shows the same kinematical characteristics. The stars have the maximum velocity gradient along the apparent major axis while the gas, also in agreement with previous observations (2), reaches the maximum rotation along an axis which is nearer to the optical minor axis. This fact, together with the low value of V_m/σ_0 , suggests, again like NGC 5077, that the gravitational potential in NGC 3962 is nearly prolate.

In the flattened galaxy NGC 2325 (E4) the stars do not seem to rotate appreciably, although a slight tendency to rotation appears along the apparent major axis. On the contrary, no rotation is detected for the gas in the two P.A. studied (major and minor axis). Since we expect that, because of dissipational processes, the gas lies in a flattened disk, the absence of rotation within $|\Delta V| = 50 \text{ km sec}^{-1}$, suggests that we are viewing the gas disk almost face-on.

The two remaining galaxies are both of EO type, but from the comparison of gas and stellar kinematics we can deduce that we are looking at two very different systems.

Our data, together with that of Ulrich et al. (2), suggest that the disk of gas in NGC 5846 is rotating along P.A. = 90° . For the stellar component our data, together with that of Peterson (7), suggest that a small velocity gradient could be present along P.A. = 4° , again a case in which stars and gas reach the maximum rotation along axes which are nearly perpendicular. In that galaxy it is also interesting to note that the velocity dispersion profile shows a strong decrease with radius. The low value of V_m/σ_0 is not surprising if this galaxy is an axisymmetric system seen near to, but not exactly along, the symmetry axis (prolate or oblate). In both cases the rotation cannot be stable and the stellar gradient represents only the projection of the rotation along the line of nodes.

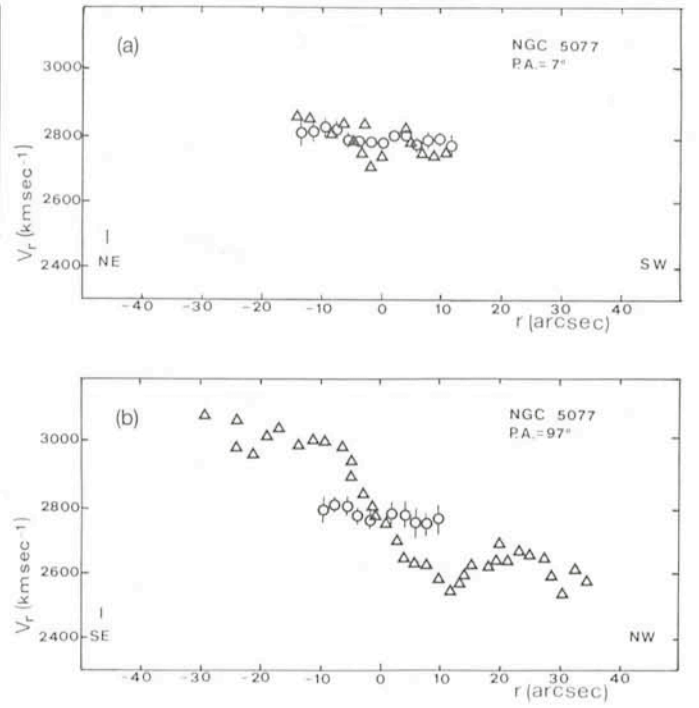


Fig. 2: Same as Fig. 1 but for NGC 5077 along the major (a) and minor (b) axis. (The data are from two $90''$ exposure spectra from the ESO 3.6 m telescope.)

The other galaxy, NGC 5898, was selected from the list of objects in which Caldwell (8) recently indicated the presence of emission lines in the central regions. Stars and gas show the maximum velocity gradient along nearly the same position angle but they are rotating in opposite senses. Again these properties could be explained if the gas had been acquired from the external regions and has not yet settled to a stable configuration.

In this small sample of elliptical galaxies with nuclear emission lines, we are surprised to detect so great a difference in the dynamics of gas and stars. The fact that in most cases there is no correlation between stellar and gaseous kinematical axes strongly suggests that the gas has been acquired from outside. In this hypothesis, if the mass of gas is negligible with respect to the total galaxy mass, its motion will be determined by the gravitational potential of the stellar body only. We know that the rotation axis of the gas disk spinning within an ellipsoidal potential should align, in a short time scale, with one of the principal axes of the ellipsoid. Different configurations are expected as the galaxy tends to be more prolate or oblate. In the first case the rotation axis coincides with the major one while in the second case it aligns with the minor axis. In the more general case of a triaxial ellipsoid the spin axis could align with the major or minor axis of the configuration depending on the infall angle within the system. Then the relative positions of the gas and stars rotation axes are different for different galaxy shapes.

The wide variety of orientations found leaves open the possibility, in the light of recent theoretical work, that all of the intrinsic shapes are possible. In fact the coincidence of gas and stars kinematical position angles in NGC 2974 suggests that in this galaxy the potential is nearly oblate. On the contrary the case of NGC 5077 cannot be interpreted in this way but is better understood as an almost prolate system.

These are two extreme cases but from these results we learn that the study of the properties of the gas in elliptical galaxies is important not only to understand its origin, but also as a new

interesting way for the comprehension of the intrinsic structure of elliptical galaxies.

References

- (1) Bertola, F., Bettoni, D., Rusconi, L. and Sedmak, G., 1984, *A. J.*, **89**, 356.
- (2) Ulrich, M.H., Butcher, H. and Boksenberg, A., 1984, ESO Preprint No. 327.
- (3) de Vaucouleurs, G., de Vaucouleurs, A. and Corwin, H.G., 1976, *Second Reference Catalogue of Bright Galaxies* (University of Texas Press).
- (4) Faber, S.M. and Jackson, R.E., 1976, *Ap. J.*, **204**, 668.
- (5) Davies, R.L., Efsthathiou, G., Fall, S.M., Illingworth, G. and Schechter, P.L., 1983, *Ap. J.*, **266**, 41.
- (6) Graham, J.A., 1979, *Ap. J.*, **232**, 60.
- (7) Peterson, C.J., 1978, *Ap. J.*, **222**, 84.
- (8) Caldwell, N., 1984, Ph.D. Thesis Yale University.

Suspected Rotation of an X-ray Cluster of Galaxies

J. Materne, Institut für Astronomie und Astrophysik, Berlin

Introduction

The universe as we observe it shows structure on many scale lengths. They start probably with the sizes of quarks having an extent of maybe 10^{-18} m and increase up to at least superclusters of galaxies with sizes of 10^{24} m. The building blocks of the large scale structure of the universe are, however, the largest gravitationally bound stellar systems, the galaxies. They are the largest systems we can observe relatively easily as whole objects.

The distribution of galaxies in the universe, that is in space, is difficult to determine. We can observe directly only very limited properties: distribution on the sky and, with a great effort, radial velocities. The third dimension, the distance, is normally lacking. Generally we replace it by the radial velocity. If we assume that the universe is expanding homogeneously – and there is no reason not to believe in this – we can convert radial velocities into distances using the Hubble law, radial velocities v_{rad} being proportional to distances D :

$$V_{\text{rad}} = H_0 D.$$

But there is a problem. Clusters of galaxies are gravitationally bound and probably relaxed. Consequently, the internal motion of the galaxies relative to the cluster centre is superimposed onto the receding motion due to the expanding universe. The Hubble flow appears distorted in the direction of clusters.

Cluster Kinematics and Dynamics

This seeming disadvantage can also be turned into an advantage. If we have some coarse ideas about the distribution of galaxies in clusters we can identify the member galaxies using a distribution function. The simplest approach is density enhancement relative to the neighbourhood and clustering in velocity distribution. Then we can define the cluster averages and investigate the behaviour of the member galaxies relative to the cluster mean. Of course, this is an iterative process and we hope that it converges to the right model.

Apart from the galaxy distribution, the X-ray emission provides an independent way of studying cluster properties. One of our main goals is to unify observations in the optical regime with the ones in the X-ray regime. The spatial form and the gravitational potential of a cluster are very well given by the X-ray emission, the dynamics can be studied best with the galaxy velocities. A simple first step is to look for correlations of the X-ray emission with other properties: total luminosity, total mass (which should be correlated to the luminosity via a mass-to-light ratio), velocity dispersion (which should be governed by the mass distribution), content in types, or cluster classification.

Therefore, many astronomers started to observe in more detail clusters which were detected by the satellites Uhuru or Ariel as X-ray sources.

An ultimate aim is to understand the phase space distribution function of the galaxies in clusters. Then we would know at each place the density of galaxies and their velocities. When using the galaxy distribution combined with the X-ray emission distribution, we have to be very careful because the dynamical age of these components may be different. An important question is whether the galaxies and the hot gas are formed together or if the galaxies have shed the gas during their lifetime into the intracluster space. The latter assumption is more plausible because the X-ray emitting gas seems to be processed material, matter which has gone through stars already and which is enriched with heavy elements.

The Cluster SC 0316-44

One of the galaxy clusters discovered with the Ariel satellite is in the southern hemisphere ($03^{\text{h}}16^{\text{m}}-44^{\circ}$). One of the first investigations of this cluster was done by the two former ESO members J. Melnick and H. Quintana. They noted some curious properties of the cluster:

(i) SC 0316-44 has a very large velocity dispersion. The radial velocities scatter over a broad range.

(ii) It belongs to the few clusters in which the central dominant cD galaxy (number 18 in the figures) is neither at the dynamical centre of the cluster nor at the bottom of the potential well. In the present case the most massive galaxy does not have the mean radial velocity though it is roughly in the geometrical centre.

(iii) It has a dominant cD galaxy. But there is also a galaxy nearly as big as the central one, far offset from the centre (number 8 in the figures). One might speculate that we have in reality two clusters centred on these two dominant galaxies.

This made the cluster interesting enough to investigate it again. We counted and determined the positions of all the galaxies with a major diameter larger than 14 kpc in the region of the cluster. For comparison, our Galaxy has a major diameter of some 30 kpc. The measurements were done with the ESO Optronics machine in Garching. The positions were measured manually but the software available made these measurements very efficient. There were nearly 1,100 galaxies. Their spatial density distribution projected on the sky reveals another remarkable fact:

(iv) The central part of the cluster is elongated in the NE-SW direction. The outer regions indicate, however, an elongation in the NW-SE direction though this is still a matter under discussion. Elongation of clusters is not so unusual. The Basel

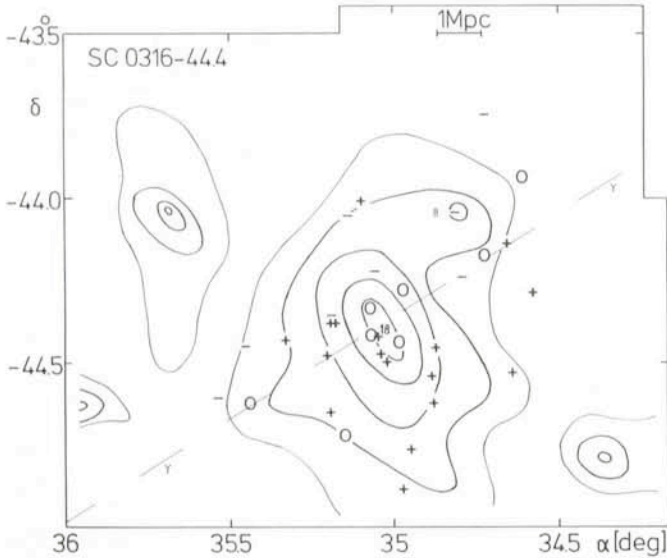


Fig. 1: This graph gives all the information on the galaxy distribution. The irregularly shaped lines are lines of constant galaxy surface density. The levels are 8, 10, 16, 21, and 26 galaxies/Mpc². In the centre the cluster has a density of approximately 35 galaxies/Mpc². The most prominent galaxies, number 18 and number 8, are also indicated. The broken line called Y is the axis of rotation. The galaxies with measured radial velocities are marked:

- : $v_{rad} < 20,000 \text{ km s}^{-1}$
- : $20,000 \text{ km s}^{-1} \leq v_{rad} < 22,000 \text{ km s}^{-1}$
- +: $22,000 \text{ km s}^{-1} \leq v_{rad}$

astronomer B. Binggeli has shown that it is a rather common fact. To illustrate this for SC 0316-44 we have plotted in Fig. 1 contours of equal galaxy number densities (so-called isopleths). The elongated central part can clearly be seen. B. Binggeli has also found that the long axis of an elongated cluster points to its neighbours. If we accept this as a general rule, the twists of the outer isopleths should have no relevance because two adjacent clusters can be seen NE and SW. The reader should be cautioned, however, that no radial velocities are available for the two neighbouring clusters, they may be just chance projections.

New Measurements

An increase of the number of radial velocities compared with those available to Melnick and Quintana seemed to be necessary. Therefore we reobserved the cluster and took more spectra with the ESO 1.52 m telescope equipped with the

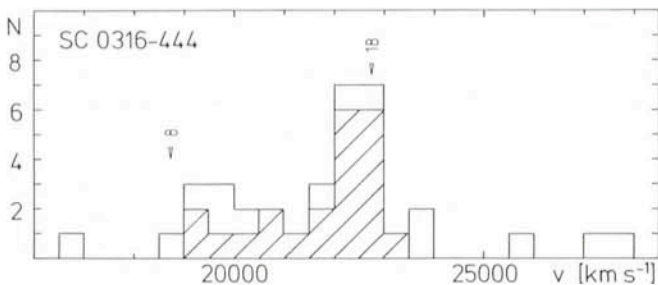


Fig. 2: In this graph we show the distribution of galaxy velocities. The two most prominent galaxies, number 18 and number 8, are marked. They are near the edges of the velocity range spanned by the cluster and not at the centre.

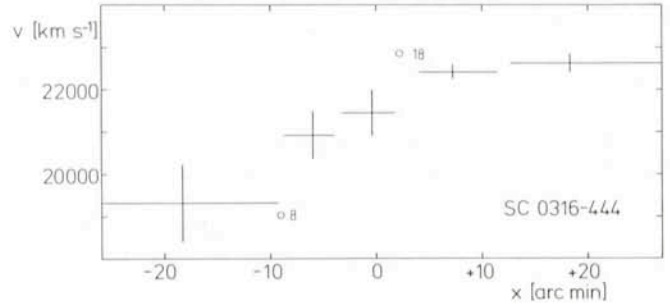


Fig. 3: In this final figure we plot the radial velocities of the galaxies versus their distance to the axis of rotation. We have averaged over several galaxies. The horizontal bars show the averaged range in distance from the rotation axis, the vertical bars the velocity errors in these ranges.

Boller & Chivens spectrograph and an image tube. This "oldtimer" of ESO can be a very efficient telescope for this kind of work, securing spectra of moderately faint galaxies. We now know radial velocities for 39 galaxies. Of these, four are foreground objects and three are in the background.

A table with these velocities is not very illustrative. Therefore, the description in form of a histogram is given in Fig. 2 in which the foreground galaxies are omitted. Most of the galaxies cluster around 22,000 km s⁻¹. To be precise, the mean velocity of the cluster is 21,400 km s⁻¹. This puts the cluster at a distance of 1,200 million light-years. Its velocity dispersion, that is the spread in velocities, is 1,500 km s⁻¹, which is high. But we can give a possible reason for this below.

In a first step we wanted to see how the galaxies for which radial velocities are available are distributed in the cluster. Therefore, we plotted these galaxies in Fig. 1. We not only marked their position but also tried to indicate their radial velocities. The small bars represent galaxies with radial velocities lower than 20,000 km s⁻¹, the circles are for galaxies in the range 20,000 to 22,000 km s⁻¹, while the crosses are taken for galaxies with velocities larger than 22,000 km s⁻¹.

The Asymmetric Velocity Distribution

When looking at Fig. 1, one has the impression that there are more crosses in the lower right part, the circles are on a strip from the lower left to the upper right, and the bars are in the upper left corner. In fact, we used a much more refined colour coding to visualize this. But this cannot be reproduced here.

In the NE the velocities are generally lower than in the SW. We looked for a method to make this effect more clearly visible. The broken inclined line called "Y" in Fig. 1 was chosen so that it separates most efficiently the low velocity galaxies from the high velocity ones. Then we plotted the radial velocities of the galaxies versus their distance from this line Y. The result can be seen in Fig. 3. There we have binned the galaxies to decrease the noise. The trend for the galaxy velocities shows up clearly. Fig. 3 displays something like a rotation curve of a disk galaxy.

We have presently two possible explanations for the effect if it is real and not an artefact of poor statistics caused by too few radial velocities:

- (i) Fig. 3 can be interpreted as a rotation curve indeed. Then the axis Y is the rotation axis of the cluster.
- (ii) We see two clusters partially overlapping, collapsing or expanding. The decision which of these two possibilities may be the right one is difficult to make.

Discussion

Generally, one believes that clusters of galaxies do not rotate. Dressler, for example, found no rotation for the very elongated cluster Abell 2029. This is analogous to the case of the elliptical galaxies which rotate, if at all, only very slowly though they are elongated. The gravitational force of the mass of the member galaxies is balanced by their kinetic energy – the velocity dispersion. The motion of the galaxies is not typically in circular orbits. Nevertheless, the aspherical shape can be maintained by an anisotropic distribution of the velocities as has been shown, for instance, by Binney.

One should keep in mind, however, that Gregory and Tifft thought they had detected some rotation for the Coma cluster which is also elongated. But these authors were careful not to exclude an anisotropic expansion.

Generally one can say that there is always a residual angular momentum for any isolated bound object in the universe. Therefore, the elongated shape of the inner part of the cluster may be caused indeed by rotation, the outer isopleths appearing distorted only because of the noise in the galaxy counts. And the dominant galaxy number 18 is not at the dynamical centre but it is roughly where one would expect it to be from the rotation curve. Also the radial velocity of the second most

prominent galaxy number 8 is approximately predicted by the rotation curve.

The two massive galaxies number 8 and number 18 are not likely the centres of two clusters being projected onto each other because the line connecting them is far away of being perpendicular to the proposed line separating high velocity galaxies from low velocity ones.

Conclusion

We have probably detected a rotating cluster of galaxies though we cannot exclude that we just observe two clusters partially overlapping. To decide on the correct answer, we have to collect much more information. We should try to determine the luminosity functions of the two possible clusters given by the low and high velocity parts and see if they are shifted, or we should try to look for different contents of types. But this is an ambitious programme.

We (Ulrich Hopp took part in this investigation) would not have been able to pursue this programme without the support by ESO. It is not only the telescope time which counts but also the possibility to reduce observations in Garching or do plate measurements there.

Wolf-Rayet Stars in “Lazy” Galaxies

*M. Joubert, Laboratoire d’Astronomie Spatiale, Marseille, France, and
D. Kunth, Institut d’Astrophysique, Paris, France*

We are all very familiar with the concept of “active galaxies” but have you ever heard about “lazy galaxies”? We shall stress that they are the ones which have been recognized as a class by Sargent and Searle (1970: *Astrophysical Journal*, **162**, 455) under the generic name of “extragalactic” H II regions. They are dwarf objects, compact on photographic atlases such as the Palomar Sky Survey or the ESO Quick Blue Survey. They have low masses but, strikingly, they are blue and their spectra resemble those of Giant H II regions. Therefore, one of us (DK) in his Ph.D., regarding as most probable the current view that these galaxies now experience star formation after a long period of quiescence, suggested they might be regarded as “lazy”. Indeed, on average they have not done much: little stellar nucleosynthesis, thus showing marked deficiencies in heavy elements, and containing large quantities of unprocessed neutral hydrogen.

Since their discovery, these unevolved objects have been very much studied. They are especially important for galactic evolution models and in various occasions were chosen for their low metallicities to study the primordial helium abundance. Along these studies—spectroscopic for most of them—a few galaxies have shown the presence of a very large number of Wolf-Rayet stars!

A Huge Number of Wolf-Rayet Stars?

André Maeder has emphasized that WR stars are “much more than a mere curiosity in the zoological garden of spectral peculiarities” (ESO Workshop: The Most Massive Stars, 1981, p. 173) and pointed out a few facts contributing to make their study a fascinating one: they power giant H II regions with large mass losses, may be useful indicators of metallicities in

galaxies, contribute to eject processed material into the interstellar medium and are supernova progenitors.

In our Galaxy, WR stars have been discovered individually in young clusters and stellar associations and their number—relative to that of the blue supergiants—is small. Should one not find them in lazy galaxies with active sites of star formation? Of course, one cannot expect to detect individual WR stars in such distant galaxies but one can detect the strongest broad emission lines formed in their atmospheres, for instance the He II 4686 Å emission.

In most of the past spectroscopic observations of giant H II regions and emission line galaxies, WR stars have been overlooked merely because observers have focussed on the intensities of the nebular emission lines for abundance determinations in the gas. As a result, very few cases were found. The broad emission waveband 4600–4700 Å around the He II line remained unnoticed until its first discovery in the emission line galaxy He2–10 by Allen et al. (1976: *Monthly Notices of the Royal Astronomical Society*, **177**, 91). Since then, spectra of several clusters in H II regions in external galaxies have also been found to exhibit the same WR features (e.g. in NGC 604 and 30 Dor) but only a few lazy galaxies are known to share these properties: Tololo 3, Mkn 750 and other peculiar galaxies such as Mkn 309, NGC 6764 and Tololo 89.

All these observations led to one surprising fact: WR stars largely outnumber the blue supergiants in number in both giant H II regions and lazy galaxies! This can be understood if one picks out objects during a very evolutionary point at which most of the massive stars in the range 25–60 M_{\odot} have entered a post-red-supergiant stage on which they exhibit WR activity in their He-burning phase. Another way of explaining the data requires that the observed broad-band emission is due to a very small number of WR stars more massive than 60 M_{\odot} .

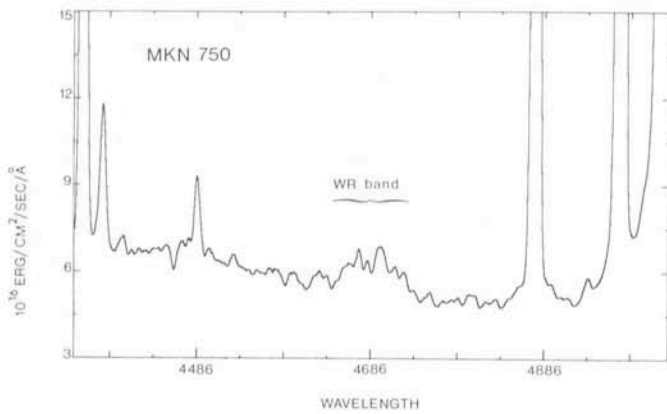


Fig. 1: Section of the spectrum of Mkn 750 taken with the ESO 3.6 m telescope and showing the WR band.

losing mass while still on the main sequence. These very massive stars would be largely responsible for the ionization of the nebulae. This shows why giant H II regions and emission line galaxies are ideal sites to test stellar evolution models of massive stars in various conditions of heavy element content and to study the initial mass function in present high rate star formation systems.

Kunth and Sargent (1983: *Ap. J.* **273**, 81) for studying the helium abundance in low heavy element extragalactic systems have been searching for galaxies with hot interstellar gas. During their search, they have accumulated a hundred spectra of these lazy galaxies as well as more luminous and more abundant ones. At this stage we have decided to reanalyse their spectra and see whether any galaxy with milder WR emission had been overlooked. Why do some show these features but not others? Would selection effects be present? In addition to the running observing programme undertaken at La Silla with the 1.5 m and the 3.6 m telescopes equipped with the IDS, we have begun to elaborate a strategy for a deep search of WR emission in relatively distant objects. This study involves a sample with a wider range of metallicity than for H II regions in a single late-type galaxy.

Observations and Analysis

The sample is composed of three sets of independent observations: one is formed by blue compact Zwicky galaxies observed with the SIT spectrograph at the Palomar 200 inch telescope; a second set is composed of lazy galaxies observed with the Varo-Reticon detector at the Cassegrain focus of the Las Campanas 2.5 m telescope, and the third with the IDS on the 1.5 and 3.6 m telescopes at La Silla. Dispersions used were in the range 114 to 240 Å/mm. The reduction procedure is not unusual and is described in our previous papers on similar objects. Since most of the WR lines occur in the He II 4686 Å region, we have measured the WR emission excess WRE above the continuum in the rest wavelength range 4600–4700 Å with allowance for the different instrumental resolutions and assuming a typical WR line of FWHM of 2,000 km/sec. This emission integrated over this wavelength range has been measured above the continuum, together with an estimate of the signal-to-noise ratio of the underlying continuum. About 50 galaxies have been reanalysed so far. As a first guess, we have considered as significant, excesses larger than about 0.8σ over the adjacent background. This lower limit, although arbitrary at this stage of the discussion, turned to finally provide a workable sample for discussing selection biases and a strategy for future observations.

Finally, WR stars have been positively detected in 3 galaxies and are suspected in 16 others at 1σ over the underlying

background. A tracing of a typical broad-band WR emission in the spectrum of Mkn 750 is shown in Fig. 1.

What About the Characteristics of Our Sample?

The redshift distributions among the various sets of observations are different, as the Palomar subset picked out fainter and therefore more distant objects than the Las Campanas/La Silla subset. The overall sample covers a range in redshift from $z = 0.002$ to 0.024 with scarce objects up to $z = 0.05$. Fig. 2 displays the redshift distribution of our sample of galaxies together with the corresponding histograms of the galaxies in which WR stars are suspected to be present or absent! A statistical test reveals a clear tendency for WR stars to be more easily detectable in nearby galaxies with redshifts not greater

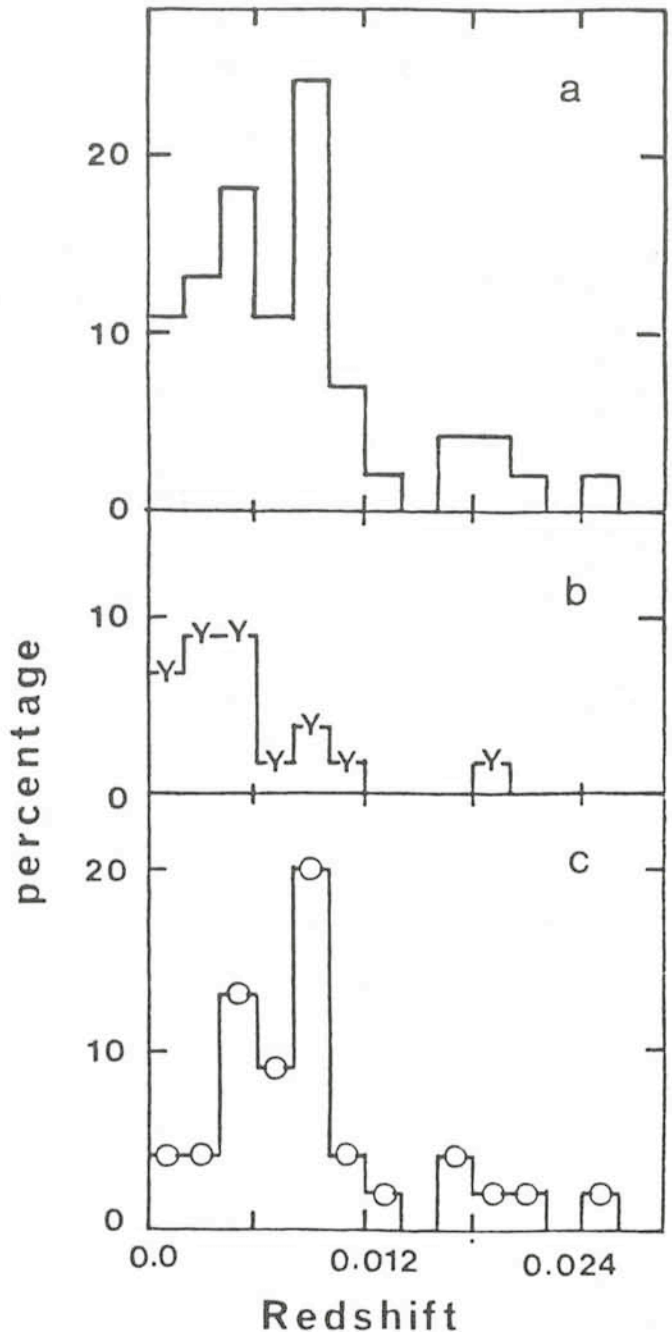


Fig. 2: a: Redshift distribution histogram of the galaxy sample; b: Histogram of galaxies exhibiting WR emission (Y); c: Histogram of galaxies with no WR emission (O).

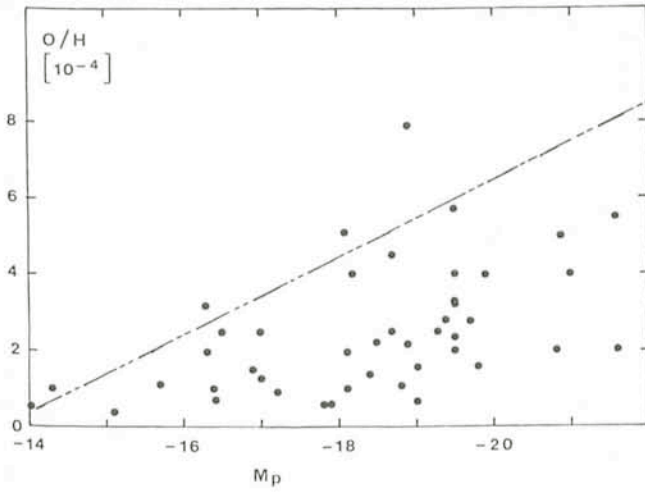


Fig. 3: Oxygen abundance versus absolute photographic magnitude of the galaxy sample. The dotted line represents the regression fit given in the text using the 12 upper points of the diagram and neglecting the discrepant one at $O/H = 8.0 \cdot 10^{-4}$.

than about 0.02. Clearly beam dilution acts against detection, unless WR are formed in unusually large numbers.

The galaxies largely differ in their metal content, they spread a range from 7.5 to 8.9 in logarithmic scale for the oxygen abundance, hence some exceeding the metallicity in the solar neighbourhood. Their luminosities from $M_p = -14$ to -21.5 include objects which are not genuinely lazy! Fig. 3 displays the oxygen abundance versus absolute magnitude, it shows that the galaxies evenly populate an area below a line $O/H = -1.4 (M_p + 13.6)$ in surprising agreement with that of Lequeux et al. (1979: *Astronomy and Astrophysics*, **80**, 155) for a sample of 8 irregular and compact galaxies. This large scatter in the diagram may not be due to observational uncertainties but more likely to dispersion in the properties of this type of galaxies such as galactic winds, infall, and variations in the yield of metals (Matteucci and Chiosi, 1983: *Astronomy and Astrophysics*, **123**, 121).

Where Are Wolf-Rayet Stars Expected to Be?

While the galaxies in our sample are well distributed over 8 magnitudes in luminosity, our study shows no tendency to detect WR stars at any preferred galactic luminosity. Contrary

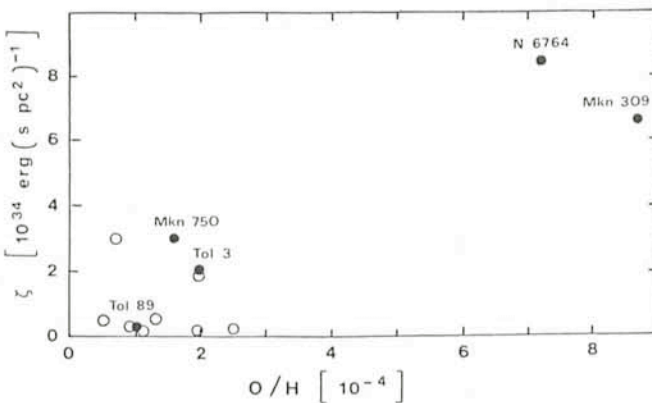


Fig. 4: Intrinsic luminosity of the WR emission per projected surface in the galaxy as a function of oxygen abundance. Symbols are: Open circles are galaxies with WR excesses larger than the 0.8σ threshold; filled circles are galaxies with WR excesses larger than the 3σ threshold.

to what had been suspected from both the distribution of galactic WR stars and their number in the Magellanic Clouds, that WR stars would be found in sites of large metallicities, emission was detected in galaxies with no preferential oxygen abundance. But what about their absolute number? In order to estimate the number of WR stars formed in all relevant galaxies we have computed the absolute luminosity of the WR emission per unit area in the galaxy, a quantity independent of the distance. Limitations of this procedure rise from the assumption that WR stars are uniformly distributed and from severe reddening corrections. Fig. 4 displays this quantity as a function of the oxygen abundance and indicates that WR stars seem to be more numerous in sites of higher metallicity.

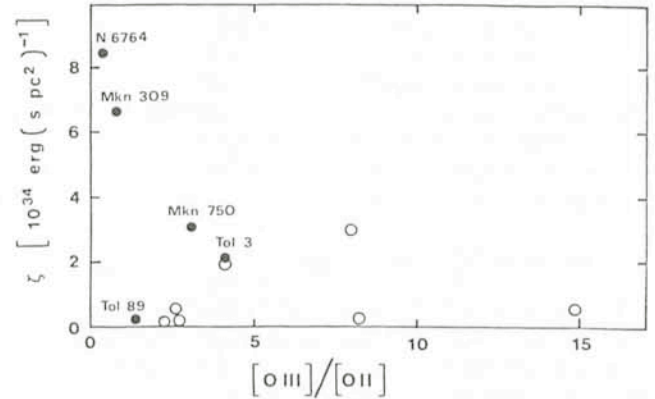


Fig. 5: Intrinsic luminosity of WR emission per projected surface in the galaxy as a function of the $[O III] \lambda 5007$ to $[O II] \lambda 3727$ ratio.

Next we have plotted in Fig. 5 the absolute WR emission per square area as a function of the mean temperature of the ionizing stellar cluster, as guessed from the line ratio $[O III] \lambda 5007/[O II] \lambda 3727$. This says that WR stars are found in larger numbers in regions of low to moderate stellar effective temperature, less than 35,000 K.

About Our Feelings Concerning the Nature of WR Stars in Lazy Galaxies

Let us finally come back to our original question: what kind of WR stars do we see in lazy galaxies? Are they supermassive ones on the main sequence or post-red-supergiant stars in a He-burning phase? Using our 3 best observed cases and the published ones, we are struck by the fact that the equivalent width of the WR feature is in no way related to that of the $H\beta$ emission line. Instead a spread in EW ($H\beta$) by a factor of more than 20 corresponds to a nearly constant WR emission equivalent width of about 8 \AA . The number of WR stars is therefore proportional to the number of stars responsible for the continuum at 4600 \AA but not at all to the number of ionizing massive ones. They probably play a minor role in ionizing the gas. This strongly indicates that WR stars in lazy galaxies occur in a population of stars less massive than $60 M_{\odot}$ evolving in their He-burning stage. They should be linked to the early evolutionary phase of the burst of star formation.

Galaxies with a continuous range of WR emission may then be found, with $8-10 \text{ \AA}$ equivalent width being an upper limit. Our observations performed last January at La Silla should answer this question and many others we hope!

On the Accuracy of the Wavelength Calibration and of the Flat-Fielding of the CCD CASPEC Spectra

S. D'Odorico and D. Ponz, ESO

Great care has to be used in the calibration of echelle spectra, both in wavelength and in intensity because most observational programmes which are carried out with CASPEC call for the highest accuracy in the velocity determinations or for the detection and measurements of faint features in the spectra.

The well-known difficulties in the reduction of the spectroscopic data in the echelle format are coupled in CASPEC with the problems of flat-fielding the CCD images.

In this short note we report on the results obtained on spectra from the commissioning phase of the instrument, using the software developed within the ESO MIDAS data reduction on the VAX computer in Garching. They represent a good reference point: the users should consider them as the minimal goal to achieve in reducing their data, but they could certainly do better by refining the calibration procedure and the reduction software.

The Wavelength Calibration

The dispersion coefficients are determined from the spectra of the Thorium-Argon hollow cathode lamp, obtained with the same instrumental configuration and at the same telescope position as the science frame.

In the reduction procedure, the orders are automatically defined via the flat-field exposure, and extracted using a sampling step of 1 pixel.

The calibration lines are then identified with a detection criterion which is based on the width of lines and their intensity above the background.

The actual position of the lines is defined as the centre of gravity of the two brightest pixels relative to the third brightest. Initial guesses for the wavelength calibration are obtained by entering manually the identification of a few lines in the frame, and then improved by comparison with the reference catalogue of thorium lines (1). The dispersion coefficients are computed by means of a regression analysis, where the equation conditions are similar to the one used in the calibration of the IUE high resolution spectra. In our case it is reduced to

$$x = a_0 + a_1 m \lambda + a_2 (m \lambda)^2 + a_3 m + a_4 \lambda + a_5 m \lambda^2 + a_6 m^2 \lambda$$

where m is the order number.

In a typical reduction, between 100 and 300 lines are used in the regression analysis. Fig. 1 shows the behaviour of the residuals for two calibration images centred at 4500 Å and 6200 Å respectively.

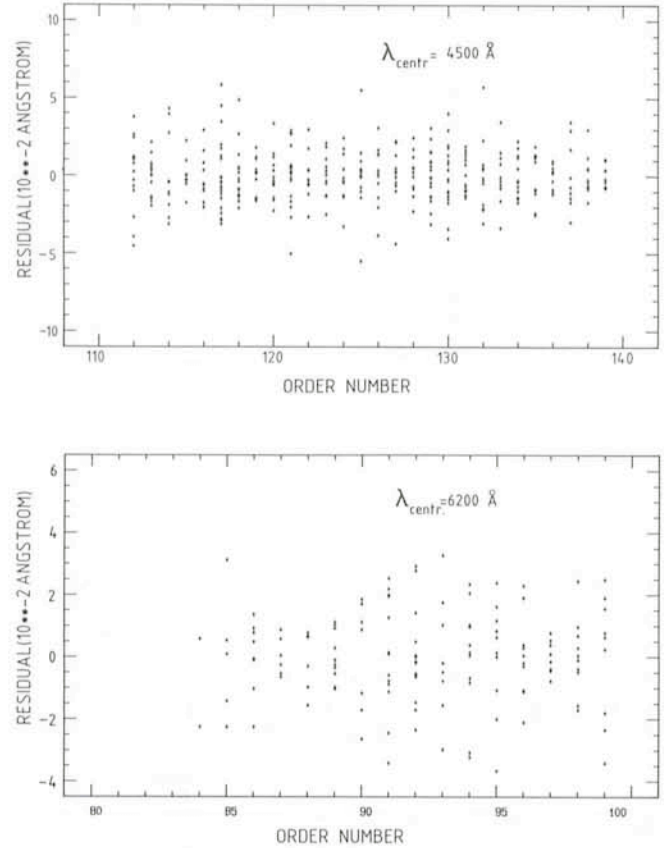


Fig. 1: Plots of the residuals ($\Delta\lambda = \lambda_{\text{obs}} - \lambda_{\text{comp}}$) of two wavelength calibrations for the velocity standard stars as a function of order number. 350 and 142 lines were used for the blue and red frame respectively with corresponding standard deviations of 0.02 and 0.01 Å.

In the commissioning phase, we have obtained nine spectra of 4 velocity standard stars (2) and reduced them with the standard procedure in MIDAS (3). Table 1 summarizes the results, Table 2 gives the list of lines which have been used in the radial velocity measurements. Typical exposure times were five minutes. When more than one spectrum per star is given, they were taken at intervals of about 15 minutes and calibrated with the same thorium exposure.

TABLE 1: OBSERVATIONS OF VELOCITY STANDARD STARS

Name HD	Spectral type	Velocity (km/sec)	Date	λ_{Cont} (Å)	Measured velocity (km/sec)	σ (km/sec)	No. lines
51250	K2 III	19.6 ± 0.5	18/1/84	6200	19.8	1.5	20
66141	K2 III	70.9 ± 0.3	14/1/84	6200	68.3	2.7	19
107328	K1 III	35.7 ± 0.3	20/6/83	6500	35.0	0.9	17
"	"	"	21/6/83	4500	35.0	3.4	18
"	"	"	"	"	34.9	3.3	18
"	"	"	"	"	35.0	3.5	18
136202	F8 IV-V	53.5 ± 0.2	20/6/83	6500	53.7	1.8	18
"	"	"	"	"	53.5	1.8	18
"	"	"	"	"	52.3	1.9	18

TABLE 2: LIST OF WAVELENGTHS USED IN THE DETERMINATION OF THE RADIAL VELOCITY

Blue spectra		Red spectra	
Ion	Wavelength (Å)	Ion	Wavelength (Å)
FeI	4152.170	Nil	6108.123
FeI	4174.917	CaI	6122.218
FeI	4191.436	FeI	6141.759
FeI	4202.031	FeI	6151.632
FeI	4219.364	CaI	6162.172
FeI	4383.547	FeI	6230.728
FeI	4404.752	FeI	6252.561
FeI	4415.125	FeI	6393.605
FeI	4427.312	FeI	6430.851
CoI	4549.656	CaI	6439.073
FeI	4611.289	CaI	6462.566
FeI	4602.944	FeI	6546.245
FeI	4654.624	H α	6562.808
H β	4861.33	FeI	6592.919
FeI	4920.505	Nil	6643.641
FeI	4934.023	FeI	6677.993
FeI	4957.609	Nil	6767.778
FeI	4973.108	Nil	6772.36
FeI	4991.277	FeI	6663.446
		FeI	6717.556
		TiI	5866.462
		NaI	5889.953
		NaI	5895.923
			5922.123

The velocities were derived from gaussian fitting of the lines in the flat-fielded, λ -calibrated and merged spectra using an IHAP command. The line FWHM is typically 2–3 pixels.

Most of the 9 spectra give velocities within 1 km/sec from the standard value, with the largest discrepancy being 2.5 km/sec and with no trace of systematic deviations.

The pixel size being about 9 km/sec, these results indicate that radial velocity measurements with an accuracy of a fraction of the pixel size can easily be achieved.

This accuracy is also confirmed by the measurements on the telluric emission lines, e.g. OI 5577 and 6300 Å, which are detected in long exposures. The radial velocities of these lines are within 2 km/sec of the zero redshift.

The Flat-Fielding of the CCD CASPEC Frames

As the use of CCD has become more and more common in astronomy, the procedure to flat-field a CCD image, that is to correct for offset values in the pixel intensity read-outs, for deviations from linearity and for chip defects, has become an art in itself. An additional feature which is particularly bothering in echelle spectra taken with the thinned, back illuminated RCA CCD is the fringing effect, due to reflections in the thinned silicon layer of the CCD. They produce an interference pattern whose variations depend on the wavelength of the incident light and the CCD thickness. The effect is as high as 30% in the red part of the spectra with the chip we used in the commissioning phase, but is less conspicuous in a new RCA chip which has recently come into operation.

We do not venture here into a discussion of the advantages of the various flat-fielding methods, but simply describe the procedures we have followed and the results we have obtained to provide, as pointed out above, a reference point to the other users.

In the standard reduction procedure implemented in MIDAS, an average dark exposure, which might incorporate the preflash exposure applied to improve poor charge transfer

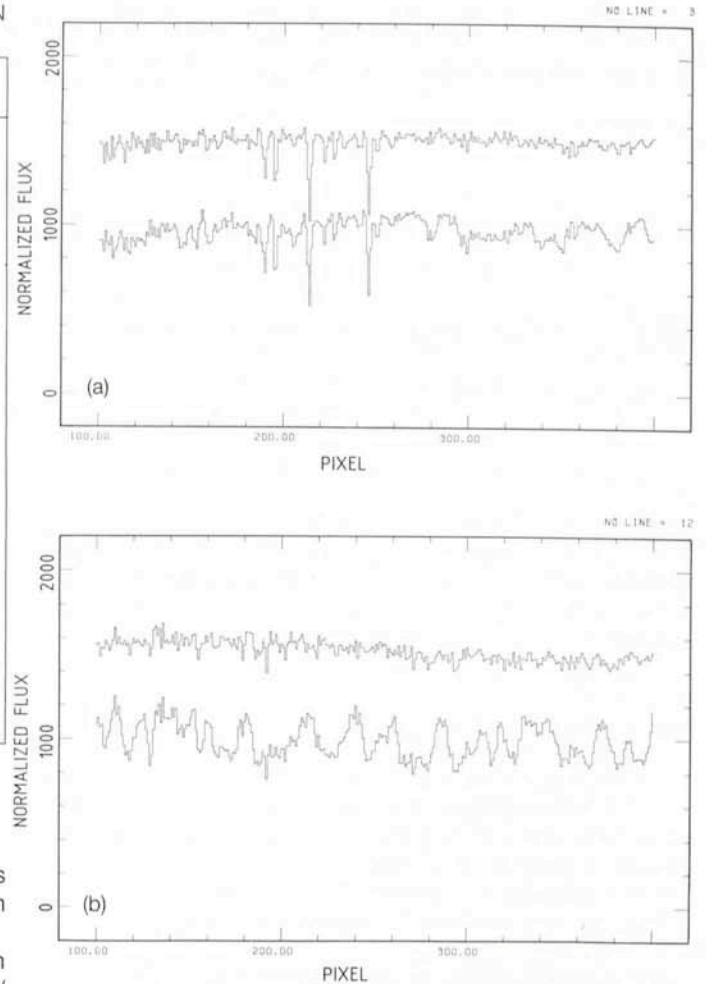


Fig. 2: Two extracted orders of a CASPEC exposure of the 12.1 m, star LTT 3864, centred at λ 5900 Å (a) and 6700 Å (b). The extraction step is the CCD pixel. Lower tracings show the spectra extracted from the original CCD frame, the upper ones from the flat-fielded image. The spectra have been normalized and shifted one with respect to the other to make the comparison easier.

efficiency, is subtracted from the science exposure and from the corresponding flat-field exposure with a continuous lamp. The residual background in the images, which is due to scattered light in the spectrograph and to the dark current of the chip, is then automatically fitted by a surface which interpolates values at interorder positions and again subtracted from the frames. The resulting background free science and flat-field exposures are then divided one by the other. Finally, the spectral orders are extracted and eventually normalized.

The flat-field exposure is taken with an internal lamp through a projection system to the slit which reproduces the focal ratio and the central obstruction of the telescope. The intensity of the flat-field spectra is sufficiently high to have a negligible shot noise but still far from saturation.

As a representative example, we show in Figure 2a, b two orders from a 25 min. exposure on the 12.1 visual magnitude star LTT 3864, a white dwarf used as a flux standard star. The orders were extracted from the original and flat-fielded frames respectively, with a step of 1 CCD pixel, and are centred on the interstellar sodium lines at 5900 Å and to the red of H α . At these wavelengths, the fringing effect in the original data is shown to be as high as 30%, but the noise is successfully

reduced to better than 3% in the flat-fielded spectrum. The equivalent widths of the faintest interstellar lines recorded in the spectrum are about 40 mÅ.

References

(1) S. D'Odorico, C. la Dous, D. Ponz and J. F. Tanné, "An Atlas of the

Thorium-Argon Spectrum for the ESO Echelle Spectrograph", ESO Scientific Report No. 2.

(2) The Astronomical Almanac, 1984, Naval Observatory and Royal Greenwich Observatory.

(3) MIDAS, Munich Image Data Analysis System, 1984, ESO Operating Manual No. 1.

IRAS* Ground-based Follow-up at ESO

T. de Jong, Astronomical Institute Anton Pannekoek, University of Amsterdam

Introduction

The InfraRed Astronomical Satellite (IRAS) was successfully launched on 26 January 1983 from Western Test Range, Lompoc, California. The satellite died when the superfluid liquid helium which kept the telescope and the infrared instrumentation at its operating temperature of a few degrees Kelvin ran out on 22 November 1983. The very good performance of the satellite, the telescope and the infrared instrumentation has surpassed most preflight expectations. Due to the excellent attitude control system IRAS source positions are generally accurate to about 20 arcseconds. The extraordinary dark current stability of the infrared detectors has made it possible to attain an overall photometric accuracy of about 10% and has in addition enabled us to also study extended emission features in the infrared sky.

The daily avalanche of infrared data accumulated over the 300 day IRAS mission has resulted in infrared parameters of about 300,000 astronomical sources. These sources are inhomogeneously distributed over the sky, with source densities varying from about 50 sources per square degree in the galactic plane (the source confusion limit) to about one source per square degree at the galactic poles. The reduction of the IRAS data and the preparation of the IRAS point source catalogue is carried out under the responsibility of the Joint IRAS Science Working Group consisting of astronomers from the three participating countries. The IRAS catalogue is presently scheduled to come out in November 1984.

The focal plane of the 60 cm Ritchey-Chretien telescope accommodated three separate instruments:

(i) The survey array, built in the US, and consisting of eight rows of altogether 62 detectors, two rows for each wavelength band (for detector sensitivities, fields of view and wavelength ranges see Table 1), and two additional Dutch instruments:

(ii) the Low Resolution Spectrometer (LRS), a slitless spectrograph, that registered 8–23 μm spectra with a spectral resolution of about 20 of all sufficiently strong ($\text{SNR} > \sim 50$) point sources observed in the survey, and

(iii) the Chopped Photometric Channel (CPC) designed to map sources at 50 and 100 μm with higher spatial resolution (1.2 arc minutes) but lower sensitivity than the survey array.

The main purpose of the IRAS mission was to systematically survey the whole sky at infrared wavelengths. About 60% of the total available observing time was spent on carrying out this survey which was successfully completed apart from a five degree wide gap roughly centred at ecliptic longitudes 160 and 340 degrees that was missed because of operational

problems. The remaining 40% observing time was spent on mapping about 3,000 preselected sources and areas of sky at higher sensitivity (survey array) and better spatial resolution (CPC).

Due to the survey character of the IRAS mission the scientific results cover a wide spectrum of astronomical scenery and astrophysical processes, ranging from comets to quasars and providing new insights in the evolution of the solar system, stars and galaxies. Since cosmic infrared radiation is predominantly emitted by small dust particles heated by starlight, regions of high density close to stars generally stand out most clearly in the infrared. This makes the infrared the wavelength range "par excellence" to study stars in the process of formation when they are still immersed in the gas and dust clouds from which they have formed as well as stars at the end of their lives when they have evolved to red giants and are blowing off their envelopes on a relatively short time scale ($\sim 10^5$ years) before turning into white dwarfs or exploding as supernovae.

Ground-based IRAS Follow-up

To illustrate the capabilities of IRAS compared to ground-based telescopes in the infrared, it is instructive to compare the performances at 10 and 20 μm where observing from the ground is possible but severely hampered by atmospheric emission. To reach the same limiting sensitivity as IRAS at 10 μm with the 3.6 m ESO telescope requires 200 times longer integration times (40 seconds) at 10 μm and about 30,000 times longer (2 hours) at 20 μm in spite of the fact that the collecting area of the 3.6 m is about 40 times larger than that of the IRAS mirror. For this estimate I have assumed that sources are pointlike (smaller than the 3 arcseconds diaphragm of the IR photometer). If, as for virtually all protostars and galaxies, the sources are extended, the integration times go up proportional to the area of the source. In fact, to reach the same surface brightness sensitivity as IRAS, one would have to integrate about 2,000 times longer than estimated above.

This little bit of trivial numerology shows that ground-based follow-up of IRAS sources in the infrared is only profitable at 10 μm and shorter infrared wavelengths and would greatly benefit from the availability of an array-photometer, now in use at several other major observatories in the world. The enhanced spatial resolution that one can reach from the ground makes it worthwhile to have such an instrument for more detailed studies of fine-scale structure in the brightest sources detected by IRAS.

Two infrared observing runs that we had in 1983 were totally unsuccessful because of bad weather but in view of the considerations above it is doubtful in retrospect how much could have been achieved with the conventional infrared photometer presently available at the 3.6 m telescope.

* The InfraRed Astronomical Satellite was developed and is operated by the Netherlands Agency for Aerospace Programmes (NIVR), the US National Aeronautics and Space Administration (NASA), and the UK Science and Engineering Council (SERC).

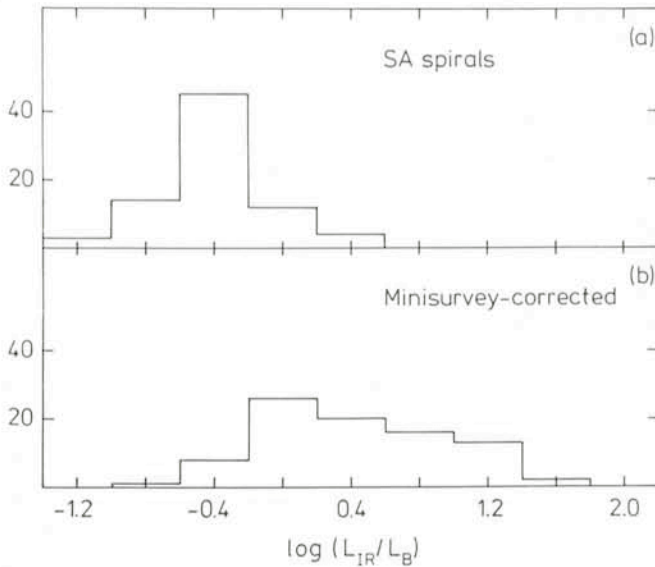


Fig. 1: Infrared excess distributions of an optically complete (a) and an infrared-complete (b) sample of galaxies.

Extragalactic IRAS Follow-up in the Optical

It is outside the scope of this short article to review all the exciting new discoveries made up to now by IRAS (see the 1 March 1984 issue of the *Astrophysical Journal Letters*). Instead I will concentrate on the extragalactic results and present ground-based optical spectra of galaxies with large infrared excesses recently obtained at ESO.

IRAS has detected infrared radiation of about 10,000 galaxies, the majority spirals. Most of these galaxies are optically faint ($B > 14$), many of them so faint that they do not appear in any presently available catalogue while some do not even show up on Palomar and ESO/SRC Sky Survey plates ($B > 19$).

Fig. 1 shows the distributions of infrared excesses of two samples of spiral galaxies, an optically complete sample ($B < 12.5$) and an infrared complete sample ($S < 60 \mu\text{m} > 0.5 \text{ Jy}$). The former is a sub-set of the optically complete sample of Shapley-Ames galaxies analysed by de Jong et al. (1984). The infrared sample is the IRAS mini-survey sample of Soifer et al. (1984). Care has been taken to treat the optical magnitudes of galaxies in both samples in the same way by attempting to correct the magnitudes of the mini-survey galaxies for systematic errors in the adopted Zwicky magnitudes and for galactic extinction.

It can be shown that the optically complete sample is representative for the local ($d \leq 100 \text{ Mpc}$) population of spiral galaxies. Thus, according to the data in Fig. 1 a, spirals emit on the average about 0.4 times as much energy in the infrared as in the visible.

The infrared sample is of course biased towards large infrared excesses. Fig. 1b shows that about 60% of the roughly 10,000 galaxies detected by IRAS emit more energy in the infrared than in the visible.

In the following I will refer loosely to galaxies which emit more than four times as much energy in the infrared as in the visible as "starburst" galaxies. Although they constitute less than 1% of all spiral galaxies, roughly 30% (about 3,000) of the galaxies detected by IRAS are starburst galaxies. The most extreme ones have recently been found to emit up to several hundred times more energy in the infrared than in the visible (Aaronson and Olszewski 1984).

The fraction of interacting galaxies among infrared galaxies is significantly higher than expected on the basis of random

statistics suggesting that (distant) encounters between galaxies may play an important role in triggering bursts of star formation.

Most starburst galaxies identified by IRAS are astronomically speaking "terra incognita". For most of them not even magnitudes are known. In order to study these galaxies in more detail we (T. de Jong, G. K. Miley, J. Lub and R. de Grijp) have started a ground-based follow-up programme at ESO.

First we selected a sample of southern starburst galaxies from the IRAS database in a roughly 1,000 square degree area of sky between RA = 10 and 14 hrs and between Dec = -40 and -60 degrees. Of these galaxies we are presently in the process of collecting optical spectra and CCD pictures. The spectra are taken at the 3.6 m telescope with the Boller and Chivens spectrograph using the IDS detector, and the CCD pictures will be taken at the 1.5 m Danish telescope. The spectra will enable us to determine redshifts and to study the ionized gas while the CCD pictures are required to accurately determine magnitudes and to investigate the distribution of the optical emission and the galaxy morphology.

In Fig. 2 we show spectra for two galaxies, IRAS 1027-395 (MCG 07-22-019) and IRAS 1318-314 (for infrared fluxes see IRAS Circular No. 13), that we obtained during a recent observing run at ESO. The spectra show strong narrow emission lines of Hydrogen ($H\alpha$ at λ 6563 and $H\beta$ at λ 4861), Nitrogen ([NII] at $\lambda\lambda$ 6548/6583), Oxygen ([OIII] at $\lambda\lambda$ 4959/5007) and Sulphur ([SII] at $\lambda\lambda$ 6716/6731). The lines are unresolved at the spectral resolution of about 13 \AA , corresponding to FWHM line widths less than 600 to 800 km s^{-1} . At this resolution the lines of the Nitrogen doublet show up as shoulders in the $H\alpha$ line and the [SII] doublet lines are blended together. The line ratios are very similar to those observed for a sample of galactic nuclei studied and appropriately referred to as "starburst" nuclei by Balzano (1983). The observed [OIII]/ $H\beta$ ratios are characteristic for regions of ionized gas excited by massive stars.

The two galaxies for which spectra are shown in Fig. 2 have redshifts of 0.0148 and 0.054, respectively, corresponding to distances of 89 and 230 Mpc (assuming a Hubble constant of $50 \text{ km s}^{-1} \text{ Mpc}^{-1}$). At these distances the $4'' \times 4''$ aperture with

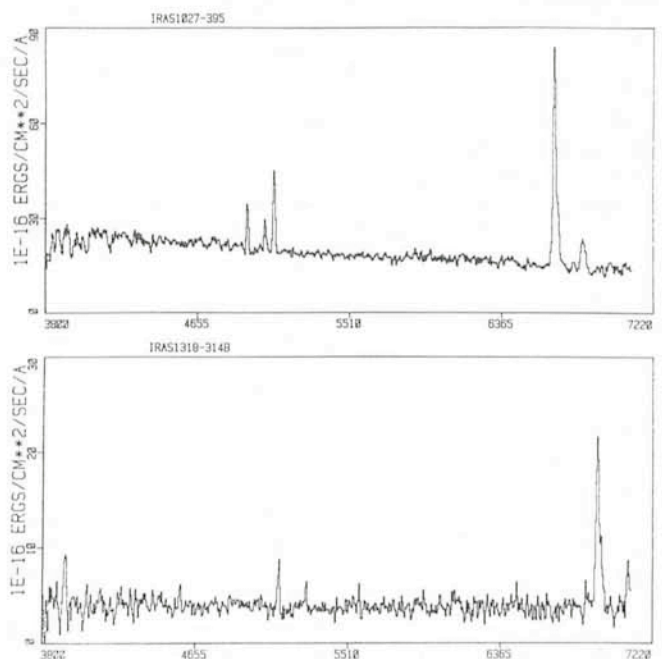


Fig. 2: IDS spectra of starburst galaxies taken with the Boller and Chivens spectrograph at the 3.6 m telescope by J. Lub and R. de Grijp.

which the spectra were taken, samples central regions with dimensions of 1.7×1.7 and 6.2×6.2 kpc².

A comparison of hydrogen recombination line intensities with infrared luminosities in principle allows the determination of the masses of the stars formed in a starburst. In practice such a comparison is complicated by the fact that the field of view of the IRAS detectors is much larger (of the order of several square arcminutes, see Table 1) than the aperture used for the spectral observations. To outline the kind of analysis that one would like to carry out on the basis of the available data, I present below a preliminary discussion of one of the galaxies shown in Fig. 2.

The galaxy associated with IRAS 1027-395 is listed in the *ESO/Uppsala Survey of the ESO (B) Atlas* (Lauberts 1982) as a disturbed SB galaxy situated in a cluster. It has optical dimensions of $66'' \times 48''$ corresponding to major and minor axes of 29 and 21 kpc at the adopted distance of 89 Mpc. The integrated blue magnitude and the optical colour in a 62 arcsecond aperture are given as $B = 13.69$ and $B-V = 0.56$. If we make standard assumptions to correct for reddening on the basis of the observed $H\alpha/H\beta$ line ratio and if we assume that the hydrogen line to continuum ratio is the same everywhere in the galaxy (a somewhat questionable assumption) we derive an integrated $H\alpha$ luminosity of 1.1×10^{-15} W m⁻² for IRAS 1027-395.

Based on the observed IRAS fluxes at 60 and 100 μ m we obtain an integrated infrared flux of 2.2×10^{-13} W m⁻² yielding a total galactic luminosity of $5.4 \times 10^{10} L_{\odot}$. Using data tabulated by Panagia (1973) we then find that the derived $H\alpha$ and total luminosities could be emitted by 2×10^6 B0V stars. Those stars have masses of about 15 M_{\odot} and main-sequence lifetimes of about 10^7 years so that we finally derive a rate of formation of massive stars of $\sim 3 M_{\odot} \text{ yr}^{-1}$. Although this result has been derived by assuming that all stars have the same mass it does not drastically change if we take into account that stars probably form with a mass spectrum that falls off steeply towards higher masses.

The derived star formation rate of massive stars may be a severe lower limit to the total rate of star formation. If the mass spectrum of stars born in a starburst has the same slope as observed for stars born in our own galaxy and if it extends down to about 0.1 solar mass the total starformation rate increases to about $30 M_{\odot} \text{ yr}^{-1}$. In that case a galaxy would use up most of its available interstellar gas during a starburst in a few hundred million years.

We hope that our study of an infrared complete sample of starburst galaxies at ESO will ultimately provide answers to such fundamental questions as:

- What triggers starbursts?
- How much mass is converted into stars during a starburst?
- How long does the starburst phase last?
- Do all galaxies at one time or another experience starbursts?
- Is there any connection between starburst and Seyfert galaxies (fuelling of central engines)?

Distribution and Access of IRAS Data in Europe

The remarks above may have sufficiently illustrated the need and the potential rewards of ground-based observational programmes to follow-up IRAS discoveries. In view of the huge size of the IRAS database and of the diversity of astronomical information that it contains this is a task that has to be taken up by the astronomical community at large. In order to get prepared for this in Europe we will briefly discuss a few relevant aspects of the future distribution and access of IRAS data in Europe.

TABLE 1. PROPERTIES OF IRAS SURVEY ARRAY DETECTORS

Central wavelength (μ m)	Wavelength range (μ m)	Detector field of view (arcminute ²)	Detector dwell time (s)	Sensitivity at SNR = 10 (Jy)
12	8.5 - 15	0.75×4.5	0.19	0.7
25	19 - 30	0.75×4.6	0.19	0.65
60	48 - 80	1.5×4.7	0.39	0.85
100	83 - 120	3.0×5.0	0.78	3.0

As presently foreseen the IRAS catalogues will be published in late November 1984. There will be two main catalogues and several so-called specialty catalogues. The main catalogues are:

1. The point source catalogue ($\sim 300,000$ sources)
2. The catalogue of small extended sources (present estimate: $\sim 50,000$ sources with sizes less than 8 arcminutes)

These will be available on tape and can be obtained in the US from the National Space Science Data Center and in Europe probably through the Centre de Données Stellaires in Strasbourg.

The paper editions of both catalogues consisting of about 5 volumes (about 3,000 pages) will come out some time in the spring of 1985.

To be able to access, display and analyse the IRAS catalogues we are presently setting up an IRAS data centre in Holland at the Astronomical Institute of the University of Amsterdam. A similar centre will be established at the Rutherford and Appleton Laboratories in Chilton, England.

At the IRAS centre in Amsterdam it will be possible to access the catalogues and to extract sources according to a variety of criteria. We have also acquired tape copies of most major astronomical catalogues for comparison with and further analysis of the IRAS data. We hope to have all software ready by November to be able to get going as soon as the IRAS catalogues become available.

Although set up initially for use by the Dutch astronomical community, European astronomers who would like to analyse IRAS data relevant for their own research programmes are invited to get in touch with the IRAS centre if they would like to make use of the facilities in Amsterdam. We will probably be able to accommodate a maximum of two visitors at any time. Interested colleagues should contact Dr. T. de Jong, Astronomical Institute Anton Pannekoek, University of Amsterdam, Roetersstraat 15, 1018 WB Amsterdam, The Netherlands.

References

- Aaronson, M., Olzsewski, E.W., 1984, *Nature* **309**, 414.
 Balzano, V.A., 1983, *Astrophys. J.* **268**, 602.
 de Jong, T., Clegg, P.E., Soifer, B.T., Rowan-Robinson, M., Habing, H.J., Houck, J.R., Aumann, H.H., Raimond, E., 1984 *Astrophys. J. (Letters)* **278**, L67.
 Lauberts, A., 1982, *The ESO/Uppsala Survey of the ESO (B) Atlas*.
 Panagia, N., 1973, *Astron. J.* **78**, 929.
 Soifer, B.T., Rowan-Robinson, M., Houck, J.R., de Jong, T., Neugebauer, G., Aumann, H.H., Beichmann, C.A., Boggess, N., Clegg, P.E., Emerson, J.P., Gillett, F.C., Habing, H.J., Hauser, M.G., Low, F.J., Miley, G., Young, E., 1984, *Astrophys. J. (Letters)* **278**, L71.

The proceedings of the First ESO/CERN Symposium on

"Large-Scale Structure of the Universe, Cosmology and Fundamental Physics"

held at CERN in Geneva from 21 to 25 November 1983, have now been published. The 456-page volume costs DM 35,- and can be obtained from ESO, Karl-Schwarzschild-Str. 2, D-8046 Garching, Federal Republic of Germany.

Observations of Comet P/Crommelin at ESO in the Near Infrared Range

T. Encrenaz, *Observatoire de Paris-Meudon, France*

D. Engels, *Universitäts-Sternwarte, Bonn, F.R.G., and J. Krautter, ESO*

Near infrared photometry has been used for a long time for cometary observations (Ney, 1982). The 1-3 μ spectral range is adequate for observing the solar light scattered by the particles, since there is no strong gaseous signature expected in this region (except in some cases a weak possible contribution from a CN band at 1.1 μ). It has been shown that photometric measurements in the J, H and K filters are useful for deriving constraints upon the nature and the distribution of the cometary dust (Campins and Hanner, 1982).

In order to prepare as well as possible the campaign of Comet Halley's ground-based observations, the International Halley Watch (IHW) has initiated a "trial run" on comet P/Crommelin. This periodic comet, which comes back every 27.7 years, arrived at perihelion on February 20, 1984, with a heliocentric distance of 0.73 AU, and presented for ground-based observers the same overall configuration as expected for the 1986 apparition of Comet P/Halley. Apart from its trajectory and expected visual magnitude, little was known on P/Crommelin itself, and nothing about its dust composition and distribution, before its 1984 apparition.

An observing campaign was organized at ESO for infrared observations of P/Crommelin, from January to March 1984, involving Dr. Drechsel (Dr.-Reimis-Sternwarte, Bamberg), Dr. Engels (Universitäts-Sternwarte, Bonn) and Dr. Krautter (ESO, Garching). The equipment used were the ESO InSb infrared photometers at the 1 m telescope and the 3.6 m telescope.

The first attempts to observe the comet in January 1984 were unsuccessful due to the low brightness of the comet.

Comet P/Crommelin was observed on March 19, 1984 at the 1 m telescope. The diaphragm was 30 arcsec, with a throw of 60 arcsec in east-west direction. Calibration was achieved with the standard star HR 1136 ($J = 1.98$; $H = 1.53$; $K = 1.44$). The air mass ranged between 1.6 and 1.9 for both the comet and the star. Results for P/Crommelin are $J = 11.4$, $H = 11.0$, $K = 11.0$ with an uncertainty of 0.1 for each filter. P/Crommelin was also observed in the J filter at the 3.6 m telescope on March 20, with a 7.5 arcsec diaphragm and a throw of 15 arcsec in east-west direction. A magnitude of 13.4 was measured, possibly overestimated.

Fig. 1 shows the quantities J-H and H-K plotted as functions of the scattering angle θ . The curves shown in Fig. 1 are theoretical curves computed by Veeder and Hanner (1981) and Campins and Hanner (1982), from Mie scattering theory, for various types of grains, assuming the Sekanina-Miller distribution (Sekanina and Miller, 1973). Among the types of grains considered are dirty ice grains, silicate grains and magnetite, a typical absorbing material present in meteorites. Our result tends to eliminate the presence of absorbing grains, as shown by the magnetite curve which corresponds to a colour redder than our result.

Icy grain models seem also incompatible with our measurement, in particular because they would lead to a (J-H) colour bluer than observed. This result is not surprising, since our diaphragm was large (30 arcsec, which corresponds to 18,000 km in the coma at the time of observation); moreover, the comet's heliocentric distance was 0.9 AU at that time, and icy grains could not survive long enough to make a significant contribution to the cometary flux. In conclusion, our measurement tends to support a silicate composition of micron-sized

particles, from both the (J-H) and (H-K) colours. P/Crommelin would thus have a dust composition different from P/Meier, P/Tuttle and P/Stefan-Oterma, for which a mixture of absorbing particles and irregular silicate grains has been suggested (Veeder and Hanner, 1981; Campins and Hanner, 1982). However, it has to be mentioned that our conclusion is not unambiguous, because different kinds of grains could eventually lead to the same (J-H) and (H-K) colours, so that the solution is not unique.

Other measurements of Comet P/Crommelin were achieved in the same filters at the UKIRT telescope on March 27 (Eaton and Zarnecki, 1984) with a 6".2 aperture and at the IRTF telescope (Hanner and Knacke, 1984) on March 31, with a 7".1 aperture. The corresponding (J-H) and (H-K) values are also plotted in Fig. 1.

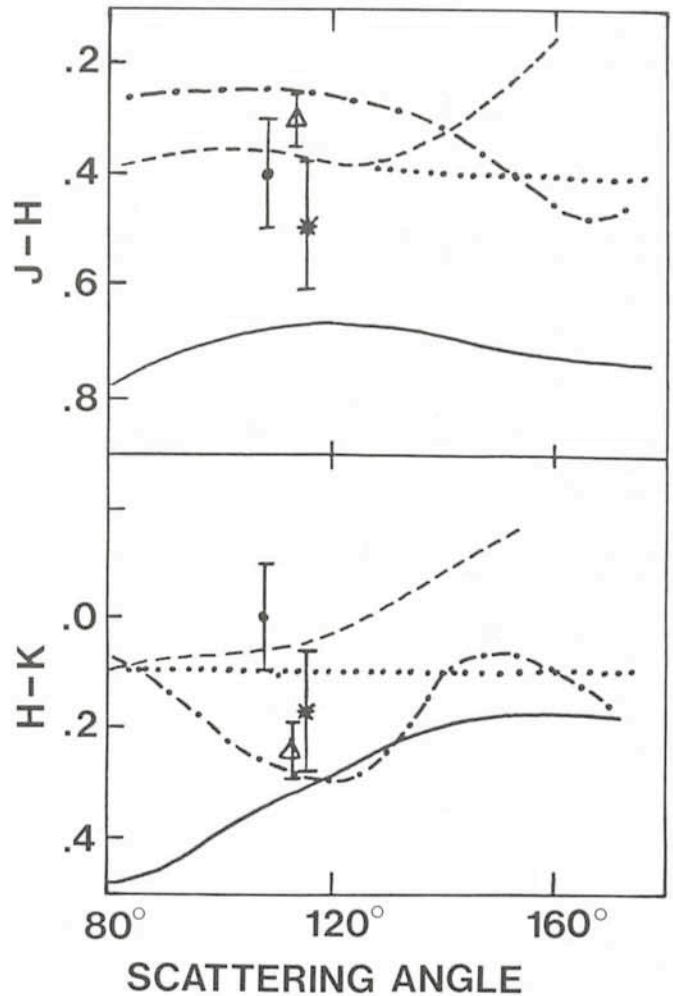


Fig. 1: (J-H) and (H-K) diagrams as functions of the scattering angle. The curves have been calculated by Veeder and Hanner (1981) and Campins and Hanner (1982). Solid curves: magnetite grains (absorbing material); dashed curves: silicate grains; dotted curves: irregular silicate grains; dash-dot curves: 20 μ slightly dirty ice grains, $n'' = 0.002$ (Campins and Hanner, 1982). The observations are from this paper (black point), Eaton and Zarnecki (triangle) and Hanner and Knacke (star).

Assuming the dust composition did not change between March 19 and March 31, and assuming the dust composition to be homogeneous within the 30 arcsec diaphragm, we can compare our (J-H) and (H-K) values to the values derived from the two other sets of observations. The agreement with Hanner and Knacke's data is reasonably good; in the case of Eaton and Zarnecki's measurement, there is some discrepancy for the (H-K) value. A possible explanation could be that Eaton and Zarnecki's results, obtained in a smaller diaphragm (6.2 arcsec) imply a contribution due to dirty ice grains; however, we would expect in this case the same behaviour in Hanner and Knacke's results, which do not appear for (J-H); moreover, the presence of a significant ice contribution in a sphere of about 3,500 km is not expected at a heliocentric distance smaller than 1 AU (Campins and Hanner, 1982). The final conclusion which can be derived from the three sets of measurements is that there is no evidence for absorbing particles in the dust composition of P/Crommelin.

Another information which could be derived from the data comparison concerns the spatial distribution of dust, using the fact that observations were performed in different diaphragms. If the dust is assumed to be ejected radially, isotropically, with a constant velocity, then the dust density at a given distance r from the nucleus varies as r^{-2} , and the number of particles inside a diaphragm of radius δ increases linearly with δ . The observed flux, either in the scattered component or in the thermal component (since the medium is optically thin) is proportional to the number of particles and thus proportional to δ . This linearity has been checked by Becklin and Westphal (1966) on Comet Ikeya-Seki for diaphragms ranging from 20 to 80 arcsec. For smaller apertures, the linear law might be altered by collisional effects or anisotropic dust ejection. However, in our case, this study requires that we are able to monitor accurately the intrinsic variations of the comet's magnitude between March 19 and March 31. The

geocentric distance of P/Crommelin remained constant within 2% between these dates; in contrast, the visual magnitude changed rapidly, not only because of the heliocentric distance, but also because of intrinsic cometary activity. Information upon the M_V curve is available from Marsden (1984) but a more complete analysis, involving more data, would be useful.

In conclusion, the preliminary results reported here show the potential interest of near IR photometry for studying cometary dust, especially for future observations of Comet P/Halley. Extension towards higher wavelengths will be necessary to obtain more constraints upon the nature and size of the dust particles. A systematic study with different size diaphragms should allow a good determination of the dust density distribution.

Acknowledgements

We thank Dr. Drechsel for his participation in the observing campaign. We are grateful to Drs. Hanner, Knacke, Eaton and Zarnecki for giving us access to unpublished data. We thank Dr. Festou for helpful comments on this paper.

References

- Becklin, E., and Westphal, J. 1966. *Astrophys. J.* **145**, 445.
 Campins, H., and Hanner, M. 1982. In *Comets*, L. Wilkening, ed. Univ. of Arizona Press.
 Eaton, N., and Zarnecki, J. 1984. In "Infrared Observations of P/Crommelin in Europe", *IHW Newsletter* n°5, Jet Propulsion Laboratories.
 Hanner, M., and Knacke, R. 1984. Private communication.
 Marsden, B.G. 1984. IAU Circular n° 3930 (March 26, 1984) and IAU Circular n° 3938 (April 12, 1984).
 Ney, E. 1982. In *Comets*, L. Wilkening, ed. Univ. of Arizona Press.
 Sekanina, Z., and Miller, F. 1973. *Science* **179**, 565.

Line Profile Shapes in Optical H II Regions

H. W. Yorke, *Universitäts-Sternwarte, Göttingen, F.R.G.*

Some of the most spectacular astronomical photographs and favourite subjects for popular astronomical slide shows are colour pictures of H II regions. Probably every astronomer, both amateur and professional, is familiar with the nebula in Orion, M 42. Shaped like an opened fan, this well-known H II region ("H II" is the technical term for ionized hydrogen) appears to be yellow in its bright core and fades out to red and then a faint bluish hue towards the outer perimeter. Of course, the exact colours and size of the Orion Nebula, M 42, is dependent on the type of colour film used and the amount of light gathered. Longer exposure times tend to make the nebula appear larger, expanding outward in the direction of the fan's perimeter. Short exposures of the nebula (or using the eye instead of film) reveal the presence of four bright stars in its core, the "Trapezium", so named because of their relative geometrical positions. These stars cannot be seen on long-exposure pictures, because the light from the nebular core saturates the film.

H II Regions – the Strömgren Theory

On the theoretical side, much has been learned about the nature of H II regions such as the Orion Nebula. An important theoretical breakthrough came when Strömgren, in 1939,

published his paper on "The Physical State of Interstellar Hydrogen" (1). Strömgren recognized that ionized hydrogen at typical interstellar densities is transparent to the extreme ultraviolet radiation from hot O and B stars, such as the Trapezium stars in the Orion Nebula. Neutral atomic hydrogen on the other hand should be very opaque to this radiation at wavelengths shorter than $\lambda = 912 \text{ \AA}$. This critical wavelength corresponds to the ultraviolet photon energy necessary to ionize the hydrogen atom, expelling its single electron. The process of absorbing ultraviolet photons and ionizing hydrogen changes the material originally opaque to ultraviolet light to material transparent to subsequent ultraviolet photons. If it were not for the fact that the electrons and protons in an ionized gas occasionally recombine to form atomic hydrogen, all the material in the Milky Way Galaxy could be converted into ionized gas by fewer than 10^4 O5 stars. The process of occasional recombination in an ionized gas makes this gas only partially transparent to the hydrogen-ionizing ultraviolet photons. Thus, an H II region, which is produced whenever a hot O or B star is embedded in a cloud of neutral material, has only a finite extent.

The equilibrium size of the ionized region can be calculated in an approximate way by equating the total number of recombinations per second in a fully ionized gas with the total

number of hydrogen-ionizing ultraviolet photons per second emitted by the embedded exciting star (or stars). A more detailed calculation by Strömgren of the ionization/recombination balance of hydrogen at each point in the nebula was thus able to determine its ionization structure. Such a nebula is almost fully ionized in its interior; the degree of ionization x (defined as the ratio of electron density to numerical hydrogen density) drops off from $x = 1$ (fully ionized) to almost $x = 0$ (fully neutral) within a narrow transition zone known as the ionization front.

Strömgren's simple calculation was very successful in explaining the occurrence of optical H II regions. We now know that whenever dust is present sufficiently close to the hot exciting star(s), the nebula will appear to be yellow—due to starlight scattered off the surfaces of the dust particles. The reddish appearance is due to light produced by the process of recombination, one of the most prominent electronic transitions within a newly recombined hydrogen atom being the $n = 3$ to $n = 2$ ($H\alpha$ transition). The $H\alpha$ line is found in the red part of the spectrum ($\lambda = 6563 \text{ \AA}$). In fact, by summing up the number of $H\alpha$ photons emitted per second by the nebulae, it is possible to determine the rate at which recombinations occur and thus the rate at which the exciting stars emit their hydrogen-ionizing ultraviolet photons. Knowing this and something about the densities of gas and dust within the nebula it is possible to construct detailed nebular "models" which match the line strengths of various hydrogen and helium lines and the many "forbidden" lines ("forbidden" only because they do obey the selection rules for simple changes of electronic states) of elements such as oxygen, nitrogen, silicon or sulfur. Actually, the analysis of data works in reverse: from measured line ratios one determines the density and temperature of the ionized gas. One normally has many independent methods at one's disposal for determining nebular conditions, so that internal consistency checks are possible. Combining radio and infrared data with optical and ultraviolet spectra it is possible to make sophisticated analyses of many H II regions.

Progress in the study of optical H II regions has not only been made in the detailed reconstruction of the ionization structure of hydrogen, helium and many other elements in Strömgren-type models, but also in their expected evolution and kinematic properties. Even in his 1939 paper, Strömgren was aware that the hydrogen-ionizing photons have more energy than necessary to merely ionize hydrogen. As shown later by Spitzer (2) this energy excess causes the H II region to heat up to a temperature higher than the surrounding neutral gas. Confirming theoretical expectations, interpretations of typical line ratios yield a fairly uniform temperature of about $T = 10^4 \text{ K}$ in the ionized gas, whereas the neutral gas temperature is generally less than 100 K. One can therefore expect the hot ionized region to expand under the influence of its own internal pressure.

Expansion Models of H II Regions

The expansion motion of the ionized gas will affect the shapes of the emission lines originating in the H II region. A photon emitted from an atom moving away from (toward) the observer will have a wavelength which is longer (shorter) than that expected from an atom at rest. The photon is "red- (blue)-shifted". Observations of these line profile shapes can thus provide an observational test of the kinematic motions predicted by theoretical evolutionary models. Let us first consider three simple kinematic models and their expected $H\alpha$ and forbidden line profiles.

The first model we will consider is a homogeneous sphere of ionized gas at rest. Such a situation is possible immediately after an ionizing source is suddenly "turned on" in a constant

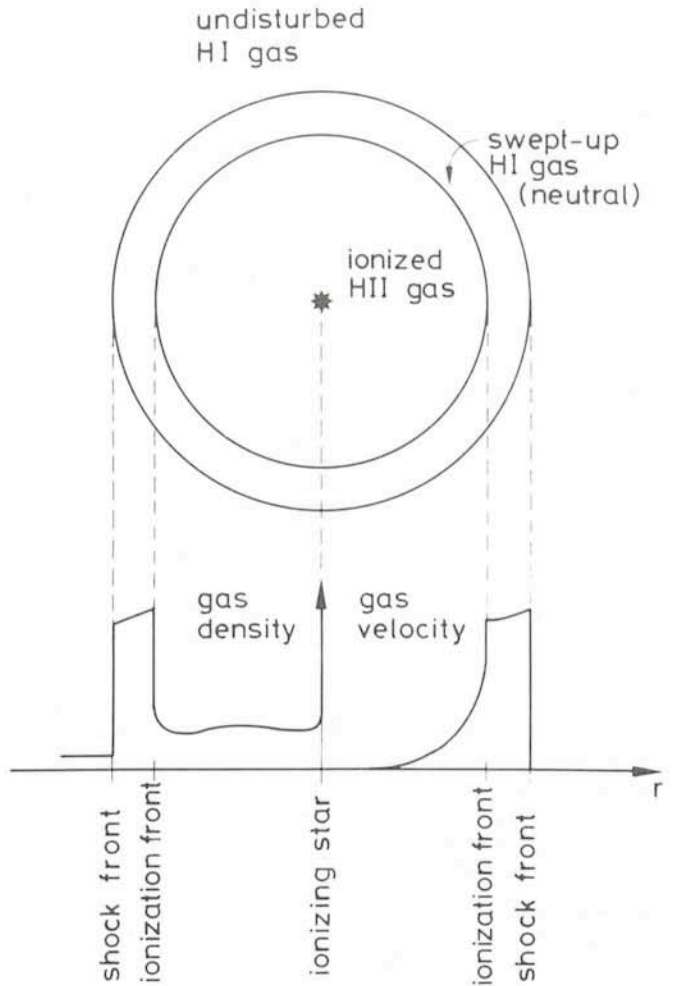


Fig. 1: Schematic representation of the density and velocity structure of a spherically symmetric, expanding H II region, initially in a constant density medium. The degree of ionization (not shown) would appear to change discontinuously from $x = 1$ on the inside to $x = 0$ at the ionization front on the scale of the drawing. The maximum expansion velocity is about 10 km/s, i. e. the sound speed of the ionized gas.

density neutral medium at rest, before the hot ionized gas has had time to expand.

The second idealized situation we will analyse is depicted schematically in Fig. 1. The ionized gas has attained expansion velocities up to 10 km/s. This velocity is much higher than the sound velocity of the surrounding neutral medium and a shock front forms here. Dense, cool material piles up in front of the ionization front. An earth-bound analogy (admittedly somewhat contrived) is a snowplow with a heated blade, piling up the snow in front of it, while at the same time melting the piled up snow in contact with its hot blade. If the snowplow moves fast enough, more snow can be piled up than melted. The expanding H II region usually does move fast enough that more neutral material is piled up into a dense shell than can be ionized away at the inner boundary of the shell. This type of expansion model has been dealt with extensively in the literature. We shall call it the "classical" expansion model.

An alternative to the "classical" expansion is the so-called "champagne" model (Fig. 2), recently proposed by Tenorio-Tagle (3), which has also been dealt with extensively since 1979. In this model a classically expanding H II region embedded in a molecular cloud encounters the sudden change of density at the cloud's edge. The ionized material is accelerated to a relatively high velocity (up to several times its sound speed) in a direction away from the cloud, because little resistance to expansion is offered by the low density material.

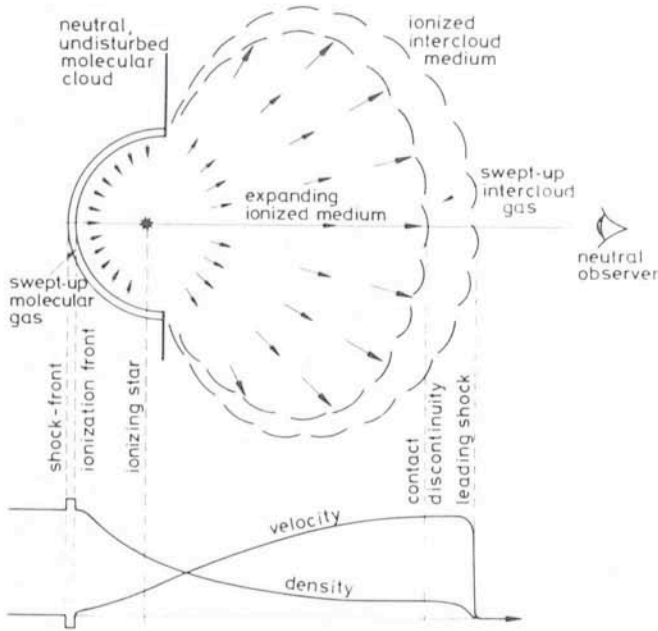


Fig. 2: Schematic representation of the champagne model for H II region evolution. The H II region appears as a "blister" on the surface of a molecular cloud. It is produced by an O star which has formed inside the molecular cloud and which subsequently erodes out a cavity by ionization. The hot, ionized gas seeks the path of least resistance and expands preferentially away from the cloud, reaching velocities of over 30 km/sec. This high velocity gas is of low density and is therefore difficult to observe directly. The density and velocity structure along a single line of sight, i.e. perpendicular to the surface of the molecular cloud, is shown.

The ionized material from the molecular cloud "fans" out, its density decreases as it moves further away from the cloud. A champagne-type flow also develops when an ionizing star is located outside (but not too far) from a molecular cloud. The fan-shaped Orion Nebula is typical for what is to be expected from an H II region during its champagne phase and bears little resemblance to what the classical expansion model would predict.

Predictions of Line Profile Shapes

The line profile shapes for hydrogen and oxygen to be expected from each type of model is shown schematically in Fig. 3. In Fig. 4 the results of a single numerical calculation of champagne flow line profiles is given. A variety of line shapes are possible with the champagne model, although the line-of-sight positions close to the ionizing source are only slightly asymmetric and the line centres are only slightly shifted with respect to zero velocity. Since these positions have the strongest emission lines, the total net line fluxes from the nebulae resemble the schematic profiles in Fig. 3.

It is interesting to note that the multiple components displayed in some of the oxygen spectra cannot be seen in the hydrogen spectra. The reason for this should be clear. Due to its lower atomic mass, the hydrogen line will be thermally broadened to a greater degree. Thus, multiple velocity components blend together. Another interesting feature of the theoretical results shown in Fig. 4 is the fact that the multiple velocity components did not arise from several different "blobs" in the champagne flow. Instead, the projected component of ionized gas velocity along a given line-of-sight changed more slowly in some parts of the nebula. This led to higher

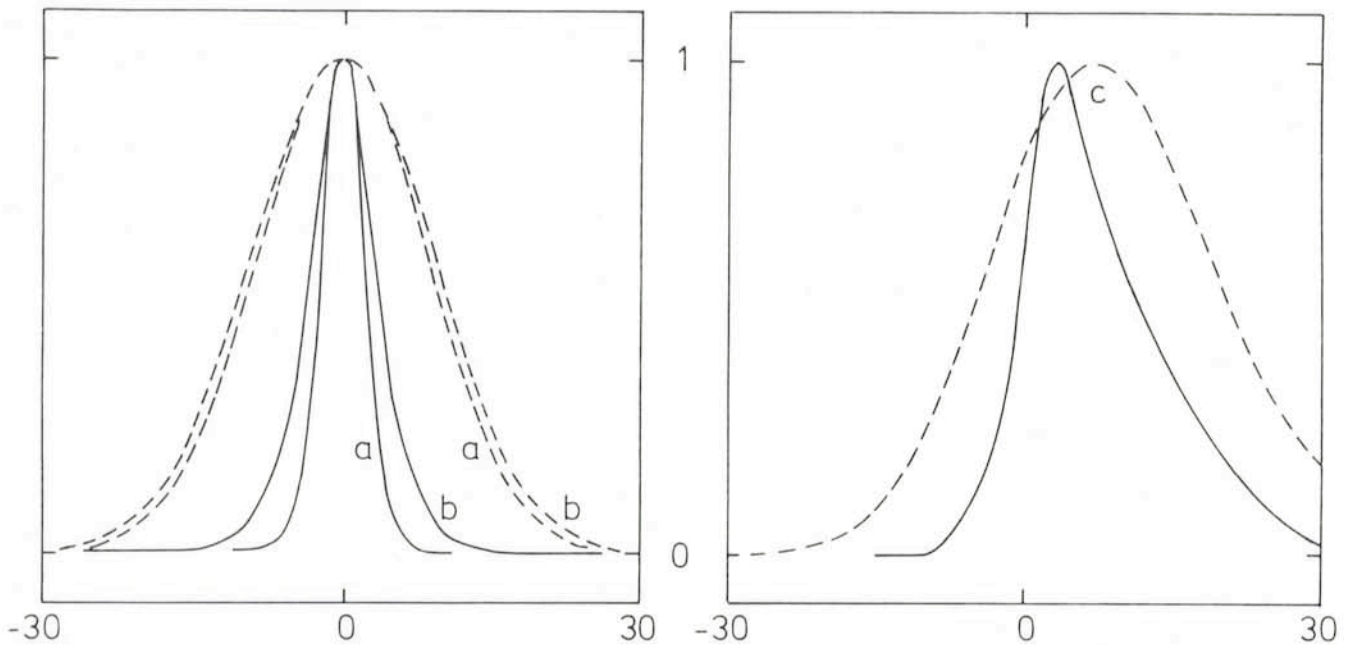


Fig. 3: Normalized line profiles predicted by H II region expansion models (see text). The dotted curves are for hydrogen, the solid curves for oxygen. The blue part of the spectrum is to the right, corresponding to positive velocities (30 km/s).

(a) No expansion: the line profiles are "smeared out" by the thermal motions of the emitting atoms and ions. The width of such thermally broadened lines depends on both the gas temperature (here assumed constant, $T = 10^4$ K) and the mass of the emitting particle.

(b) Classical expansion model (see Fig. 1, text): the line profiles are only slightly broader than in (a).

(c) Champagne model (see Fig. 2, text): depending on viewing angle, spatial resolution and position within the nebula a variety of line shapes can be expected (see also Fig. 4). In general one can expect the line centre to be shifted by several km/s and the profiles to be asymmetric by varying degrees. Note that for such asymmetric profiles the maximum line intensity for hydrogen and oxygen may appear to be shifted with respect to one another.

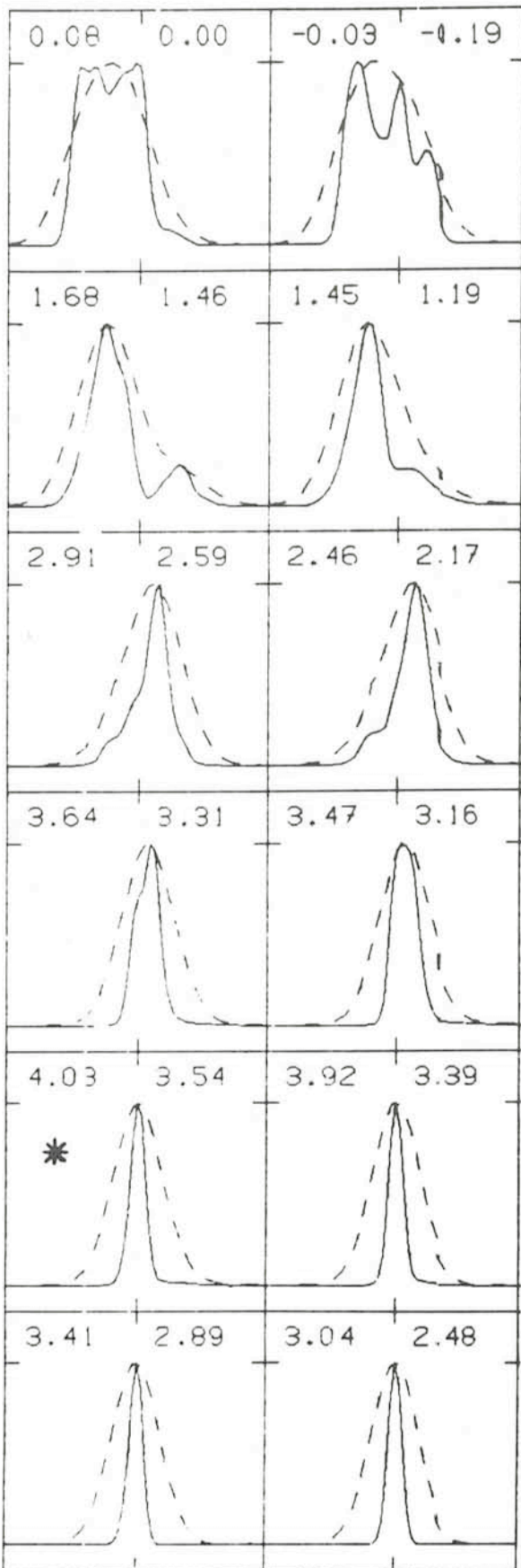


Fig. 4: Normalized line profiles of oxygen (solid curves) and hydrogen (dotted curves) at selected positions in an H II region during the champagne phase (4). The velocity scale runs from -60 km/s to $+60$ km/s. The logarithm of the line strengths for oxygen (hydrogen) are given in the upper left (right) corner of each box. The "starred" box displays the profiles at the line-of-sight centred on the projected position of the ionizing source. More details are given in (4).

integrated column densities at some parts of the spectrum than at others. Two extreme (theoretical) cases leading to line splitting are shown in Fig. 5. Thus, the common interpretation of line splitting in H II regions, multiple filaments or sheets of high density ionized material, should be viewed with greater skepticism.

Observations of M 8, the Lagoon Nebula

The Lagoon Nebula, an H II region, and its associated star cluster, NGC 6530, lie near the inner edge of the Sagittarius spiral arm, about 6,000 light-years from the solar system. Three bright O stars (HD 165052, 9 Sagittarii, Herschel 36) are probably members of the star cluster and the main sources of ionizing photons for the nebula. Lynde and O'Neil (5) interpreted their spectroscopic observations of M 8 as four H II regions, one surrounding each of the O stars with the exception of the bright Hourglass Nebula which is located between Herschel 36 and the associated molecular cloud. Parameters for each of these H II regions are given in Table 1. The relative locations of these H II regions, one behind the other in the order given in Table 1 (the Hourglass Nebula is furthest from the earth and closest to the background molecular cloud), is consistent with the interpretation of Lada and co-workers (6) that M 8 is an H II blister on the surface of the molecular cloud.

TABLE 1: THE H II REGIONS COMPOSING M 8 (5)

Star	Size in light-years	Gas density atoms/cm ³	Effective temperature of star
HD 165052	90	1	37,500
9 Sgr	9.6	100	37,500
H 36	3.3	250	35,000
Hourglass	1.0	4,000	35,000

The interpretation of M 8 as four superimposed constant density H II regions, each with a very different gas density and size, seems to be very unlikely. Most likely M 8 is a fan-shaped champagne flow with a continuously varying gas density which is being viewed face-on. The O stars are probably at different distances from the molecular cloud — as suggested by Lynds and O'Neil — so that the resulting champagne flow is somewhat more complicated than that predicted by the simplest models with a single ionizing source. In spite of this, M 8 should be an excellent candidate for studying and comparing line profile shapes with model predictions.

The author was allotted 12 nights of observing time with ESO's 1.4 m Coudé Auxiliary Telescope (CAT) in August 1983. Poor weather conditions (high winds and clouds) resulted in a loss of about two thirds of the observing time. Even in the remaining third, observing was sometimes restricted to inconvenient areas of the sky. It was possible to keep the CAT dome open for a full night only once. The other eleven (exasperating) nights were spent opening and closing the dome, watching the wind meter and keeping an eye on the humidity. Still, a number of high resolution spectra ($10^5 \pm 3$ km/s) were obtained in the spectral regions $\lambda\lambda 6535-6590$ and $\lambda\lambda 4990-5025$ at several selected positions in the M 8 region. Detailed line profiles of H_α, [N II] 6548, 6584 and [O III] 5007 were extracted from the data. Some of these are shown in Fig. 6.

There are several features of the spectra shown in Fig. 6 and other spectra taken but not shown here which can be termed "typical" for champagne-type flows. First of all, the lines are much broader than the thermal width; a radial velocity dispersion of $10-20$ km s⁻¹ can be surmised after removal of thermal and instrumental broadening. Secondly, indications of multi-

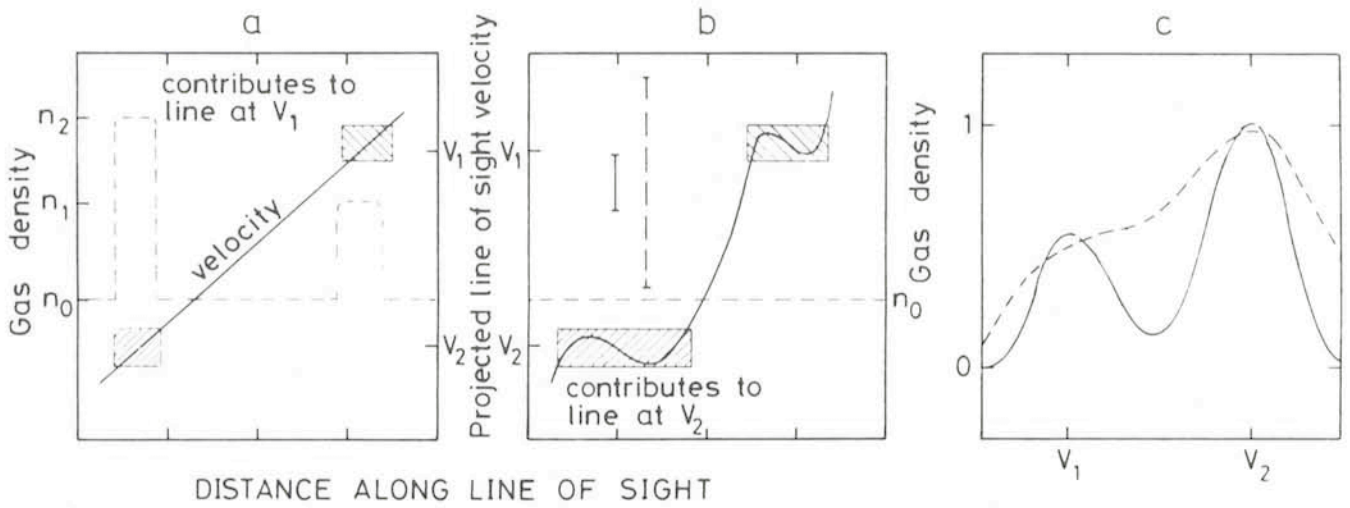


Fig. 5: Two hypothetical situations leading to line splitting. The density and gas velocity are depicted as dashed and solid curves, respectively, in (a) and (b).

- (a) Two high density clumps of material lying along the line-of-sight of the observer have different radial velocities, v_1 and v_2 .
 (b) The variation of velocity in a constant density medium leads to long integration paths (and high column densities) at certain wavelengths. The error bars show amounts of thermal broadening for oxygen (solid bar) and hydrogen (dashed bar).
 (c) Resultant line profiles for cases (a) and (b) (schematic). The hatched boxes in (a) and (b) show the projected velocities contributing to the emission at v_1 and v_2 . The solid curve (for example [N II] or [O II] forbidden lines) can show splitting, whereas the hydrogen line profile (dashed curve) may show little or no indication splitting.

ple components and marked asymmetries are present, which can be most clearly seen in the [N II] and [O III] lines. The lines' complexity increases as line-of-sight positions in the peripheral zones (away from the Hourglass Nebula) are considered.

There is a surprising feature which is barely discernable in the H_α profile of Fig. 6b. This line displays extended wings out to -38 km s^{-1} blue-shifted with respect to the position of maximum and $+58 \text{ km s}^{-1}$ (red-shifted) at an intensity level of a few per cent of the maximum. This effect will be difficult to explain by a simple champagne flow alone. If M 8 is a "blister" on the surface of the molecular cloud, expanding towards us, then why is such a large red-shifted contribution (implying velocities $\sim 50 \text{ km s}^{-1}$ away from the observer) present? Scattering by moving dust can broaden spectral lines. A photon emitted away from us by an atom moving towards at 20 km s^{-1}

which is then scattered towards us by a dust particle moving away from us at 20 km s^{-1} will appear to be red-shifted by 60 km s^{-1} . How likely is this situation? Probably it is not too likely. The interpretation of M 8 will require more detailed models. The observational results from M 8 and their interpretation will be the subject of a forthcoming paper.

References

- (1) Strömgren, B.: 1939, *Astrophys. J.* **89**, 526.
- (2) Spitzer, L.: 1949, *Astrophys. J.* **107**, 6.
- (3) Tenorio-Tagle, G.: 1979, *Astron. Astrophys.* **71**, 59.
- (4) Yorke, H.W., Tenorio-Tagle, G., Bodenheimer, P.: 1984, *Astron. Astrophys.* **243** (in press).
- (5) Lynds, B.T., O'Neil, E.J.: 1982, *Astrophys. J.* **263**, 130.
- (6) Lada, C.J., Gull, T.R., Gottlieb, C.A., Gottlieb, E.W.: 1976, *Astrophys. J.* **203**, 159.

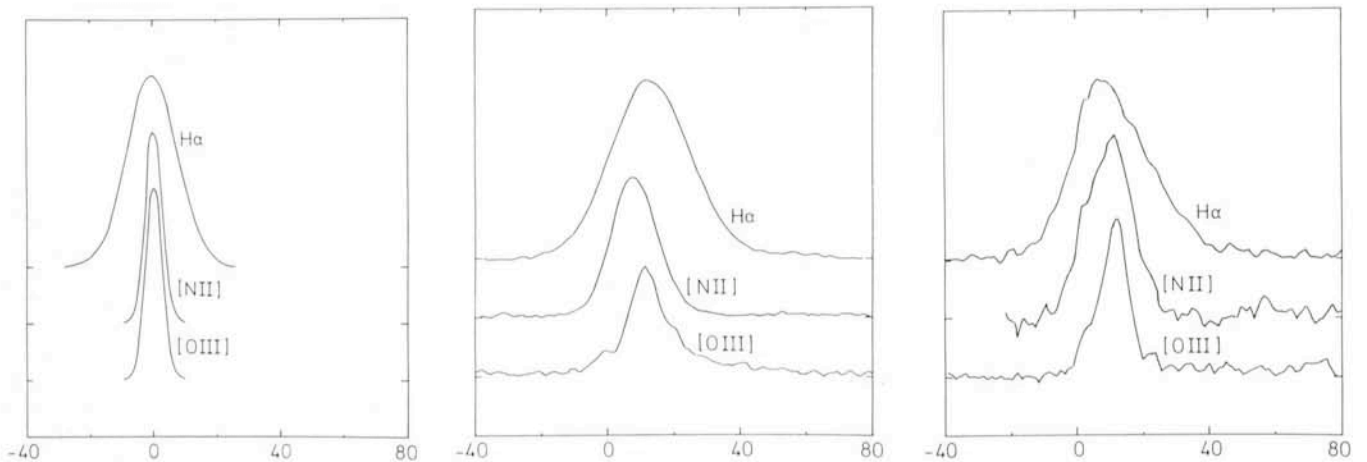


Fig. 6: Line profiles of H_α , [N II] 6584 and [O III] 5007. Zero velocity has been arbitrarily set to reference frame of the earth.
 (a) Theoretical profiles expected from a $T = 10^4 \text{ K}$ ionized gas at rest. The profiles have been spread out by the measured Coudé Echelle Spectrograph's instrument profile at a spectral resolution of 10^5 (corresponding to 3 m s^{-1}).
 (b) Measured profiles at a position in the north part of the Hourglass Nebula. The intensity scale is in arbitrary units.
 (c) Measured profiles at a position 86 arcseconds to the north-east of the Hourglass Nebula. The net intensity of the lines at this position is about a factor of four lower than those of 6b).

IDS Spectroscopy of Faint Emission-Line Objects

I. Lundström and B. Stenholm, Lund Observatory, Sweden

Introduction

During the last decades we have seen the advent of new technology detectors, which no longer contain a photographic emulsion as a last step. These detectors, such as the IDS (Image Dissector Scanner) for spectroscopic work and the CCD (Charge-Coupled Device) for field imaging, produce digitized data, which can easily be stored on a disk or on a magnetic tape.

In this short article we will report some of our experiences of the IDS devices of ESO. The IDS at the 3.6 m telescope was taken into use in 1978 and the one at the 1.52 m telescope followed two years later. Although we have had the opportunity to use both instruments we will concentrate on a programme performed exclusively with the 1.52 m telescope.

The Instrument

The IDS is mounted on a conventional B & C spectrograph. The spectral images fall on an image tube arrangement which ends with an output phosphor. This phosphor, in which an intensified spectral image is formed, is "read" by a scanning device dividing the one-dimensional image into 2,048 pixels. The reading-out procedure goes on continuously during the observation, one cycle being about 1 ms. The building-up of the spectrum can be followed by the observer on a screen, and it can thus immediately be checked that the correct object is observed, provided a rough spectral type is known. This property has been very advantageous in the programme described below.

The IDS actually sees two windows in the decker of the spectrograph simultaneously. One window contains the object and the sky, the other the sky only. In the reduction process these two windows are subtracted from each other, producing, in the ideal case, a clean spectrum of the observed object. The data are stored on disk (and normally copied on tape) ready for reduction with the IHAP (Image Handling and Processing) system, either directly at La Silla or at a later date at ESO Garching or some other astronomical institute in Europe where the IHAP system is available.

The IDS is a very efficient tool for low-resolution spectroscopy of faint emission-line objects. The advantages we particularly appreciate are:

- high sensitivity;
- continuous watching during the observation;
- efficient reduction via the IHAP system.

There are, however, also some disadvantages. The only one that is really important for the present programme is the very low sensitivity of the IDS in the violet and ultraviolet, which effectively hinders the detection of spectral features below ≈ 400 nm.

The Programme

The programme described here concerns low-resolution spectroscopy of faint emission-line objects in the southern Milky Way. Originally, the object list was based on objects found in an objective prism survey near the galactic plane ($-7^\circ < b < 7^\circ$) in the longitude intervals $210^\circ < l < 260^\circ$ and $0^\circ < l < 40^\circ$. We were particularly interested to find new Wolf-Rayet star candidates, but all kinds of emission-line objects were noted. In this way about 130 objects were found, many noted in earlier surveys but normally lacking reliable

classification. However, several of the objects were not previously known as emission-line objects. We later decided to include also a number of objects from other discovery lists and catalogues. Many of these objects were near the detection limit of the original surveys, and their nature was in many cases unclear. It is, for example, sometimes impossible to discern on an objective-prism plate between an emission-line object, where only the most intense features show up as a faint spot, from a plate flaw of regular shape. In other cases, the lack of a wavelength calibration makes it difficult to correctly identify the object on a direct plate and can also lead to incorrect line identifications.

The IDS is an ideal instrument for observing emission-line objects with uncertain identifications. One can test without much loss of observing time several objects in the field and in this way make sure that only the correct object is fully exposed. Moreover, faint M stars are sometimes mistaken for emission-line objects. Also in this case the error can be quickly detected, thus saving valuable observing time. The high sensitivity of the IDS also makes it possible to get sufficiently good spectrograms (at least of the line spectrum) with reasonable exposure times even for very faint objects.

Some Preliminary Results

Our programme has been allotted observing time during three different periods. At the two first occasions, in June 1982 and May 1983, the weather was not good and only a very limited number of objects were observed. Nevertheless, one part of the programme, spectroscopy of faint WR stars, was successfully completed during these two periods (Lundström and Stenholm, 1984). However, during the third period, in April 1984, the weather conditions were excellent and we managed to complete the whole programme. Altogether we have collected spectrograms of about 160 emission-line objects in the wavelength region 400–750 nm with a dispersion of 17 nm/mm. The majority of the objects are planetary nebulae, but there are also numerous symbiotic stars, Be and Bep stars, compact HII regions and a number of objects that cannot easily be put into these categories. Only one new WR star has been found (see below), an unexpectedly low number. The material has still not been entirely reduced and we will give here only a few examples of the various types of objects encountered.



Fig. 1: The observers desk at the 1.52 m telescope with the IDS control equipment.

WR Stars

There are two WR stars in our material. One of these, PK 309 $-4^{\circ}1$ (= He 2-99) was previously classified as a planetary nebula with a WC9 star as central star (Jones, 1969). Our observations confirm this. The other example is PK 337 $+1^{\circ}1$, which appears as No. 67 in the list of misclassified or doubtfully classified planetary nebulae by Sanduleak (1976). The reason for this was the finding by Webster (1969), who from photometric observations concluded that the normally strong [O III] line at 500.7 nm seemed to be absent in PK 337 $+1^{\circ}1$. A spectrogram of this object is shown in Fig. 2 (upper). The strongest lines are H α and the [N II] doublet at 654.8 and 658.4 nm. H β and [N II] at 575.5 nm are also narrow and relatively strong. The [N II] line is surrounded with broader features, which also can be found near 465 nm and in the red end of the spectrum.

A so-called "high-cut" version of the spectrum (Fig. 2) reveals that these features are due to lines typical for a Wolf-Rayet star of type WC9. In fact the object is very similar to PK 309 $-4^{\circ}1$, which also has very weak [O III] lines, a property that is normal for planetary nebulae with late WC type central stars. The most natural interpretation is to regard also PK 337 $+1^{\circ}1$ as a planetary nebula with a WC9 type central star.

However, the line widths of the emission lines are normally smaller for planetary nuclei of WR type than for "classical" WR stars of the same type (Smith and Aller, 1971). A comparison with the classical WC9 star, WR103, which was observed during the same observing run, did not show any significant differences in line widths or line intensities between the two stars. One must therefore also consider the possibility that PK 337 $+1^{\circ}1$ might be a normal WC9 star surrounded with a compact H II region. Hopefully, the finally reduced data will permit a more unambiguous interpretation of this object.

Symbiotic Stars

Fig. 2 (middle) shows a spectrum of our object 209, also known as No. 324 in the list of H α emission objects by Stephenson and Sanduleak (1977). The true nature of this object was previously unknown, but our spectrogram clearly shows a symbiotic object, with a high excitation line spectrum superposed on a late-type stellar spectrum.

Planetary Nebulae

Our final example is a spectrogram of our object 88 ($\alpha = 18^{\text{h}}46^{\text{m}}11$, $\delta = -5^{\circ}59'8$). This object does not, as far as we know, appear in any other list of emission line objects. The spectrum (Fig. 2, lower) is typical of a planetary nebula of medium excitation.

There are of course several other interesting objects in our material, but since almost no reductions have yet been made, we feel that a discussion of these must be postponed to a later occasion. Let us only once more emphasize that the IDS is an excellent tool for studying faint emission-line objects and that we certainly intend to make use of this fine equipment for future investigations of similar kind. For example, with the

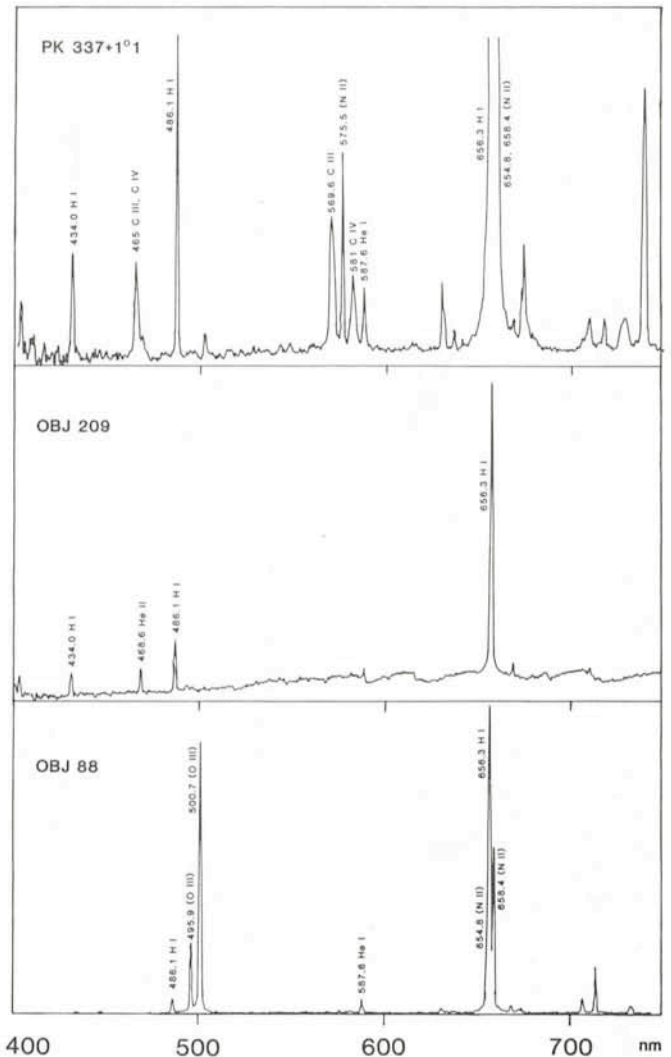


Fig. 2: Spectral signatures of three objects mentioned in the text. Not finally reduced, no calibration of the ordinate is done.

experience hitherto gained, we are now designing a programme for ESO in which we will investigate all known or suspected planetary nebulae in the southern sky. This project, which will not require very much telescope time, will go into a planned catalogue of planetary nebulae as proposed by Agnès Acker at the Strasbourg Observatory.

References

- Lundström, I. and Stenholm, B.: 1984, *Astron. Astrophys.* (in press).
- Jones, D. H. P., Evans, D. S. and Catchpole, R. M.: 1969, *Observatory* **89**, 18.
- Sanduleak, N.: 1976, *Publ. Warner & Swasey Obs.* **2**, 3.
- Smith, L. F. and Aller, L. H.: 1971, *Astrophys. J.* **164**, 275.
- Stephenson, C. B. and Sanduleak, N.: 1977, *Astrophys. J. Suppl.* **33**, 459.
- Webster, B. L.: 1969, *Monthly Not. Roy. Astron. Soc.* **143**, 79.

Colour Gradients in Elliptical Galaxies – Some Results from CCD Photometry

E. Sadler, ESO

The use of charge-coupled device (CCD) cameras in galaxy photometry offers a number of significant advantages over

traditional photoelectric and photographic techniques. CCDs have a high quantum efficiency compared to photographic



Fig. 1: *B-R colour map of the dust-lane galaxy NGC 1947.*

plates, and their response is linear over a large range of brightness. Since they are two-dimensional detectors, the centring problems of photoelectric photometers are avoided, and object and sky can be observed simultaneously. Of course, there are also some disadvantages; the CCD is much smaller in area than a photographic plate, and the read-out noise is a limiting factor for short exposures. However, one area in which CCD detectors are particularly valuable is in studying the inner regions of nearby galaxies, and in particular the colours and colour gradients in galactic nuclei. Here, the smaller size of the CCD is no disadvantage as we are studying objects 1–2 arc minutes in angular size. Since the luminosity profile of a galaxy rises sharply towards the centre, saturation effects and the non-linear response of the emulsion present problems for photographic work, while it is extremely hard to obtain photoelectric aperture photometry with diaphragms smaller than 10–15" because of the difficulty in centring the galaxy accurately. The resolution of the CCD image, on the other hand, is limited only by the pixel size (0".47 at the Danish

1.5 m telescope) and the seeing (usually 1–2" at La Silla). This allows us a fascinating glimpse into the innermost regions of many nearby galaxies, and may provide new insight into the mechanisms responsible for "active" nuclei in galaxies.

The existence of colour gradients in the outer parts of some elliptical galaxies is well known (e.g. Strom and Strom 1978 *A.J.* **83**, 73), although the number of galaxies for which detailed information is available is still small. Generally, the galaxy becomes bluer in colour further out from the centre, and this is generally explained as being due to a gradient in the abundance of heavy elements. However, it is also very interesting to know how the colour of the galaxy nucleus compares with that in the outer parts, because several phenomena which are believed to take place in the central 1 kpc of the galaxy may have an observable effect on the colour of the central region. Despite the classical picture of elliptical galaxies as essentially gas-free systems of old stars, there is mounting evidence that modest ($\sim 10^6 M_{\odot}$) amounts of ionized gas are a normal feature of these galaxies. A group of us (L. Binette and

E. Sadler at ESO, together with M. Dopita, M. Phillips and C. Jenkins) have found weak $H\alpha$ and [NII] emission lines in more than half of a sample of 200 elliptical and S0 galaxies. A similar result for emission lines of [OII] has been reported by Caldwell (1982 Ph.D. Thesis, Yale University), who also argues that recent bursts of star formation have occurred in some ellipticals. If this is the case, the young stars should be concentrated in the nucleus of the galaxy where most of the gas resides, and their effect will be to change the colour of the central region relative to the galaxy background.

In March 1984, I spent three nights observing with the CCD camera at the Danish 1.5 m telescope at La Silla. A description of the CCD was given in a previous issue of the *Messenger* (Pedersen and Cullum, December 1982). The weather during this run was very good, with excellent seeing (often better than 1"). Images were obtained with B, V and R broad-band filters for 15 galaxies as part of a project to study the relationship between gas, radio emission and the stellar population in elliptical galaxies. A number of standard stars were observed each night, and were used to transform the observations to the standard Cousins BVR system after flat-fielding and dark subtraction had been done. Although only 5–6 stars were observed each night, the transformation was accurate to about 0.02 mag. in V and 0.01 mag. in B–V and V–R. This is encouraging since it shows that, at least for bright objects, the CCD can produce results comparable in accuracy with photoelectric photometry.

At this stage, we can derive the brightness distribution in each galaxy out to about 25 mag./(arcsec^2) in B (i.e. at least 2 magnitudes fainter than the La Silla night sky) and corresponding levels in V and R. However, some further processing is necessary to obtain the B–V and B–R colour maps. It is important that the point spread function have exactly the same width and shape in each frame before they are subtracted. If, for example, the seeing is better in the red frame than the blue, then subtraction of the two frames will produce an artificially "red" nucleus because the red profile is narrower and so the central few pixels contain proportionally more light. Other effects, such as guiding errors (which are very small at the Danish telescope thanks to the autoguider) or focus drift can produce an asymmetric image. Each frame must therefore be broadened to the same "seeing" profile with a two-dimensional gaussian function and aligned exactly with the others before subtraction. This is done by measuring the position and half-width in X and Y directions of 6–10 stellar images in each frame. The stellar images also provide a check on the final colour map – they should be circular in shape and of uniform colour if the subtraction has been done correctly.

Fig. 1 shows a B–R map of the dust-lane S0 galaxy NGC 1947. North is at the top, east to the right, and darker and lighter areas represent bluer and redder colours respectively. The area to the top and left of the picture shows only noise since it lies outside the galaxy image. The reddening due to the dust-lanes on the NE side of the galaxy is clearly seen, and the structure of the dust itself is reminiscent of that in Centaurus A (see e.g. Ebneter and Balick 1983 *PASP* **95**, 675 for a recent photograph) although NGC 1947 is somewhat more distant and intrinsically fainter. Fig. 2 shows the blue luminosity profile and B–R colour gradient for a region perpendicular to the dust-lane. The dust manifests itself both as absorption in B and as a sharp reddening in B–R. The colour gradient in the underlying galaxy is very small (≤ 0.1 mag. in B–R over 70" on the SW (dust-free) side).

What is interesting is that this "dust-lane signature" is also seen in the inner regions of a number of apparently "normal" elliptical galaxies. Figs. 3 and 4 show the E2 galaxy IC 3370 in which the B–R map reveals a small ($\sim 10''$) long dust lane which is clearly seen in the B–R profile even though it is barely visible

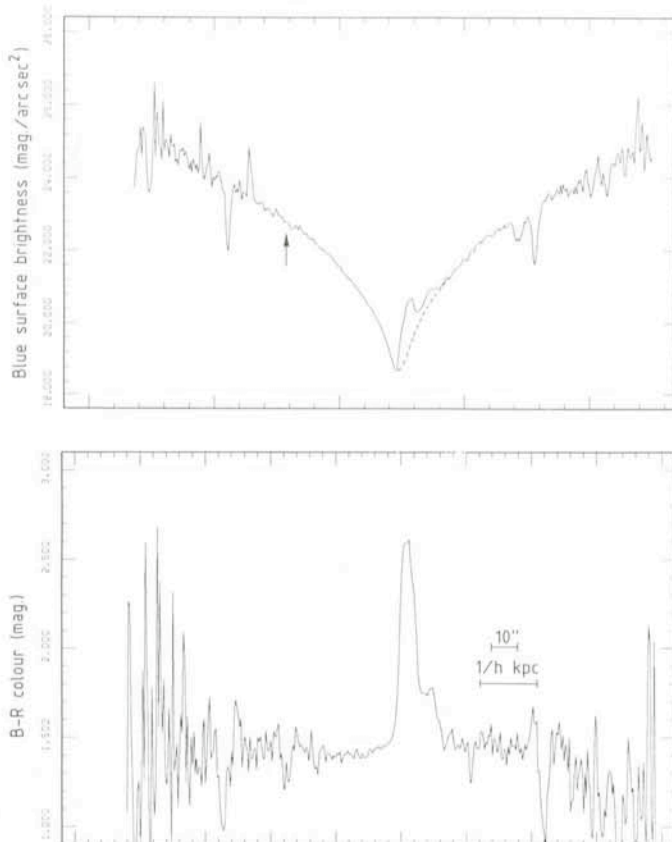


Fig. 2: Profiles in blue luminosity and B–R colour along a line perpendicular to the dust-lane of NGC 1947 and passing through the nucleus. An arrow indicates the brightness of the night sky at La Silla at the time of observation, while the dotted line is the reflection of the (dust-free) south-west side about the nucleus. The bright "spikes" far from the nucleus are due to foreground stars.

as an absorption kink in the luminosity gradient and certainly cannot be detected on photographic plates. This dust-lane has a diameter of about $1.3/h$ kpc ($H_0 = 100$ h km/s/Mpc), compared to $3\text{--}4/h$ kpc for the NGC 1947 dust-lane and $10\text{--}15$ kpc for the dust lane in Centaurus A. CCD surface photometry

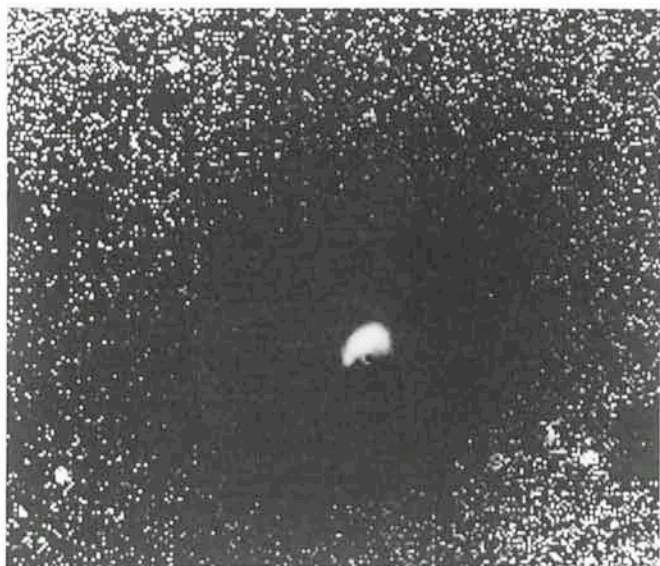


Fig. 3: B–R colour map of the elliptical galaxy IC 3370, revealing a small dust-lane in the nucleus.

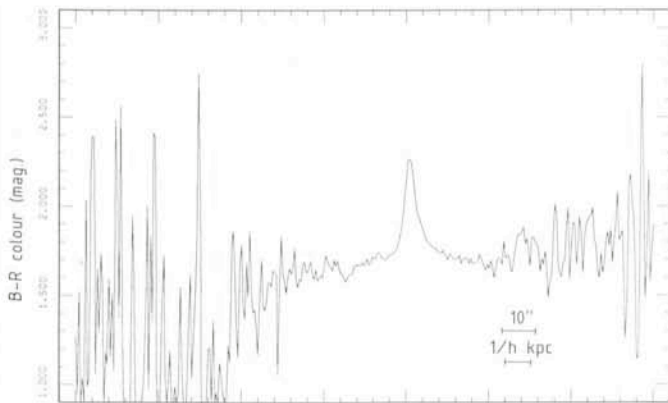
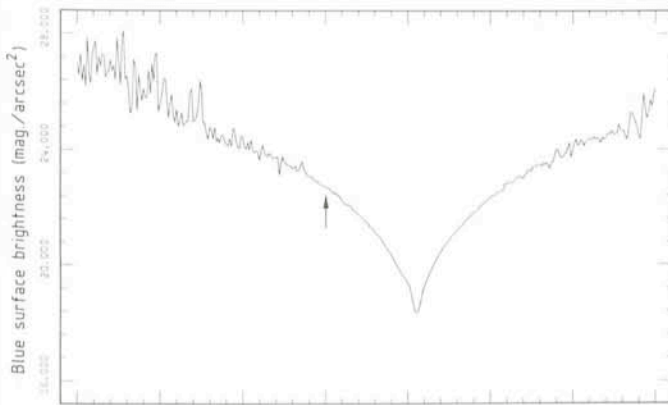


Fig. 4: As Fig. 2, for IC 3370. Note the similarity to Fig. 2 despite the smaller size of the absorbing region.

seems to be a powerful method of revealing "hidden" dust in the nuclei of elliptical galaxies because at least three other galaxies in the small sample so far observed show resolved red nuclei similar to that in IC 3370. All these galaxies show

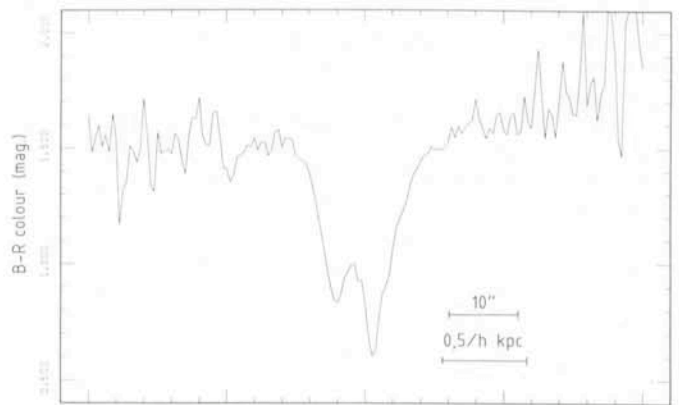


Fig. 5: *B-R* profile of the star-forming elliptical galaxy NGC 2328. The blue nucleus is clearly seen.

weak emission lines in their nuclei and also contain small radio sources, suggesting that all these factors may be linked.

NGC 2328 is an example of an early-type galaxy currently undergoing a strong burst of star formation. It is very blue in colour, and has an emission-line spectrum characteristic of HII regions. The two-dimensional *B-R* map shows a ring of blue regions which encircle the centre of the galaxy, and several of them can be resolved. Fig. 5 shows a profile through the nucleus.

These preliminary results from a project which is still in progress show the power of CCD photometry in the study of galactic nuclei and reveal once again that elliptical galaxies are by no means the "simple" systems they were once believed to be.

I should like to thank Holger Pedersen and H. Jørgensen for their advice and help during the CCD observing run, and Preben Grosbøl for guiding me during several stages of the photometric reduction.

PERSONNEL MOVEMENTS

STAFF

Arrivals

Europe

DEIRIES, Sebastian (D), Technician, 1.9.1984
 MAASWINKEL, Alphonsus (NL), Project Engineer in Astronomical Instrumentation, 1.10.1984

Chile

JUTZI, Christian (CH), Administrator, 1.9.1984
 LE BERTRE, Thibaut (F), Astronomer, 6.9.1984
 MERTL, Wenzel (CH), Electronics Engineer, 1.10.1984

Departures

Chile

MEINEN, Inge (D), Administrator, 31.8.1984

ASSOCIATES

Departures

Europe

KRAUTTER, Joachim (D), 30.11.1984

ALGUNOS RESUMENES

Un telescopio submilimétrico de 15 m en La Silla

En su última reunión del 7 de junio de 1984 el Consejo de la ESO aprobó el acuerdo entre el Consejo Sueco de Investigaciones de Ciencias Naturales y la ESO por la instalación y operación en La Silla de un telescopio submilimétrico de 15 m y el acuerdo entre IRAM y ESO por el cual IRAM proporcionará el telescopio.

El tiempo de observación será compartido en períodos iguales entre Suecia y ESO. Gran parte de la responsabilidad técnica para el proyecto quedaría a cargo del Observatorio Espacial de Onsala que ya opera un telescopio submilimétrico de 20 m en Onsala. Está programado que el telescopio submilimétrico Sueco-ESO (SEST) opere a partir de 1987.

El Señor Profesor L. Woltjer fue nombrado nuevamente como Director General por el Consejo de la ESO para el período del 1° de enero de 1985 al 31 de diciembre de 1989.

ESO, the European Southern Observatory, was created in 1962 to . . . establish and operate an astronomical observatory in the southern hemisphere, equipped with powerful instruments, with the aim of furthering and organizing collaboration in astronomy . . . It is supported by eight countries: Belgium, Denmark, France, the Federal Republic of Germany, Italy, the Netherlands, Sweden and Switzerland. It operates the La Silla observatory in the Atacama desert, 600 km north of Santiago de Chile, at 2,400 m altitude, where thirteen telescopes with apertures up to 3.6 m are presently in operation. The astronomical observations on La Silla are carried out by visiting astronomers – mainly from the member countries – and, to some extent, by ESO staff astronomers, often in collaboration with the former. The ESO Headquarters in Europe are located in Garching, near Munich. ESO has about 120 international staff members in Europe and Chile and about 120 local staff members in Santiago and on La Silla. In addition, there are a number of fellows and scientific associates.

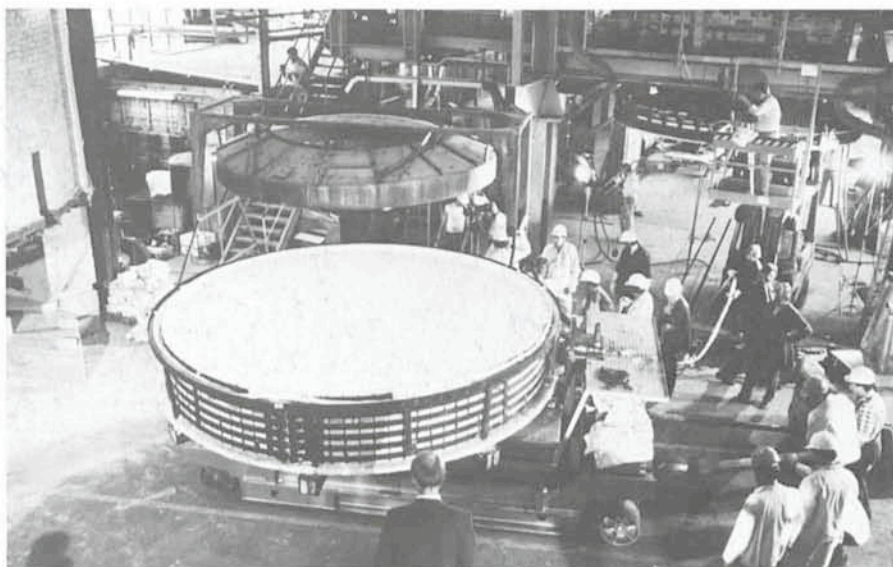
The ESO MESSENGER is published four times a year: in March, June, September and December. It is distributed free to ESO personnel and others interested in astronomy. The text of any article may be reprinted if credit is given to ESO. Copies of most illustrations are available to editors without charge.

Editor: Philippe Véron
 Technical editor: Kurt Kjær

EUROPEAN
 SOUTHERN OBSERVATORY
 Karl-Schwarzschild-Str. 2
 D-8046 Garching b. München
 Fed. Rep. of Germany
 Tel. (089) 32006-0
 Telex 5-28282-0 eo d

Printed by Universitätsdruckerei
 Dr. C. Wolf & Sohn
 Heidemannstraße 166
 8000 München 45
 Fed. Rep. of Germany

ISSN 0722-6691



Casting of the blank for the 3.5 m NTT primary mirror took place at the Schott Glaswerke in Mainz, on July 25, 1984. Coming out of the furnace, the glass had a temperature of approximately 1,400° C and was cooled in the mold to 600° C within two hours.

In this photograph the blank is seen immediately before entering into the brick oven in which it will stay for several months. During renewed heating the glass will be transformed into ZERODUR glass ceramics with very low thermal expansion characteristics. Photo: C. Madsen

El moldeo del vidrio del espejo primario de 3.5 m para el NTT se efectuó en la fábrica Schott en Mainz el 25 de julio de 1984. Al salir del horno el vidrio tenía una temperatura de aproximadamente 1400° C y fue enfriada en el molde a 600° C dentro de dos horas.

La fotografía muestra el vidrio inmediatamente antes de entrar al horno de ladrillos refractarios en donde permanecerá durante varios meses. A través de un renovado calentamiento el vidrio será transformado en cerámica de vidrio ZERODUR con muy bajas características de expansión térmica. Fotografía: C. Madsen

Contents

A 15 Metre Submillimetre Telescope on La Silla	1
G. Raffi and M. Tarengi: The Remote Control Run from La Serena, June 10–17, 1984	1
Tentative Time-table of Council Sessions and Committee Meetings in 1984	3
R. G. Gratton and S. Ortolani: Oxygen Abundances in Metal Poor Stars	3
Visiting Astronomers (October 1, 1984 to April 1, 1985)	5
H. Dekker and S. D'Odorico: First QSO Spectra with EFOSC	7
T. J.-L. Courvoisier: Study of the Overall Spectrum of the QSO 3C273	8
I. Furenlid and T. Meylan: The Sun and α Cen A	10
A. Heske and H. J. Wendker: Roaming in the Sco OB 1 Association	11
S. Vidal: Data Saving and Banking at La Silla	13
B. Reipurth: Two Bok Globules with Active Star Formation	14
List of Preprints Published at ESO Scientific Group (June–August 1984)	16
D. Bettoni: Rotation Axes of Gas and Stars in Elliptical Galaxies	17
J. Materne: Suspected Rotation of an X-ray Cluster of Galaxies	19
M. Joubert and D. Kunth: Wolf-Rayet Stars in "Lazy" Galaxies	21
S. D'Odorico and D. Ponz: On the Accuracy of the Wavelength Calibration and of the Flat-Fielding of the CCD CASPEC Spectra	24
T. de Jong: IRAS Ground-based Follow-up at ESO	26
T. Encrenaz, D. Engels and J. Krautter: Observations of Comet P/Crommelin at ESO in the Near Infrared Range	29
H. W. Yorke: Line Profile Shapes in Optical HII Regions	30
I. Lundström and B. Stenholm: IDS Spectroscopy of Faint Emission-Line Objects	35
E. Sadler: Colour Gradients in Elliptical Galaxies – Some Results from CCD Photometry	36
Personnel Movements	39
Algunos Resúmenes	39
Casting of the Blank for the 3.5 m NTT Primary Mirror	40